Rheological Characterization of Polymer Additives for Mist Control and Drag Reduction

Thesis by
Red C. Lhota

In Partial Fulfillment of the Requirements for the
Degree of
Doctor of Philosophy in Chemical Engineering

Caltech

CALIFORNIA INSTITUTE OF TECHNOLOGY
Pasadena, California

2022
Defended 2022/05/16

© 2022

Red C. Lhota
ORCID: 0000-0002-8481-3716

ACKNOWLEDGEMENTS

I dedicate this thesis to grandmothers, Marilyn Lhota and Marie Peterson, who both passed away in April 2021. Their lifetime love of learning and teaching will always be an inspiration to me as I move forward in teaching and learning more.

I would like to thank my parents, Wendy Peterson and James Lhota, who encouraged me to explore math, science, and engineering from a very early age. Thank you to Barb Lhota and Lisa Hezceg, my aunts, who I know I can always talk to about life.

Thank you to Dara Zirlin, my oldest friend–when I mistook you for my student host as a new student back in fifth grade, I didn't know how lucky I would be to get to know you that first day.

I would like to thank my friends from my time in college in Chicago: Emily Moorman, Sunjay Kumar, Kira Cozzolino, and Eli Klein for the regular calls keeping me connected and giving me excuses to visit.

Thank you to my many friends I met through Caltech: my former roommates, Elliott Williams and Rayden Styer, for your emotional support through the hardest period in my life; my gaming group, Sarida Pratuangtham, Jade Asher, and Tristan Murphy, for all the stories we've told together; my labmates, especially Rob Learsch and Lealia Xiong, for being a touchpoint for what is reasonable and encouraging me to have work-life balance.

I would like to acknowledge the tremendous help of Grace Ho, occupational therapist—graduating was much less painful and felt much more possible because of your support.

Thank you to the Darbs, the students of Dabney Hovse, for whom I was a

Resident Associate for three years. Dabney felt like a home to me because of all of the amazing interactions I had with you all.

Thank you to my dance community–all of the friends I made through Do Something Blue, Lindygroove, and California Twirl. Special shoutout to Jenny Cannon, for watching out for me and making sure I felt like I belonged in the blues community—thank you for "adopting" me at that first dance.

I would like to thank my advisor, Julie Kornfield, would made this work possible. Thank you for teaching me about science communication and how to give talks that include as many members of the audience as possible. I would like to thank my committee for their feedback and expertise–in particular, Beverley McKeon for her continued advice and mentorship throughout our collaboration. Thank you to Jacque Tawney, for keeping our collaboration alive and for making the last few years of research much more fun and rewarding.

ABSTRACT

Long flexible polymers in solution at low concentrations strongly change the extensional properties of fluids due to chain stretching that resists flow, while their compact conformation in shear has weak effects. This dramatic difference between their effects on extension and shear is desirable in a variety of applications–controlling drop size in sprayed mists, reducing drag in turbulent flow, and preventing rebound in drop impact. Traditional long covalent polymers, however, are not practical in many applications because they undergo mechanical degradation, i.e. chain scission, under strong flow conditions. Megasupramolecular polymer systems, consisting of long end-associative telechelic polymers that assemble in solutions into multi-million molecular weight supramolecules, meet this practical need. Through association, they act like traditional covalently-bonded polymers in extension, while reversibly dissociating under the strong flows that cause scission for those long polymers.

This thesis examines the interplay of flow and degradation that imposes an upper-bound on useful lengths of invididual end-associative chains (how long is too long) (Chapters 2 and 3); the quiescent coil size that affects the onset of stretching in fluids of interest (water and polyalphaolefin lubricant) (Chapters 2 and 4); rheological approachs to detect variations in the degree of end-functionalization that affect formation of ultra-long supramolecules (Chapter 5); and the changes to turbulent flow when long polymers are present at low concentration (Chapter 3). Ultimately, the audience who might enjoy this thesis is limited by barriers of rheological jargon. In the pursuit of broader rheological and overall scientific understanding, I describe evidence-based pedagogical techniques and my approach to implementing them in chemical engineering and polymer physics classrooms (Chapter 6).

TABLE OF CONTENTS

vii

LIST OF ILLUSTRATIONS

LIST OF SCHEMES

LIST OF TABLES

C h a p t e r   1

CONTROLLING FLUID PROPERTIES THROUGH POLYMER ADDITIVES

This chapter covers applications of polymers as rheological modifiers (Section 1.1), essential ideas in polymer physics and rheology leveraged in the contained work (Section 1.2), a description of the theory and practice of dripping-onto-substrate extensional rheometry (Section 1.3), and a brief introduction to megasupramolecules (Section 1.4). This chapter is intended as a broad overview to introduce a more general audience to the core ideas in the thesis and is by no means exhaustive.

1.1 Desirable Effects of Polymer Additives on Solution Properties

Polymer additives are a ubiquitous part of the industrial toolkit for modifying the rheology (and other properties) of fluids in transportation, manufacturing, and consumer use. In this section, I will discuss three key applications where high extensional resistance is desirable and where there is an unmet need due to the vulnerability of existing additives to mechanical degradation.

Mist Control

When a liquid is sprayed, the average drop size and distribution of drop sizes determine much of the resulting behavior.[1,2] In agricultural spraying applications, small droplets may drift, while large droplets may rebound off leaves (as discussed more below).[2–8] In a fuel injector in an engine, drops must be small and uniform enough to rapidly and completely combust.[9] In an accidental release of a flammable fluid, small droplets can quickly evaporate and contribute to a fire in the presence of an ignition source.[10–12]
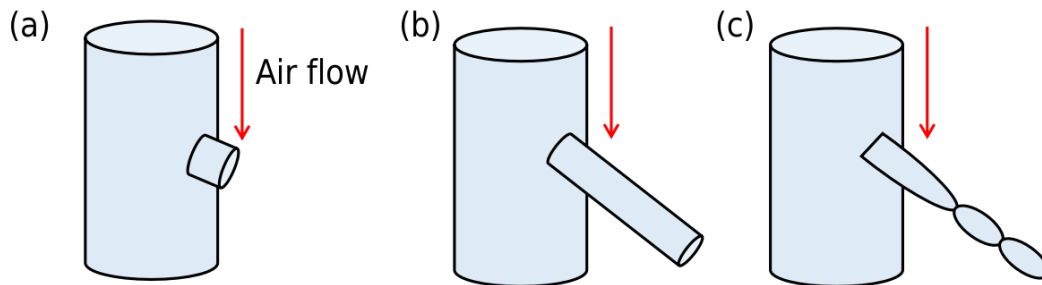
Figure 1.1: Ligament formation and pinchoff. (a) An instability results in a protrusion of the fluid into the surrounding stream. (b) A ligament forms and extends from the main body of the fluid. (c) The ligament pinches off under the capillary action of surface tension.

Controlling both the drop size and the distribution is thus desirable. Polymeric additives are attractive for many mist control and antimisting applications because they have a profound effect on the breakup of jets into drops without greatly increasing the shear viscosity (see Section 1.2 below for discussion of modification of shear versus extension). When a polymer is added into a fluid that is then sprayed, the fluid is observed to form drops of larger average size[2,10,11,13] and fewer tiny satellite droplets.[3,14]

The effect on jet and spray breakup by polymers can be attributed to their resistance to elongational flow. When a jet is breaking up, instabilities cause perturbations extending into the surrounding flow (Figure 1.1(a)). As the surrounding flow extends these perturbations, thin ligaments of fluid are formed (Figure 1.1(b)) and extend. As the ligaments extend, surface tension is driving pinchoff into droplets (Figure 1.1(c)). This process is highly extensional, and a polymer solution will strongly resist that pinchoff, leading to suppression of droplet formation and larger droplets if pinchoff still occurs.[14,15]

Droplet Deposition

When a fluid droplet impacts a surface, it experiences one of multiple fates. It could rebound and leave the surface, it could slide along an angled surface and
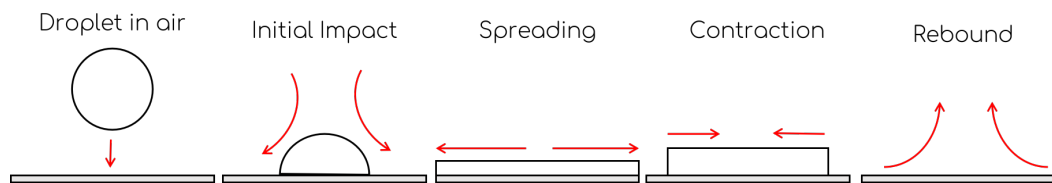
Figure 1.2: Typical stages of droplet impact and rebound. Left-to-right: pre-impact, impact, spreading, contraction, and rebound.

fall off, or it could deposit and be retained. Understanding droplet deposition is important to a number of applications, from distributing fertilizers and pesticides to crops,[3,7,16] to applying coatings and paints to materials,[17,18] to uncovering how viral droplets stick to surfaces.[19]

When a droplet impacts a surface, the kinetic energy from falling results in a series of stages where the droplet impacts, spreads, contracts, and can then rebound (Figure 1.2). During spreading, the kinetic energy is translated into surface energy, which then drives the contraction and extent of rebound, depending on how much energy was dissipated due to viscosity and interaction with the surface.

When a high molecular weight polymer is added into the solution at very low treat rates (less than 0.1 wt %), the contraction is substantially slowed and rebound can be suppressed.[5,20] This effect occurs for multiple polymer backbones, indicating it is a physical interaction, rather than a chemical interaction with the surface.[5,21]

The initial hypothesis put forth to explain these dramatic changes in droplet behavior was that the polymer additives changed the bulk extensional viscosity and thus dissipated more energy, keeping surface tension from driving rebound as it does in the Newtonian case.[5,20] That conclusion, however, has been heavily contested in the literature with additional experiments and analysis. Follow-up experiments with small targets[15,22] and Leidenfrost drops (where

a thin layer of vapor is created between the drop and the surface)[23,24] show that the effect of the polymer additive disappears when surface interaction is removed, contracting that the modification to the bulk elongational properties is the source. Studies of the behavior at the contact line between the drop and the surface showed that the effect of the polymer appears to be concentrated at the contact line, where chains are strongly stretched.[21,25] While the bulk extensional properties appear to not be the direct cause, the extensional behavior (i.e., stretching) of the polymers in solution appears to be intimately tied to their ability to increase droplet retention on surfaces.[7]

Drag Reduction

When fluid is flowing, it experiences friction (drag) that must be overcome to continue flow. In transporting fluids long distances or circulating within a closed system, we use pumps to keep the fluid flowing, at great energy cost. A phenomenon discovered in the 1940s, polymeric drag reduction, reduces the drag experienced by a fluid during turbulent flow.[26–29] Increasing bulk Reynolds number ($Re = \rho U D / \eta_{shear}$, where ρ is the density, U is the mean velocity, D is the length scale of the flow, and η_{shear} is the shear viscosity) and increasing polymer concentration experimentally results in increased drag reduction, up to a maximum drag asymptote.[30,31]

Describing the mechanism driving polymeric drag reduction is an active field of study, due the complexity of both the polymer conformation behavior and the chaotic nature of turbulence.[32,33] When characterizing wall-bounded turbulent flow (such as that in a pipe), researchers identify eddies, coherent flow structures with an associated size and characteristic velocity that vary in time and space throughout the flow. Energy is transferred in the flow from the large scale eddies (on the order of the size of the geometry) to the smallest scale

where viscous dissipation dominates (the Kolmogorov scale).[34] To give a sense of the scale, at $Re = 50,000$, this smallest scale is $3*10^-4$ of the largest scale. Turbulence consists of a cycle of bursts and sweeps–high velocity eddies move towards the wall and interact with the slower flow near the wall (sweeps), causing that near-wall fluid to rapidly move away from the wall (bursts).[35] These bursts are highly elongational, which motivates characterizing the extensional properties of the dilute polymer solutions used in polymeric drag reduction.

The complexity of the field of drag reduction is discussed in more depth in Chapter 3.

Chain Scission

Long, covalently-bonded polymers are used as rheological modifiers in a vast number of applications, from paints to foods to construction. The specific applications just discussed—mist control, droplet deposition, and drag reduction— share a trait in common where these existing additives may not be useful: prior to their use, the fluid will often be pumped, mixed or otherwise subjected to a strong flow. Traditional polymer additives are highly prone to shear as their molecular weight increases. The study of chain scission has been of particular interest in the drag reduction community because it greatly limits where drag-reducing additives can be used industrially.[33,36–43]

Chain scission occurs at lower extension rates as molecular weight increases, although literature disagrees on the exact dependence.[44–49] Careful development of flow geometries were required to extract meaningful information about polymer behavior, and mischaracterization of the flow (i.e., laminar versus turbulent) in a number of studies has led to inconsistent relationships between extension rate and molecular weight of chain scission.[49] Chain scission studies primarily have used molecular weight distributions to characterize the inter-

action between flows and polymer additives, leading to relationships that are backbone dependent, rather than capturing underlying explanations from rheology or polymer physics. This specificity limits applicability to novel polymer additives, motivating further study.

1.2 Essential Polymer Physics and Rheology

Polymer Solution Regimes

A flexible polymer chain at equilibrium in solution adopts a coiled configuration, determined by the interaction between the solvent and the chain, and as concentration increases, the chain and the chains around it. These coils take up space in the solution, the "pervaded volume," and different regimes of polymer solution behavior occur depending on how much of the solution is pervaded by polymer (Figure 1.3). In the dilute regime, polymer coils do not interact, and each chain can be treated individually. As concentration increases, the polymer coils pervade more of the volume until they touch, a point we call the overlap concentration (c^*). Above the overlap concentration, the polymer chains begin to interact, changing the solution properties substantially—the semi-dilute regime. If the chains are long enough and the concentration is above the entanglement concentration, the chains will intertwine and create physical cross-links. In this work, we will focus primarily on concentrations at or below the overlap concentration for polymer backbones. Chapter 5 discusses some semi-dilute solutions.

The above narrative description of the overlap concentration hides nuance about what is the precise choice of when overlap occurs and that the transition between regimes is not necessarily sharp. The literature contains a number of answers, basing the definition on different measures of the size of the polymer coil. Throughout this work, Equation 1.1[50] (where $[\eta]$ is the intrinsic viscosity,
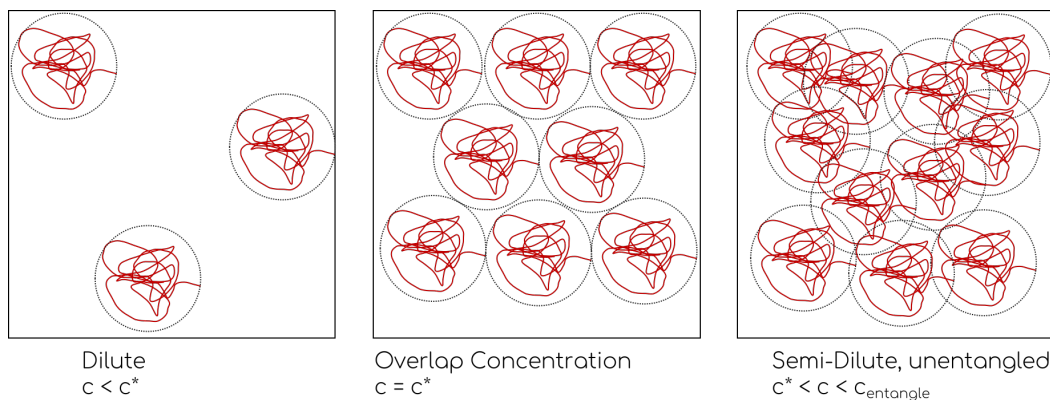
Figure 1.3: Regimes of low-to-moderate concentration (c) for polymer in solution. Left-to-right: Dilute solution (concentrations below overlap, $c < c^*$), overlap concentration (c^*), and semi-dilute, unentangled ($c^* < c < c_{entangle}$, where $c_{entangle}$ is the entanglement concentration).

discussed more below) will be used as the definition of overlap concentration, in order to facilitate comparisons to literature studies of dripping-onto-substrate extensional rheometry in which the same definition was applied. This definition is based on an average chain spacing of twice the radius of gyration at infinite dilution.

$$c^* = \frac{0.77}{[\eta]} \tag{1.1}$$

The overlap concentration is a function of both the polymer molecular weight and the interaction between the solvent and the backbone, as discussed below.

Solvent Quality

The size of a flexible polymer coil in dilute solution depends on the relative solvent-chain and chain-chain interaction. If the chain has no preference between intra-chain and solvent interactions, it will adopt an ideal random walk of its segments (accounting for steric hinderance and limited flexibility due to chemical bonds)—the fluid is a theta solvent. If the chain prefers the solvent to intra-chain interactions, the chain will swell—the fluid is a good solvent. If

the chain prefers intra-chain to solvent interactions, the coil will collapse and if concentration is sufficiently high, the polymer can precipitate. The overlap concentration, discussed above, captures the pervaded volume of a particular chain, and can be calculated from the intrinsic viscosity ($[\eta]$), a measure of the contribution of polymer to the shear viscosity at infinite dilution. The Kuhn-Mark-Houwink-Sakurada equation (Equation 1.2) is an empirical relationship between $[\eta]$ and molecular weight (M) for a particular polymer backbone-solvent-temperature combination.

$$[\eta] = K(M)^a \tag{1.2}$$

K is an empirical prefactor with units of $[\eta]$. In the studies in this work, K and $[\eta]$ will have units of 1/wt %, and the molecular weight M will be chosen to be the weight-average molecular weight M_w[51] with units of g/mol. The exponent a is often used as a proxy for solvent quality as a a value of 0.5 indicates the polymer-solvent combination is at the theta condition, where the chains are in their ideal configuration, and a greater than 0.5 indicates a swollen chain. For flexible chains, a reaches a maximum of 0.8 in a good solvent. a greater than 0.8 indicates a semi-flexible or rigid chain.

To compare a to other measures of solvent quality, Zimm theory scaling gives $[\eta] \sim M_w^{3\nu-1}$, where ν is the Flory exponent, i.e., the exponent relating the radius of gyration to the molecular weight. Thus, a can be related to the Flory exponent as $a \approx 3\nu - 1$. $\nu = 0.5$ indicates a theta solvent (ideal chain behavior) and $\nu = 0.6$ is the limit for a flexible chain in a good solvent.

Dilute Polymer Solutions in Shear Versus Extension

Every flow can be broken down into two components: shear and extension (Figure 1.4). A typical way to apply shear is by placing a material between two surfaces and moving one relative to the other. In shear, the stress is

Shear   **Extensional**

Velocity Gradient   Velocity Gradient   Stress

Stress
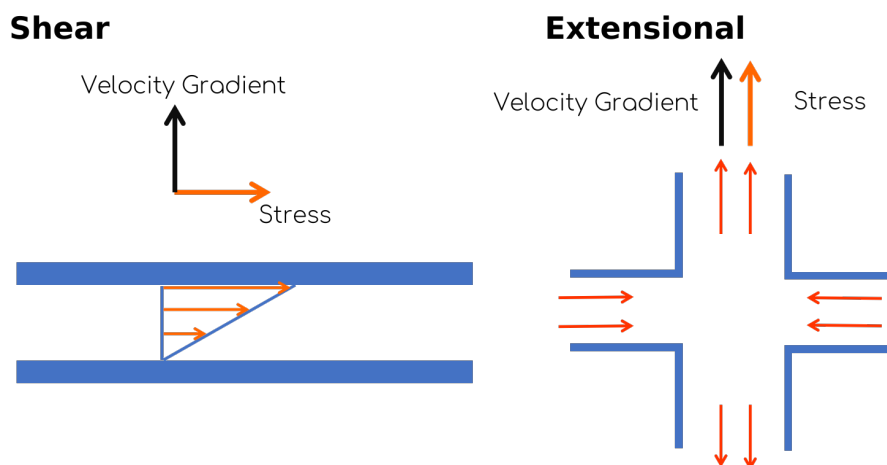
Figure 1.4: Diagram of shear versus extensional flow.

perpendicular to the velocity gradient. Extensional flows involve stretching fluid elements, such as in cross-slot flow or rapidly separating two plates with a material in between. In extension, stress is parallel to the velocity gradient.

The behaviors of dilute polymer solutions in shear and in extension differ strongly, particularly as the molecular weight of the polymer increases. In shear, polymer coils do not fully extend, and instead tumble with the flow. Addition of polymer in the dilute regime does increase the shear viscosity, but in very dilute solutions, that effect can be neglible. In extension, on the other hand, the effects of polymer addtives can be quite dramatic, with potential increases in the extensional viscosity of the solution of over 10,000. These large changes in the extensional properties are due to the polymer chains resisting the stretching of fluid elements. Additionally, the effects of concentration differ between shear and extension. Solutions that are considered dilute (below overlap concentration) in shear may exhibit inter-chain interactions in extensional flow, leading to stronger dependence on concentration for extensional properties.[52]

The ability to modify the extensional properties is dependent on the polymer backbone stiffness and extensibility, with flexible backbones having more impact on the flow.[53,54]

1.3 Dripping-onto-Substrate Extensional Rheometry (DoSER)

Because of the vast differences in polymer solution behavior in shear versus extension and the effects of these behaviors on mist control and drag reduction, measurements of these solutions in elongational flow fields can illuminate application-relevant properties. While polymer melt extensional rheology has long been part of the rheologist's toolbox, polymer solutions have presented additional challenges due to difficulties setting up an appropriate and controlled flow field, as clamping the ends of a sample is not feasible, and due to the increasingly low relaxation times as viscosity of the solution decreases, requiring higher speed flow field setup and measurement.[55–57] Capillary-breakup extensional rheometry (CaBER) solved many of these challenges for solutions with shear viscosities greater than 20 mPa-s by constructing a flow field by rapidly separating plates at a known rate and then observing the thinning of the midpoint of the formed liquid bridge using a laser micrometer.[55]

The minimum diameter of the liquid bridge (D) as a function of time (t) in capillary-breakup rheometry is observed to take on the characteristics of three regimes, depending on the relative properties of the fluid. In Newtonian fluids, two regimes are observed, controlled by the Ohnesorge number, $Oh = \eta_{shear}/\sqrt{\rho\sigma d}$ a dimensionless group comparing the viscous forces to the inertio-capillary forces, where η_{shear} is the shear viscosity of the fluid, ρ is the density of the fluid, σ is the surface tension, and d is a characteristic length scale.

In Newtonian fluids of high viscosity compared to inertia ($Oh > 1$), the liquid bridge thins according to Equation 1.3, a balance between viscous and capillary

(a) Visco-capillary (polyalphaolefin). (b) Inertio-capillary (water). (c) Elastocapillary (6M PEO in water at 0.02 wt %).
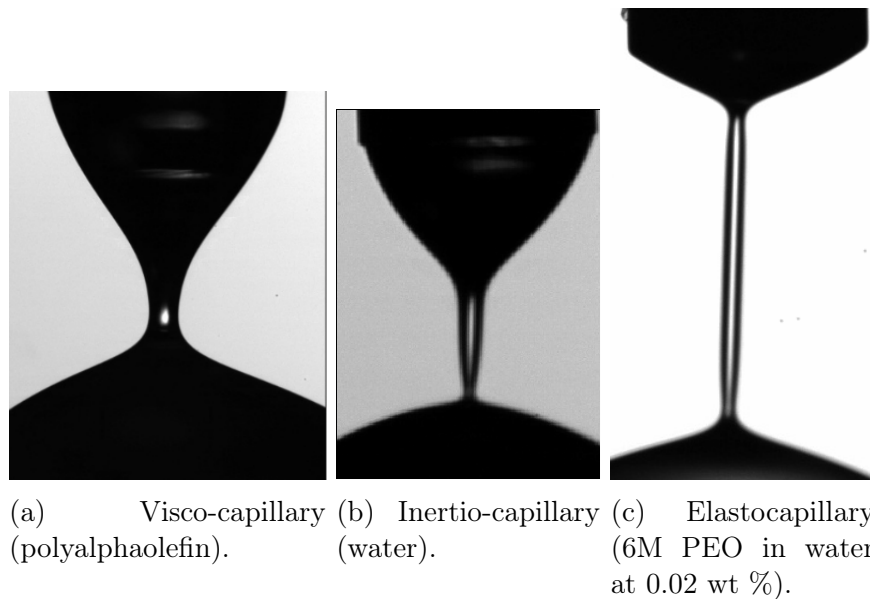
Figure 1.5: Images demonstrating expected shapes of liquid bridge necks for the three regimes of capillary breakup.

(surface tension) forces, the visco-capillary regime.

$$\frac{D(t)}{D_0} = 0.0709 \frac{2\sigma}{\eta_{shear} D_0}(t_p - t) \tag{1.3}$$

D_0 is the starting diameter of the liquid bridge. t_p is the pinchoff time. The neck of the liquid bridge forms a characteristic cylindrical shape in this regime (Figure 1.5a).[58]

In low viscosity Newtonian fluids, where $Oh \ll 1$, the inertial forces balance capillary forces in the inertio-capillary regime of thinning, following Equation 1.4.

$$\frac{D(t)}{D_0} = 0.8 \left(\frac{t_p - t}{(\rho D_0^3 / 8\sigma)^{1/2}} \right)^{2/3} \tag{1.4}$$

The neck of the liquid bridge forms a characteristic conical shape in this regime (Figure 1.5b).[58]

In viscoelastic fluids, such as polymer solutions, the thinning is initially visco-capillary or inertio-capillary, depending on the value of Oh; however, if the elastic forces exceed the viscous or inertial forces respectively, the behavior

will transition to the elastocapillary regime where the balance of elastic and capillary forces controls the thinning (Figure 1.6). In capillary-breakup experiments, this transition occurs at a Weissenburg number ($Wi = \lambda_E \dot{\epsilon}$) of 2/3, where λ_E is the extensional relaxation time and $\dot{\epsilon}$ is the extensional strain rate. The liquid bridge observed in the elastocapillary regime is a cylinder (Figure 1.5c) that thins with a characteristic time scale related to the extensional relaxation time (Equation 1.5).

$$\frac{D(t)}{D_0} = \sum_i \left(\frac{g_i D_0}{4\sigma}\right)^{1/3} e^{-t/3\lambda_{E,i}} \approx \left(\frac{G D_0}{4\sigma}\right)^{1/3} e^{-t/3\lambda_E} \tag{1.5}$$

g_i and $\lambda_{E,i}$ are the corresponding extensional modulus and relaxation time for a mode i; throughout this work, we adopt the hypothesis of Entov and Hinch and assume that the longest relaxation time dominates the observed capillary-breakup behavior, and thus we can approximate the elastocapillary regime with a single modulus G and relaxation time λ_E.[58,59]

Because polymers are not ideal springs with the ability to extend infinitely, finite extensibility limits the duration of the elastocapillary regime, leading to a more rapid fall-off in the observed diameter at long time than expected from Equation 1.5 (Figure 1.6).

As solution viscosity decreases, either by using lower viscosity solvents or lowering polymer concentration, the duration of inertial effects due to the initial separation of the plates begins to exceed the liquid break-up time and thus the elastocapillary regime is not measurable. To solve this limitation with CaBER instruments, the Sharma group developed dripping-onto-substrate extensional rheometry (DoSER), a form of capillary-breakup extensional rheometry. In DoSER, a drop of fluid is dispensed from a nozzle (often a blunt-tipped needle) onto a substrate, and a liquid bridge forms between the nozzle and the substrate. The thinning of the liquid bridge is observed as a function of time
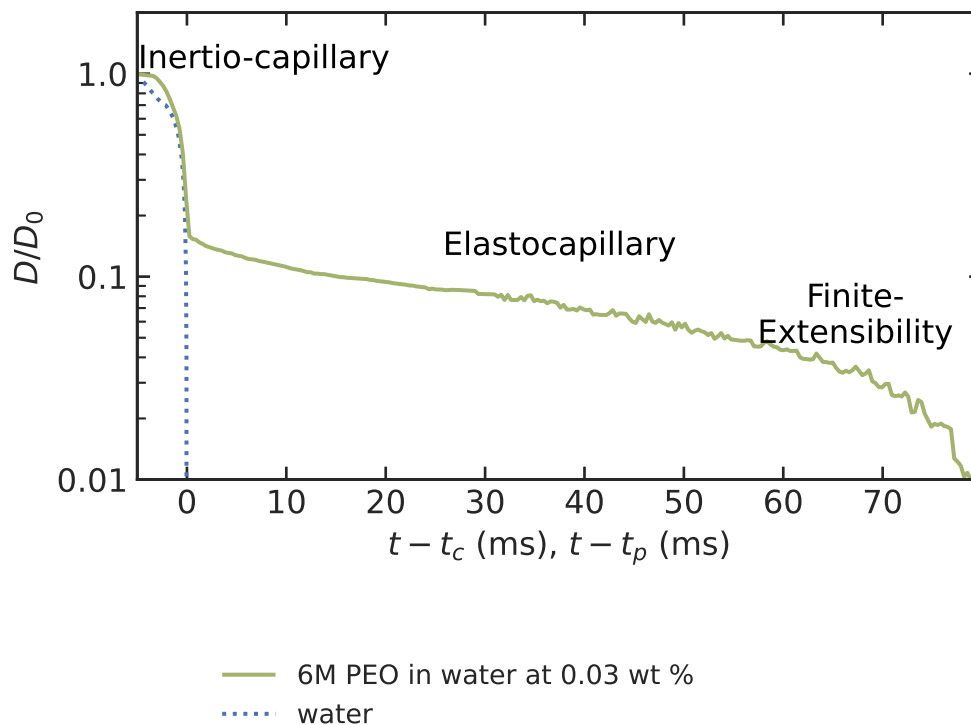
Figure 1.6: Example of measured capillary thinning for a polymer solution compared to water, demonstrating transitions for the polymer solution from the inertio-capillary regime (corresponding to water alone) to the elastocapillary regime, followed by finite-extensibility.

using a high-speed camera. Because the strain rate of thinning is imposed by the fluid rather than the separation of plates as in traditional CaBER, much higher strain rates are possible, allowing access to measurement of much smaller relaxation times, and correspondingly, lower solution viscosities. The lower limit on measurable relaxation times is controlled by the camera's spatial and temporal resolutions—small relaxation times require both high speeds and high resolution–as well as vibrations due to air currents and inertial ringing of the drop contacting the substrate obscuring the short time behavior. The upper limit on measureable relaxation times is primarily controlled by the memory available in the camera, which can be mitigated by recording at lower frame rates for high relaxation time samples.
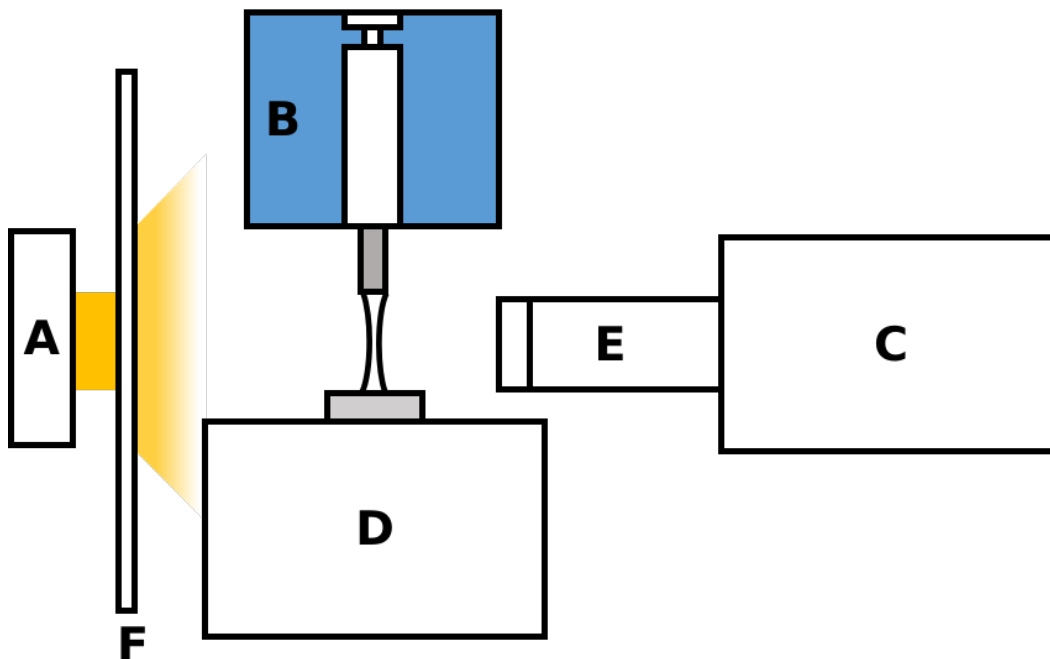
Figure 1.7: Schematic of dripping-onto-substrate extensional rheometer (not to scale).

DoSER Methodology

A dripping-onto-substrate extensional rheometry (DoSER) instrument (Figure 1.7) consists of a light source (**A**), a syringe pump for solution delivery (**B**), a (preferably high-speed) camera (**C**), an optical train that resolves the length scales desired (**E**), and a substrate (**D**). The light passes through a diffuser (**F**) before reaching the measurement plane. To set up the flow fluid, a syringe with a blunt-tip metal needle is attached to the syringe pump above the substrate holder.

The following is a brief discussion of our methodology for collecting and analyzing data using DoSER, further discussion of the analysis package we developed, dosertools, appears in Appendix A.

The substrate is chosen to be phobic to the solvent of the solution, such that a drop beads up, to prevent undesired additional flow fields away from the

primary extensional flow. The height between the substrate and nozzle is chosen based on the optimal range of height-to-initial-droplet-diameter—initial droplet diameter is a function of both nozzle diameter and surface tension of the solution.[60] Detailed discussion of selection of the height between the nozzle and the substrate is planned to be discussed in Robert Learsch's thesis.

DoSER experiments are performed using the following procedure. An aliquot is slowly loaded into a syringe through a blunt-tip needle. The syringe is attached to the syringe pump and the syringe pump is slowly advanced until solution is observed to drip from the needle. A clean set of aluminum substrates is loaded onto the substrate holder and the first substrate is aligned below the needle tip. The light is turned on and the camera is focused and aligned with the needle tip. The substrate is then raised or lowered to the correct height (as describe above) relative to the needle tip. A background video with a droplet-free needle and substrate is acquired. A drop is dispensed from the needle tip by the syringe pump at a rate of 0.02 mL/min, until the drop is nearly touching the substrate. The syringe pump is stopped prior to droplet-substrate contact. The droplet contact through liquid bridge formation and pinchoff is recorded (referred to as an experimental video or "run"). A new substrate is then placed below the needle tip. Dispensing drops onto a clean substrate is repeated until sufficient runs are recorded.

The data collected is processed using the *dosertools* Python package, developed by Robert Learsch and Red Lhota (Appendix A). A summary of the steps involved appears below.

The experimental and background videos are cropped to remove the substrate from the frame. The background is averaged and subtracted from the experimental video to remove any non-uniformity in pixel intensity due to the light
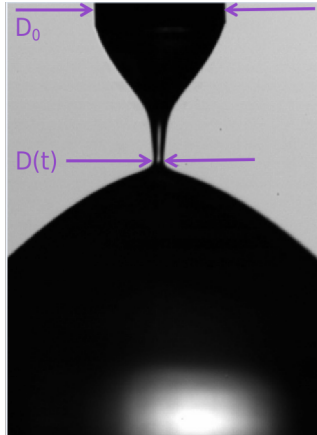
Figure 1.8: Example DoSER image showing the needle diameter D_0 and the minimum diameter of the liquid bridge $D(t)$.

source or lens. The resulting image is then turned into a binary image using an Otsu threshold. The minimum thread diameter is detected as a function of time, and normalized using the nozzle diameter (treated as the initial liquid bridge diameter, D_0, for thinning) (Figure 1.8). The needle diameter is measured from the experimental or background video, whichever video has the most clearly defined boundaries of the nozzle tip.

The normalized diameter is then analyzed to determine the critical time and the relaxation time. The critical time (t_c) is defined as the time of transition from the visco-capillary or inertio-capillary regime to the elastocapillary regime. Plotting normalized diameter data as a function of time past the critical time $(t - t_c)$ removes differences between datasets due to when recordings were started relative to the physical behavior. Equation 1.5 can be rewritten as a function of $t - tc$ (Equation 1.6).

$$\frac{D(t)}{D_0} = \left(\frac{D_{tc}}{D_0}\right)^{1/3} e^{-(t-t_c)/3\lambda_E} \tag{1.6}$$

D_{tc} is the diameter at the critical time.

Prior literature determined the critical time by inspection.[53,54,57,58,61] Robert Learsch developed a method for detecting the critical time through finding the

moment of maximum strain rate within the window of normalized diameter in which transition occurs, which was implemented in the dosertools package. By finding the critical time systematically rather than by inspection, we significantly reduced user-to-user variation in analysis.

After finding the normalized diameter as a function of time past the critical time, Equation 1.6 is fit to the elastocapillary regime, chosen to have an upper bound of $D/D_0 = 0.1$ or D_{t_c}/D_0, whichever is lower, and a lower bound of 0.045. From this fit, the extensional relaxation time is calculated for each sample (fitting details in Appendix A).

1.4   Megasupramolecules

End-associative telechelic polymers of sufficiently long backbone length can associate in solution to form supramolecular polymer exceeding 1Mg/mol in total weight, called megasupramolecules (Figure 1.9). Each telechelic polymer unit acts as a unimer in this large polymer, and can reversibly associate and disassociate both at equilibrium and in flow. This reversibility gives long, end-associative telechelic polymers a substantial advantage over traditional, long-chain polymer additives because the ability to disassociate under strong flows can prevent chain scission.[12] The megasupramolecules exhibit an equilibrium distribution of linear and ring supramolecules—linear supramolecules have a larger rheological impact and thus are usually more desirable. By using pairwise association and keeping unimer lengths sufficiently long, the distribution can be biased towards linear megasupramolecules.[12,62]

Megasupramolecular systems have a number of aspects that can be tuned to achieve their desired rheological behaviors and thus their performance. The unimer backbone length can be adjusted depending on desired effective molecular weight after association, as long as it is neither too long (and thus vul-
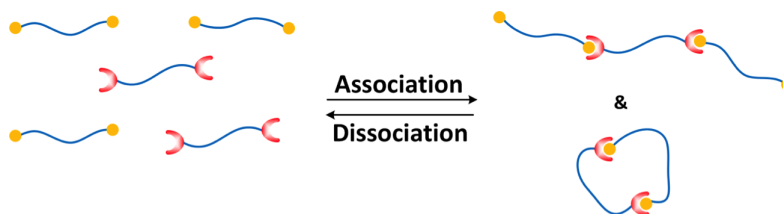
Figure 1.9: Schematic depicting the association and disassociation of end-associative telechelic polymers. Functional groups on the chains may be self-associative or pairwise associative, forming megasupramolecules in solution.

nerable to chain scission) or too short (and thus primarily forming ineffective rings[12,62] or networks[63]). The solvent quality of the backbone in the fluid of choice also affects the rheological behavior and vulnerability to chain scission through changes in the swelling of the coil—too poor of a solvent can cause loss of performance via precipitation.[64] The association strength between polymer units can be manipulated by changing the end-group or by altering the association through interaction with the solvent, which will modify the expected distribution of long linears versus small rings.[12,62] Absence of some end-groups can suppress the formation of long linear chains, but also formation of rings, by acting as end-cappers, usually to the detriment of the total contribution to the rheological properties.[62]

Chapters 2 and 3 discuss considerations in choosing an appropriate backbone length to resist chain scission. Chapter 4 looks at the effects of solvent on the backbone solvent quality and on the effective association strength, in addition to how concentration changes observed association. Chapter 5 outlines the impact of backbone length and end-group fidelity on megasupramolecular formation.

References

[1] E. Villermaux. "Fragmentation". In: *Annual Review of Fluid Mechanics* 39.1 (Jan. 2007), pp. 419–446. ISSN: 0066-4189, 1545-4479. DOI: `10.1146/annurev.fluid.39.050905.110214`. URL: `http://www.annualreviews.org/doi/10.1146/annurev.fluid.39.050905.110214` (visited on 05/06/2020).

[2] S. Kooij et al. "What Determines the Drop Size in Sprays?" In: *Physical Review X* 8.3 (July 20, 2018). ISSN: 2160-3308. DOI: `10.1103/PhysRevX.8.031019`. URL: `https://link.aps.org/doi/10.1103/PhysRevX.8.031019` (visited on 06/11/2020).

[3] R. W. Lewis et al. "Polymeric Drift Control Adjuvants for Agricultural Spraying". In: *Macromolecular Chemistry and Physics* 217.20 (Oct. 2016), pp. 2223–2242. ISSN: 10221352. DOI: `10.1002/macp.201600139`. URL: `https://onlinelibrary.wiley.com/doi/10.1002/macp.201600139` (visited on 03/23/2022).

[4] E. Hilz. "Spray Drift Review: The Extent to Which a Formulation Can Contribute to Spray Drift Reduction". In: *Crop Protection* (2013), p. 9.

[5] V. Bergeron et al. "Controlling Droplet Deposition with Polymer Additives". In: *Nature* 405.6788 (June 2000), pp. 772–775. ISSN: 0028-0836, 1476-4687. DOI: `10.1038/35015525`. URL: `http://www.nature.com/articles/35015525` (visited on 08/05/2020).

[6] W. Wirth, S. Storpb, and W. Jacobsenb. "Mechanisms Controlling Leaf Retention of Agricultural Spray Solutions". In: *Pesticide Science* 33.4 (1991), pp. 411–420.

[7] M. Xu et al. "Quantifying the Effect of Extensional Rheology on the Retention of Agricultural Sprays". In: *Physics of Fluids* 33.3 (Mar. 1, 2021), p. 032107. ISSN: 1070-6631, 1089-7666. DOI: `10.1063/5.0038391`. URL: `https://aip.scitation.org/doi/10.1063/5.0038391` (visited on 03/15/2021).

[8] Y. Yeong, J. Burton, and E. Loth. "Drop Impact and Rebound Dynamics on an Inclined Superhydrophobic Surface". In: *Langmuir* 30 (2014), pp. 12027–12038. DOI: `10.1021/la502500z`.

[9] M. Sens et al. "Effects of Highly-Heated Fuel and/or High Injection Pressures on the Spray Formation of Gasoline Direct Injection Injectors". In: *Fuel Systems for IC Engines*. Elsevier, 2012, pp. 215–238. ISBN: 978-0-85709-210-6. DOI: `10.1533/9780857096043.6.215`. URL: `https://linkinghub.elsevier.com/retrieve/pii/B9780857092106500167` (visited on 07/09/2020).

[10] K. K. Chao et al. "Antimisting Action of Polymeric Additives in Jet Fuels". In: *AIChE Journal* 30.1 (Jan. 1984), pp. 111–120. ISSN: 0001-1541, 1547-5905. DOI: `10.1002/aic.690300116`. URL: `http://doi.wiley.com/10.1002/aic.690300116` (visited on 03/23/2016).

[11] R. S. Marano et al. "Polymer Additives as Mist Suppressants in Metal-working Fluids Part I: Laboratory and Plant Studies - Straight Mineral Oil Fluids". In: *S.A.E. Transactions* 104 (Section 5 1995), pp. 136–146.

[12] M.-H. Wei et al. "Megasupramolecules for Safer, Cleaner Fuel by End Association of Long Telechelic Polymers". In: *Science* 350.6256 (Oct. 2, 2015), pp. 72–75. ISSN: 0036-8075, 1095-9203. DOI: `10.1126/science.aab0642`. URL: `http://www.sciencemag.org/cgi/doi/10.1126/science.aab0642` (visited on 03/17/2016).

[13] B. Keshavarz et al. "Studying the Effects of Elongational Properties on Atomization of Weakly Viscoelastic Solutions Using Rayleigh Ohnesorge Jetting Extensional Rheometry (ROJER)". In: *Journal of Non-Newtonian Fluid Mechanics* 222 (Aug. 2015), pp. 171–189. ISSN: 03770257. DOI: `10.1016/j.jnnfm.2014.11.004`. URL: `http://linkinghub.elsevier.com/retrieve/pii/S0377025714002055` (visited on 01/06/2017).

[14] R. P. Mun, J. A. Byars, and D. V. Boger. "The Effects of Polymer Concentration and Molecular Weight on the Breakup of Laminar Capillary Jets". In: (1998), p. 13.

[15] A. N. Rozhkov. "Dynamics and Breakup of Viscoelastic Liquids (A Review)". In: 40.6 (2005), p. 19.

[16] C. Shan et al. "Effects of Droplet Size and Spray Volume Parameters on Droplet Deposition of Wheat Herbicide Application by Using UAV". In: *International Journal of Agricultural and Biological Engineering* 14.1 (2021), pp. 74–81. ISSN: 1934-6344. DOI: `10.25165/j.ijabe.20211401.6129`. URL: `https://ijabe.org/index.php/ijabe/article/view/6129` (visited on 04/30/2022).

[17] D. Brian et al. "Impact Dynamics and Deposition of Perovskite Droplets on PEDOT:PSS and TiO2 Coated Glass Substrates". In: *Experimental Thermal and Fluid Science* 105 (July 2019), pp. 181–190. ISSN: 08941777. DOI: `10.1016/j.expthermflusci.2019.03.021`. URL: `https://linkinghub.elsevier.com/retrieve/pii/S0894177718319745` (visited on 04/30/2022).

[18] S. Chandra. "Coating Deposition by Thermal Spray Processes". In: *Annual Review of Heat Transfer* 20.1 (2017), pp. 121–148. ISSN: 1049-0787. DOI: `10.1615/AnnualRevHeatTransfer.2018019747`. URL: `http://www.dl.begellhouse.com/references/5756967540dd1b03,562e7b3835dec96e,5e195ff86bce1ea9.html` (visited on 04/30/2022).

[19] H. Yu, H.-L. Yen, and Y. Li. "Deposition of Bronchiole-Originated Droplets in the Lower Airways during Exhalation". In: *Journal of Aerosol Science* 142 (Apr. 2020), p. 105524. ISSN: 00218502. DOI: `10.1016/j.jaerosci.2020.105524`. URL: `https://linkinghub.elsevier.com/retrieve/pii/S0021850220300136` (visited on 04/30/2022).

[20] R. Crooks and D. V. Boger. "Influence of Fluid Elasticity on Drops Impacting on Dry Surfaces". In: *Journal of Rheology* 44.4 (July 2000), pp. 973–996. ISSN: 0148-6055, 1520-8516. DOI: `10.1122/1.551123`. URL: `http://sor.scitation.org/doi/10.1122/1.551123` (visited on 08/05/2020).

[21] M. I. Smith and V. Bertola. "Effect of Polymer Additives on the Wetting of Impacting Droplets". In: *Physical Review Letters* 104.15 (Apr. 15, 2010). ISSN: 0031-9007, 1079-7114. DOI: `10.1103/PhysRevLett.104.154502`. URL: `https://link.aps.org/doi/10.1103/PhysRevLett.104.154502` (visited on 08/05/2020).

[22] A. Rozhkov, B. Prunet-Foch, and M. Vignes-Adler. "Impact of Drops of Polymer Solutions on Small Targets". In: *Physics of Fluids* 15.7 (July 2003), pp. 2006–2019. ISSN: 1070-6631, 1089-7666. DOI: `10.1063/1.1580480`. URL: `http://aip.scitation.org/doi/10.1063/1.1580480` (visited on 08/11/2020).

[23] V. Bertola. "An Experimental Study of Bouncing Leidenfrost Drops: Comparison between Newtonian and Viscoelastic Liquids". In: *International Journal of Heat and Mass Transfer* 52.7-8 (Mar. 2009), pp. 1786–1793. ISSN: 00179310. DOI: `10.1016/j.ijheatmasstransfer.2008.09.028`. URL: `https://linkinghub.elsevier.com/retrieve/pii/S0017931008005875` (visited on 08/06/2020).

[24] V. Bertola. "Effect of Polymer Concentration on the Dynamics of Dilute Polymer Solution Drops Impacting on Heated Surfaces in the Leidenfrost Regime". In: *Experimental Thermal and Fluid Science* 52 (Jan. 2014), pp. 259–269. ISSN: 08941777. DOI: `10.1016/j.expthermflusci.2013.09.019`. URL: `https://linkinghub.elsevier.com/retrieve/pii/S0894177713002306` (visited on 09/02/2020).

[25] D. Bartolo et al. "Dynamics of Non-Newtonian Droplets". In: *Physical Review Letters* 99.17 (Oct. 26, 2007), p. 174502. ISSN: 0031-9007, 1079-7114. DOI: `10.1103/PhysRevLett.99.174502`. URL: `https://link.aps.org/doi/10.1103/PhysRevLett.99.174502` (visited on 07/29/2020).

[26] M. D. Graham. "Drag Reduction in Turbulent Flow of Polymer Solutions". In: *Rheology Reviews* 2 (2004), pp. 143–170.

[27]   "Some Distinctive Rheological Concepts and Phenomena". In: *Rheology Series*. Ed. by R. Tanner and K. Walters. Vol. 7. Elsevier, 1998, pp. 159–186. ISBN: 978-0-444-82945-0. DOI: `10.1016/S0169-3107(98)80008-7`. URL: `https://linkinghub.elsevier.com/retrieve/pii/S0169310798800087` (visited on 04/28/2022).

[28]   B. A. Toms. "Some Observations on the Flow of Linear Polymer Solutions through Straight Tubes at Large Reynolds Numbers". In: *Proceedings of the International Congress on Rheology* II (1949), pp. 135–141.

[29]   B. A. Toms. "On the Early Experiments on Drag Reduction by Polymers". In: *Physics of Fluids* 20.10 (1977), S3. ISSN: 00319171. DOI: `10.1063/1.861757`. URL: `http://scitation.aip.org/content/aip/journal/pof1/20/10/10.1063/1.861757` (visited on 03/18/2016).

[30]   P. S. Virk. "Drag Reduction Fundamentals". In: *AIChE Journal* 21.4 (July 1975), pp. 625–656.

[31]   C. M. White, V. S. R. Somandepalli, and M. G. Mungal. "The Turbulence Structure of Drag-Reduced Boundary Layer Flow". In: *Experiments in Fluids* 36.1 (Jan. 1, 2004), pp. 62–69. ISSN: 0723-4864, 1432-1114. DOI: `10.1007/s00348-003-0630-0`. URL: `http://link.springer.com/10.1007/s00348-003-0630-0` (visited on 04/29/2022).

[32]   L. Xi. "Turbulent Drag Reduction by Polymer Additives: Fundamentals and Recent Advances". In: *Physics of Fluids* 31.12 (Dec. 1, 2019), p. 121302. ISSN: 1070-6631, 1089-7666. DOI: `10.1063/1.5129619`. URL: `http://aip.scitation.org/doi/10.1063/1.5129619` (visited on 07/13/2021).

[33]   E. J. Soares. "Review of Mechanical Degradation and De-Aggregation of Drag Reducing Polymers in Turbulent Flows". In: *Journal of Non-Newtonian Fluid Mechanics* 276 (Feb. 2020), p. 104225. ISSN: 03770257. DOI: `10.1016/j.jnnfm.2019.104225`. URL: `https://linkinghub.elsevier.com/retrieve/pii/S0377025719304197` (visited on 11/19/2020).

[34]   P. A. Davidson, ed. *A Voyage through Turbulence*. Cambridge ; New York: Cambridge University Press, 2011. 434 pp. ISBN: 978-0-521-19868-4 978-0-521-14931-0.

[35]   J. Southard. "4.8: More on the Structure of Turbulent Boundary Layers-Coherent Structures in Turbulent Shear Flow". In: *Introduction to Fluid Motions, Sediment Transport, and Current-Generated Sedimentary Structures*. LibreTexts, July 19, 2019. URL: `https://geo.libretexts.org/Bookshelves/Sedimentology/Book%3A_Introduction_to_Fluid_Motions_and_Sediment_Transport_(Southard)/04%3A_Flow_in_Channels/4.08%3A_More_on_the_Structure_of_Turbulent_Boundary_Layers-_Coherent_Structures_in_Turbulent_Shear_Flow` (visited on 05/26/2022).

[36] W. Brostow. "Drag Reduction and Mechanical Degradation in Polymer-Solutions in Flow". In: *Polymer* 24.5 (1983), pp. 631–638. ISSN: 0032-3861. DOI: `10.1016/0032-3861(83)90119-2`.

[37] W. Brostow, H. Ertepinar, and R. P. Singh. "Flow of Dilute Polymer Solutions: Chain Conformations and Degradation of Drag Reducers". In: *Macromolecules* 23.24 (1990), pp. 5109–5118. URL: `http://pubs.acs.org/doi/abs/10.1021/ma00226a013` (visited on 05/05/2016).

[38] M. W. Liberatore et al. "Turbulent Drag Reduction of Polyacrylamide Solutions: Effect of Degradation on Molecular Weight Distribution". In: (2004), p. 10.

[39] V. N. Kalashnikov. "Degradation Accompanying Turbulent Drag Reduction by Polymer Additives". In: (2002), p. 18.

[40] J. M. J. Den Toonder et al. "Degradation Effects of Dilute Polymer Solutions on Turbulent Drag Reduction in Pipe Flows". In: *Applied scientific research* 55.1 (1995), pp. 63–82. URL: `http://link.springer.com/article/10.1007/BF00854224` (visited on 05/05/2016).

[41] T. Moussa and C. Tiu. "Factors Affecting Polymer Degradation in Turbulent Pipe-Flow". In: *Chemical Engineering Science* 49.10 (May 1994), pp. 1681–1692. ISSN: 0009-2509. DOI: `10.1016/0009-2509(93)E0029-C`.

[42] S. U. Choi, Y. I. Cho, and K. E. Kasza. "Degradation Effects of Dilute Polymer Solutions on Turbulent Friction and Heat Transfer Behavior". In: *Journal of Non-Newtonian Fluid Mechanics* 41.3 (Feb. 1992), pp. 289–307. ISSN: 03770257. DOI: `10.1016/0377-0257(92)87003-T`. URL: `https://linkinghub.elsevier.com/retrieve/pii/037702579287003T` (visited on 11/19/2020).

[43] S. Jouenne et al. "Degradation (or Lack Thereof) and Drag Reduction of HPAM Solutions During Transport in Turbulent Flow in Pipelines". In: *Oil and Gas Facilities* 4.01 (Feb. 12, 2015), pp. 80–92. ISSN: 2224-4514. DOI: `10.2118/169699-PA`. URL: `https://onepetro.org/OGF/article/4/01/80/207287/Degradation-or-Lack-Thereof-and-Drag-Reduction-of` (visited on 03/24/2022).

[44] T. Q. Nguyen, G. Yu, and H.-H. Kausch. "Birefringence of a Polystyrene Solution in Elongational Flow: Effects of Molecular Weight and Solvent Quality". In: *Macromolecules* 28.14 (July 1995), pp. 4851–4860. ISSN: 0024-9297, 1520-5835. DOI: `10.1021/ma00118a010`. URL: `http://pubs.acs.org/doi/abs/10.1021/ma00118a010` (visited on 09/13/2016).

[45] T. Q. Nguyen and H.-H. Kausch. "Chain Scission in Transient Extensional Flow Kinetics and Molecular Weight Dependence". In: *Journal of non-newtonian fluid mechanics* 30.2-3 (1988), pp. 125–140. URL: `http://www.sciencedirect.com/science/article/pii/0377025788850201` (visited on 09/11/2016).

[46] A. Keller and J. A. Odell. "The Extensibility of Macromolecules in Solution; A New Focus for Macromolecular Science". In: *Colloid & Polymer Science* 263.3 (Mar. 1985), pp. 181–201. ISSN: 0303-402X, 1435-1536. DOI: 10.1007/BF01415506. URL: http://link.springer.com/10.1007/BF01415506 (visited on 04/06/2022).

[47] T. Moussa, C. Tiu, and T. Sridhar. "Effect of Solvent on Polymer Degradation in Turbulent Flow". In: *Journal of Non-Newtonian Fluid Mechanics* 48 (1993), pp. 261–284.

[48] S. A. Vanapalli, M. T. Islam, and M. J. Solomon. "Scission-Induced Bounds on Maximum Polymer Drag Reduction in Turbulent Flow". In: *Physics of Fluids* 17.9 (2005), p. 095108. ISSN: 10706631. DOI: 10.1063/1.2042489. URL: http://scitation.aip.org/content/aip/journal/pof2/17/9/10.1063/1.2042489 (visited on 05/05/2016).

[49] S. A. Vanapalli, S. L. Ceccio, and M. J. Solomon. "Universal Scaling for Polymer Chain Scission in Turbulence". In: *Proceedings of the National Academy of Sciences* 103.45 (Nov. 7, 2006), pp. 16660–16665. ISSN: 0027-8424, 1091-6490. DOI: 10.1073/pnas.0607933103. URL: http://www.pnas.org/cgi/doi/10.1073/pnas.0607933103 (visited on 09/11/2016).

[50] W. Graessley. "Polymer Chain Dimensions and the Dependence of Viscoelastic Properties on Concentration, Molecular Weight and Solvent Power". In: *Polymer* 21.3 (Mar. 1980), pp. 258–262. ISSN: 00323861. DOI: 10.1016/0032-3861(80)90266-9. URL: https://linkinghub.elsevier.com/retrieve/pii/0032386180902669 (visited on 04/28/2021).

[51] M. Bohdanecký, V. Petrus, and B. Sedláček. "Estimation of the Characteristic Ratio of Polyacrylamide in Water and in a Mixed Theta-solvent". In: *Die Makromolekulare Chemie* 184.10 (Oct. 1983), pp. 2061–2073. ISSN: 0025116X, 0025116X. DOI: 10.1002/macp.1983.021841011. URL: http://doi.wiley.com/10.1002/macp.1983.021841011 (visited on 02/04/2021).

[52] C. Clasen et al. "How Dilute Are Dilute Solutions in Extensional Flows?" In: *Journal of Rheology* 50.6 (Nov. 2006), pp. 849–881. ISSN: 0148-6055, 1520-8516. DOI: 10.1122/1.2357595. URL: http://sor.scitation.org/doi/10.1122/1.2357595 (visited on 05/14/2021).

[53] J. Dinic and V. Sharma. "Macromolecular Relaxation, Strain, and Extensibility Determine Elastocapillary Thinning and Extensional Viscosity of Polymer Solutions". In: *Proceedings of the National Academy of Sciences* 116.18 (Apr. 30, 2019), pp. 8766–8774. ISSN: 0027-8424, 1091-6490. DOI: 10.1073/pnas.1820277116. URL: http://www.pnas.org/lookup/doi/10.1073/pnas.1820277116 (visited on 05/05/2021).

[54] J. Dinic and V. Sharma. "Flexibility, Extensibility, and Ratio of Kuhn Length to Packing Length Govern the Pinching Dynamics, Coil-Stretch Transition, and Rheology of Polymer Solutions". In: *Macromolecules* 53.12 (June 23, 2020), pp. 4821–4835. ISSN: 0024-9297, 1520-5835. DOI: 10.1021/acs.macromol.0c00076. URL: https://pubs.acs.org/doi/10.1021/acs.macromol.0c00076 (visited on 05/05/2021).

[55] S. L. Anna and G. H. McKinley. "Elasto-Capillary Thinning and Breakup of Model Elastic Liquids". In: *Journal of Rheology* 45.1 (2001), p. 115. ISSN: 01486055. DOI: 10.1122/1.1332389. URL: http://scitation.aip.org/content/sor/journal/jor2/45/1/10.1122/1.1332389 (visited on 03/22/2016).

[56] G. H. McKinley and T. Sridhar. "Filament-Stretching Rheometry of Complex Fluids". In: *Annual Review of Fluid Mechanics* 34.1 (2002), pp. 375–415. URL: http://www.annualreviews.org/doi/abs/10.1146/annurev.fluid.34.083001.125207 (visited on 03/23/2016).

[57] J. Dinic et al. "Extensional Relaxation Times of Dilute, Aqueous Polymer Solutions". In: *ACS Macro Letters* 4.7 (July 21, 2015), pp. 804–808. ISSN: 2161-1653, 2161-1653. DOI: 10.1021/acsmacrolett.5b00393. URL: http://pubs.acs.org/doi/abs/10.1021/acsmacrolett.5b00393 (visited on 03/17/2016).

[58] J. Dinic, L. N. Jimenez, and V. Sharma. "Pinch-off Dynamics and Dripping-onto-Substrate (DoS) Rheometry of Complex Fluids". In: *Lab on a Chip* 17.3 (2017), pp. 460–473. ISSN: 1473-0197, 1473-0189. DOI: 10.1039/C6LC01155A. URL: http://xlink.rsc.org/?DOI=C6LC01155A (visited on 02/10/2020).

[59] V. Entov and E. Hinch. "Effect of a Spectrum of Relaxation Times on the Capillary Thinning of a Filament of Elastic Liquid". In: *Journal of Non-Newtonian Fluid Mechanics* 72.1 (Sept. 1997), pp. 31–53. ISSN: 03770257. DOI: 10.1016/S0377-0257(97)00022-0. URL: https://linkinghub.elsevier.com/retrieve/pii/S0377025797000220 (visited on 04/02/2021).

[60] R. Learsch. "Investigation in Experimental Conditions and Automation of Dripping-onto-Substrate Rheology". American Chemical Society Spring Meeting (San Diego, CA). Mar. 23, 2022.

[61] J. Dinic, M. Biagioli, and V. Sharma. "Pinch-off Dynamics and Extensional Relaxation Times of Intrinsically Semi-Dilute Polymer Solutions Characterized by Dripping-onto-Substrate Rheometry". In: *Journal of Polymer Science Part B: Polymer Physics* 55.22 (Nov. 15, 2017), pp. 1692–1704. ISSN: 08876266. DOI: 10.1002/polb.24388. URL: http://doi.wiley.com/10.1002/polb.24388 (visited on 03/05/2020).

[62]   R. L. A. David. "Associative Polymers as Antimisting Agents and Other Functional Materials via Thiol-Ene Coupling". Pasadena, California: California Institute of Technology, Mar. 7, 2008. 189 pp. URL: `http://thesis.library.caltech.edu/2173/`.

[63]   B. Li. "Ring/Chain versus Network: Architecture Induced by Self- versus Pairwise- Association of Telechelic Polymers". Pasadena, California: California Institute of Technology, 2016. 244 pp.

[64]   A. Dupas et al. "Mechanical Degradation Onset of Polyethylene Oxide Used as a Hydrosoluble Model Polymer for Enhanced Oil Recovery". In: *Oil & Gas Science and Technology – Revue d'IFP Energies nouvelles* 67.6 (Nov. 2012), pp. 931–940. ISSN: 1294-4475, 1953-8189. DOI: `10.2516/ogst/2012028`. URL: `http://ogst.ifpenergiesnouvelles.fr/10.2516/ogst/2012028` (visited on 01/15/2019).

Chapter 2

CHARACTERIZING CHAIN SCISSION IN AQUEOUS POLYMER SOLUTIONS

2.1 Introduction

Aqueous Sprays in Agriculture

In an agricultural setting, water-based sprays feature prominently, from irrigation of crops to application of relevant chemicals, such as fertilizers and pesticides. Substantial amounts of chemicals intended for crop leaves have off-target landing sites, such as on plants in other fields, on the soil, or on local wildlife.[1,2] Groundwater and well-water contamination by pesticides is a significant and pervasive long-term health and environmental hazard, in addition to consequences of acute exposure.[3–6]

Spray-based application of chemicals faces two major challenges related to droplet size. Fine droplets (typically defined as having diameters in the range 50-200 µm) may drift on the wind away from the intended crops.[7,8] Large droplets may rebound or roll off leaf surfaces (particularly an issue for hydrophobic, angled leaves, such as those of corn).[1,2,9,10] Controlling both droplet size and deposition behavior is desirable to mitigate these challenges.[11–13] Additive candidates include surfactants (outside the scope of this work) and polymers, along with other surface tension and rheological modifiers. As discussed in detail in Chapter 1, polymers have a substantial effect on droplet average size, distribution of sizes, and impact, motivating study of water-soluble polymers with large effective sizes in solution as additives in agricultural applications.[7,9,11,14–16]

Current implementation of polymer additives in agricultural settings is limited

by efficacy in field-relevant settings. Commercially available long water-soluble homopolymers, such as poly(ethylene oxide), suffer from significant degradation when undergoing pumping.[7,17–19] Due to this vulnerability to scission, these long polymers lose efficacy in their performance as mist control and drag reduction agents as their effective size decreases.[7,11,15,20]
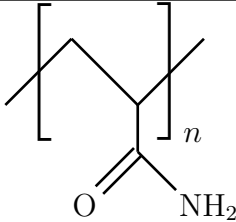
To combat degradation, our group has designed aqueous end-associative polymers to reversibly form supramolecular moeities, with synthesis conducted by Hojin Kim and characterization conducted by Hojin Kim and Robert Learsch. To establish an upper bound on the unit length for these end-associative polymers and better understand the threshold for chain scission, I compared homopolymers of two different water-soluble backbones, poly(ethylene oxide) (PEO, widely available and studied) and polyacrylamide (PAM, the backbone for the end-associative polymers). In addition to establishing guidelines for how long the unimers can be for a pumping-tolerant additive, understanding how chain scission impacts the extensional properties, and thus expected effects on the application relevant behavior, is key to designing additives that are tolerant to varying application conditions and bounding the range of outcomes if an additive system is mishandled, either in storage or use.

Comparing Properties of Polyacrylamide and Poly(ethylene oxide)

Though both water-soluble polymers, the anticipated changes to the extensional flow, and thus to chain scission, due to PAM versus PEO were not immediately apparent due to inconsistencies and gaps in literature data on PAM in water. Relevant properties of the two backbones are discussed below and summarized in Table 2.1.

When an application is limited by polymer additive loading by mass, minimizing molecular weight per backbone atom is one metric for increasing the

Table 2.1: Structure and properties of polyacrylamide (PAM) and poly(ethylene oxide) (PEO).

	polyacrylamide (PAM)	poly(ethylene oxide) (PEO)
structure		
molecular weight per backbone atom (g/mol/BBA)	35.5	14.7
Kuhn-Mark-Houwink-Sakurada Exponent in Water (a)	0.62-0.8[21–23]	0.68-0.78[24,25]
characteristic ratio	8.5[26] 12.7[27]	6.7[28] 6.9[27]
chain scission force (nN)[29]	4.38 ± 0.16	2.30 ± 0.22
backbone bond theoretical strength (nN)[29]	4.1 (C-C)	4.1 (C-C) 4.3 (C-O)

effective length of a polymer additive at a particular weight concentration. PEO has all heavy atoms in the backbone, leading to a molecular weight per backbone atom (BBA) of 14.7 g/mol/BBA, while PAM is heavier, at 35.5 g/mol/BBA, due the side groups on the backbone.

In addition to differences in length due to proportion of atoms in the backbone to side groups, effective size at equilibrium is modified by the solvent quality of the backbone (see discussion of the Kuhn-Mark-Houwink-Sakurada equation and the relationship to the Flory exponent in Chapter 1). Literature data for PAM is relatively sparse, with disagreement about the value of the exponent

indicating solvent quality (a in Equation 1.2), ranging from 0.62-0.8 for PAM in water at 30 °C over a similar range of molecular weights.[21–23] Literature on PEO in water is more available, although with some disagreement on the value of a—at similar temperatures to those studied for PAM, a is reported in the range 0.68-0.78.[24,25] Further comparison of Kuhn-Mark-Houwink-Sakurada exponents across literature sources for PAM and PEO appears in Table 2.3 in the Results section. The expansion of the chain is both due to interactions with the solvent and due to the chain's self-interactions and steric hinderance. PAM's side groups prevent the chain from adopting an ideal chain configuration at small length scales, leading to a higher mean square end-to-end distance at equilibrium for the same number of backbone bonds than PEO.[26,27] Available characteristic ratio values for each backbone are reported in Table 2.1.

Prior work comparing the behavior of PAM and PEO indicated that PEO undergoes chain scission at lower force on the backbone than PAM. Vanapalli, et al. used drag force scaling from turbulent flow at the Kolmogorov scale to calculate the maximum force a backbone can survive, given the weight-average molecular weight acheived at steady state after repeated chain scission (Equation 2.1).[29]

$$F_{max} = A^{3/2} \frac{\pi \eta_{solv} Re^{3/2} L^2}{4 \rho d^2 \ln{(L/a_d)}} \tag{2.1}$$

A is an order 1 factor based on the geometry, which Vanapalli et al. assumed to be 1 in calculations of the bond strength. η_{solv} is the solvent viscosity. $Re = \frac{\rho U d}{\eta_{solv}}$ is the Reynolds number, ρ is the fluid density, U is the mean velocity, and d is the dimension of the geometry. L is the contour length of the chain. a_d is the chain diameter. Based on the body of literature of chain scission data for which laminar scaling does not correspond, Vanapalli, et al.'s estimations of the force for scission of PEO was 2.30 ± 0.22 nN and for PAM was 4.38 ± 0.16 nN, assuming a chain diameter of 1 nm.[29] Incorporating

differences in chain diameter due to PAM's bulky side groups compared to PEO into their calculation would further amplify this difference between PAM and PEO, implying that we should expect PAM to resist chain scission up to a higher force compared to PEO, although with the trade-off of increased drag on PAM's backbone.

Based on the above survey of properties of homopolymer PAM and PEO, PAM is expected to have a smaller effect on shear and extensional properties per unit mass and that PEO is expected to degrade more significantly in chain scission events.

Extensional Rheology of Polyacrylamide and Poly(ethylene oxide)

To contextualize results in this study, a brief survey of literature results for the extensional rheology and implications for mist control applications of PAM and PEO is included below. More discussion on chain scission can be found in Chapter 1. Further discussion of PAM and PEO as drag reducing agents and the degradation that occurs in turbulent flow experiments can be found in Chapter 3.

The extensional properties of PEO have been correlated with modification of droplet formation during spraying[16] and retention upon impact,[2,9,30] although the precise mechanism for retention has been contested (further discussion in Chapter 1).[14,31,32] At relatively low loadings by mass (<0.1 wt %), long PEO (>1 Mg/mol) dissolved in water has been shown to suppressing small (satellite) droplets in sprays[16] and prevent droplet rebound from both synthetic and plant hydrophobic surfaces.[2,9,30] These studies highlighted the resistance to extension or stretching of the polymer chain as the primary modifier of the solution behavior.[9,16]

Although PEO is a potent mist control and droplet retention agent in the lab,

chain scission inhibits practical applications in the field.[7,17–19] To characterize chain scission, degradation studies have typically looked at relationships between extension rate and molecular weight at scission, with the underlying mechanism hypothesized to be the extensional forces exceeding the polymer's ability to dissipate energy through conformation changes—if the polymer is fully extended, the critical extensional rate would be inversely related to the extensional relaxation time.[33–35] The extensional properties, however, of weakly viscoelastic solutions of relatively low solvent viscosities, such as low concentrations of PEO and PAM in water, were historically difficult to measure quantitatively.[36] Many studies of degradation of PEO primarily focused on the semi-dilute regime.[37,38] Prior studies of dilute solutions indirectly probed extensional properties, for example, by measuring pressure drop during flow through a packed bed[20,39] or by using opposing jets, for which substantial empirical corrections must be applied, even in the Newtonian case.[30]

Tools to directly measure the extensional properties of highly dilute solutions in low viscosity solvents (such as water) have only been developed in recent years—dripping-onto-substrate extensional rheometry (DoSER)[36] and Rayleigh Ohnesorge jetting extensional rheometry (ROJER)[16] enable extensional studies of solutions with relaxation times and viscosities below what is accessible in traditional capillary-breakup extensional rheometry (CaBER)[40] and microfluidic instruments.[37,38] The methodology of DoSER is described in detail in Chapter 1.

Recent extensional results using DoSER and ROJER utilized PEO as a baseline for comparison to other viscoelastic materials.[16,36,41–45] Aqueous, dilute PEO solutions demonstrated concentration-dependent behavior in extensional flow well below the overlap concentration,[36,43] further supporting hypotheses of chain-chain interaction in extensional flow even when the solution is suf-

ficiently dilute at equilibrium conditions.[46] Direct comparisons of PAM and PEO solutions are sparse—comparing results of semi-dilute solutions of PEO and PAM in glycerol/water mixtures from different sources demonstrates similar relaxation times for similar ranges of shear viscosity; however, variations in glycerol/water ratios prevents quantitative analysis of differences[42,47]

In this work, I considered the relative solvent quality of PAM and PEO at the temperature of our chain scission and extensional experiments. To account for differences in relative swelling of the chains, solutions used in chain scission were prepared at the same reduced concentration. I used dripping-onto-substrate extensional rheology to track the degradation of PAM and PEO homopolymers dissolved in water during pumping, and compared to direct measurements of molecular weight using gel permeation chromatography.

2.2   Experimental Methods

Materials

Polyacrylamide (PAM) was prepared by Hojin Kim. PAM synthetic details to be included in the thesis of Hojin Kim. Low dispersity poly(ethylene oxide) (PEO) acquired from Agilent. High dispersity PEO was acquired from multiple sources as noted in Table 2.2. Table 2.2 includes number-average molecular weight (M_n), weight-average molecular weight (M_w), dispersity (Đ), and source for each polymer used in this chapter.

Solution Preparation

Solutions for Kuhn-Mark-Houwink-Sakurada (KMHS) intrinsic viscosity measurements were prepared by dissolving polymer in deionized water (DI water), rolling for a minimum of overnight (for polymers of molecular weights less than 50 kg/mol) to a maximum of one week (for polymers with molecular weights greater than 1 Mg/mol) at 10 rotations per minute (rpm). Stock solutions

Table 2.2: Molecular weights, dispersities, and sources for polyacrylamide (PAM) and poly(ethylene oxide) (PEO) samples.

Backbone	M_w (Mg/mol)	M_n (Mg/mol)	Đ	Usage	Sample Name	Source
PAM	0.18	0.17	1.0	KMHS		HK
PAM	0.49	0.48	1.0	KMHS		HK
PAM	0.75	0.73	1.0	KMHS		HK
PAM	1.65	1.50	1.1	KMHS		HK
PAM	2.34	1.40	1.7	KMHS		HK
PAM	4.19	3.21	1.3	CS	4M PAM	HK
PAM	4.80	3.00	1.6	KMHS		HK
PAM	6.70	5.00	1.3	KMHS, CS	6.7M PAM	HK
PEO	0.02	0.02	1.1	KHMS		Agilent
PEO	0.10	0.09	1.1	KHMS		Agilent
PEO	0.27	0.25	1.0	KHMS		Agilent
PEO	0.49	0.21	2.3	OC		Aldrich
PEO	0.97	0.87	1.1	KHMS	1M PEO	Agilent
PEO	1.38	1.14	1.2	KHMS		Agilent
PEO	1.40	0.38	3.7	OC		Dow WSRN12K
PEO	2.00	0.42	4.8	OC		Aldrich
PEO	2.10	0.98	2.1	OC		Aldrich
PEO	6.00	3.80	1.6	OC, CS	6M PEO	Dow WSR301

M_w: Weight-average molecular weight, M_n: Number-average molecular weight,
Đ: Dispersity index (M_w/M_n)
PAM: Polyacrylamide, PEO: Poly(ethylene oxide),
KMHS: Kuhn-Mark-Houwink-Sakurada (Figures 2.1 and 2.2),
OC: Overlap concentration (Figure 2.2),
CS: Chain scission (Figures 2.3-2.8),
HK: Hojin Kim.

were then diluted with DI water to appropriate concentrations and allowed to roll for a minimum of overnight.

Solutions for chain scission were prepared by dissolving polymer in deionized water at 0.38 times or 0.16 times the overlap concentration determined through KMHS measurements, as appropriate, and allowed to roll for a week at 10 rpm. Solutions prepared at 0.38 times the overlap concentration were divided in two, with one portion used for chain scission experiments immediately and one portion further diluted to 0.19 times the overlap concentration and allowed to roll overnight before chain scission experiments.

Chain Scission

I collected aliquots of the as-prepared solutions, and after 1, 5, 10, and 20 passes through the pump for analysis with DoSER and GPC. PAM solutions for c/c* = 0.16 and all 6M PEO solutions were run on the same pump. To prevent cross-contamination, a new separate pump was used for PAM solutions for the experiments for c/c* = 0.19 and 0.38. Each pump was washed with soap and water, thoroughly rinsed with deionized water, and allowed to dry between the solutions. The pump model used in all experiments was a 20W Imagitarium Aquarium Powerhead, with an operating speed of 303 gal/hour.

Shear Rheological Measurements

Shear viscosity measurements were performed on an Anton Paar MCR 302 WESP rheometer using a cone-and-plate fixture of 50 mm diameter and 2.007° angle, with a truncation of 0.207 mm. Solutions were loaded by depositing 1.1 mL of the solution on the center of the plate, lowering the cone to 0.217 mm, removing excess to create a flat edge, and then lowering to 0.207 mm to create a spherical edge condition. The plate was cooled to 15 ± 0.1 °C using a Peltier plate to regulate temperature and match ambient conditions experienced in

extensional rheology. Solutions were allowed to thermally equilibrate and relax for 5 min. Shear rate sweeps were performed from 1 to 100 1/s. The solution edge was examined to check for evidence of evaporation and none was observed.

Dripping-onto-Substrate Extensional Rheometry (DoSER)

A dripping-onto-substrate extensional rheometry (DoSER) instrument was constructed by Robert Learsch and Red Lhota consisting of a GSVitec MultiLED G8 with QT lamp head (12000 lumen light source, Figure 1.7**A**), a Harvard Elite 11 syringe pump on an adjustable track (solution delivery, **B**), Photron FASTCAM Nova S12 type 1000K-M-32GB (high-speed camera, **C**) equipped with an optical train as described below, and a custom holder for aluminum substrates (**D**). The optical train consisted of a Resolve4K 7:1 Zoom Video microscope lens, two rear projection lenses, a 1.0x objective lens, and a coupler, resulting in a resolution limit at full zoom of 3.5 µm (**E**). The camera was operated at 25,000 frames per second with a shutter speed of 150,000 Hz (i.e., 7 µs exposure). The light passes through a diffuser before reaching the measurement plane (**F**).

A syringe with a 22G blunt-tip stainless-steel needle (outer diameter 0.718 mm) was mounted to the syringe pump. The substrate was positioned at a height of 2.8 mm below the tip of the needle, corresponding to a height-to-needle-diameter ratio of 4 or a height-to-initial-droplet-diameter ratio of 1, which is within the optimal range for water solutions.[48] Ambient temperature was measured with each experiment and was in the range 15 ± 1 °C.

For each solution, DoSER was performed using the following procedure. An aliquot was slowly loaded into a syringe through a 22G stainless-steel blunt-tip needle. The syringe was attached to the syringe pump and the syringe pump was slowly advanced until solution was observed to drip from the needle, and

Figure 1.7: Schematic of dripping-onto-substrate extensional rheometer (not to scale). (repeated from page 14)

then the needle tip was cleaned. A clean set of aluminum substrates was loaded onto the substrate holder and the first substrate was aligned below the needle tip. The light was turned on and the camera was focused and aligned with the needle tip. The substrate was then raised or lowered to the correct height (as describe above) relative to the needle tip. A background video with a droplet-free needle and substrate was acquired. A drop was dispensed from the needle tip by the syringe pump at a rate of 0.02 mL/min, until the drop was nearly touching the substrate. The syringe pump was stopped prior to droplet-substrate contact. The events of droplet contact through liquid bridge formation and pinchoff were recorded (referred to as an experimental video or "run"). A clean substrate was then placed below the needle tip. Dispensing drops onto a clean substrate was repeated until five total runs were recorded. The videos were analyzed using the *dosertools* Python package, described in detail in Appendix A, to obtain the normalized diameter as function of time

after the critical time (time of transition between solvent behavior and elasto-capillary response). The decay of the normalized diameter is used to evaluate the extensional relaxation time. In our experiments, run-to-run variation on the DoSER instrument was observed to be more significant than errors in fitting–errors in measured relaxation times are thus quantified using the run-to-run variation. Solutions with relaxation times of 0.05 ms and lower were difficult to consistently characterize on our instrument.

Further discussions of DoSER theory and analysis are available in Chapter 1 and Appendix A respectively.

Gel Permeation Chromatography

Aliquots collected pre- and post-pumping were diluted using DI water to sufficiently low concentrations for characterization with aqueous gel permeation chromatography (GPC). PEO solutions were diluted to 0.0025 wt % or lower. PAM solutions were diluted to 0.02 wt % or lower. Solutions were passed through a 0.45 µm syringe filter after dilution.

The molecular weights and dispersity index of the polymers in solution were determined on a GPC system with an Agilent PL Aquagel-OH Mixed-H 8µm 300 x 7.5mm column, Wyatt DAWN 8 multi-angle laser light scattering detector (λ=658.9nm), and a Waters Optilab differential refractometer (RI) (λ=658nm). Water with 200 ppm sodium azide and 8.5 g/L sodium nitrate was used as the eluent at the flow rate of 0.3mL/min with a temperature of 25°C. The data were analyzed using Wyatt Astra Software (version 7.3.2.19) using the Zimm fitting formula with $dn/dc = 0.136$ mL/g for PEO and $dn/dc = 0.159$ mL/g for PAM in water to obtain the weight-average molecular weight (M_w) for each polymer reported.

Characterizing high molecular weight poly(ethylene oxide) aqueous solutions

Backbone	Temperature (°C)	$K * 10^4$ (1/wt %)	a	Source
PAM	15	4.3	0.61 ± 0.04	This study
PEO	15	3.2	0.70 ± 0.06	This study
PAM	30	0.63	0.8	Scholtan (1954)[21]
PAM	30	6.8	0.66	Collinson, et al. (1957)[22]
PAM	30	0.65	0.62	Misra, et al. (1979)[23]
PEO	15	5.0	0.68	Gregory, et al. (1986)[24]
PEO	30	1.2	0.78	Bailey, et al. (1958)[25]

Table 2.3: Kuhn-Mark-Houwink-Sakurada prefactor (K) and exponent (a) (Equation 1.2) for polyacrylamide and poly(ethylene oxide) in water.[21–25] (a $\pm$ one standard deviation, K standard deviations were less than 10^{-8})

via gel phase chromatography (GPC) can be challenging due to column interactions and polymer aggregation. PEO with weight-average molecular weight can be well-characterized up to 2.5 Mg/mol and PAM up to 5 Mg/mol.[49]

2.3   Results

Comparisons in Solvent Quality

Intrinsic viscosity as a function of weight-average molecular weight was compared to available literature values for Kuhn-Mark-Houwink-Sakurada coefficients for PAM and PEO (Figure 2.1, Table 2.3). Logarithmic fits of the Kuhn-Mark-Houwink-Sakurada equation (Equation 1.2) to the measured data produced $K = 4.3 * 10^{-4}$ (1/wt %) and $a = 0.61 \pm 0.04$ for PAM and $K = 3.2 * 10^{-4}$ (1/wt %) and $a = 0.70 \pm 0.06$ for PEO ($a \pm$ one standard deviation, K standard deviations were less than 10^{-8}).

The overlap concentration was calculated from the intrinsic viscosities measured using Equation 1.1 (Figure 2.2). High dispersity ($M_w/M_n > 1.3$) PEO samples were also characterized in addition to PAM and the low dispersity ($M_w/M_n < 1.3$) PEO samples shown in Figure 2.1. The weight-average num-
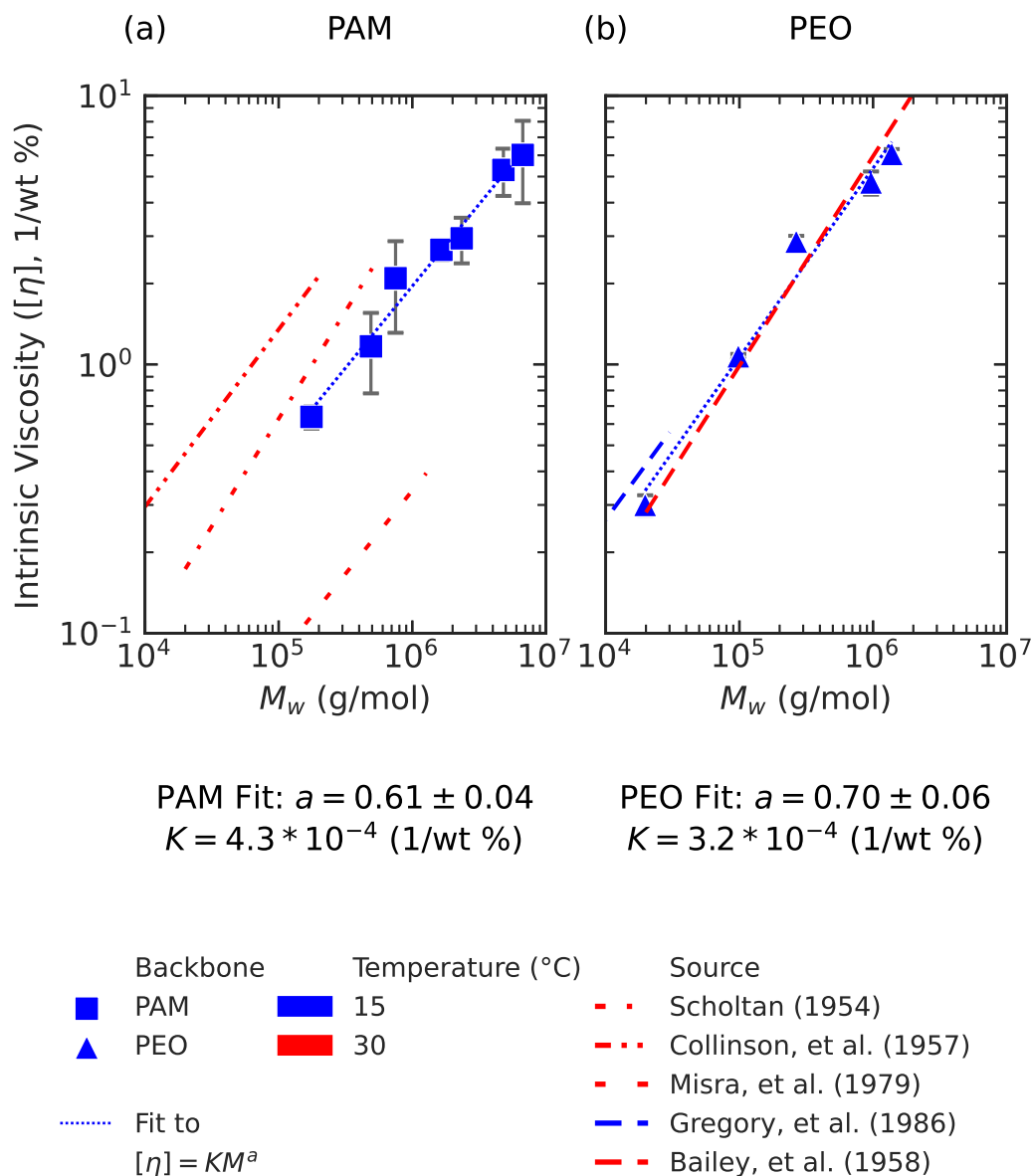
Figure 2.1: Intrinsic viscosity ($[\eta]$, 1/wt %) as a function of weight-average molecular weight (M_w, g/mol) for (a) polyacrylamide (PAM) and (b) poly(ethylene oxide) (PEO) at 15°C. Kuhn-Mark-Houwink-Sakurada (KMHS) fits to experimental results (blue dotted line) are (a) $K = 4.3 * 10^{-4}$ (1/wt %) and $a = 0.61 \pm 0.04$ for PAM, and (b) $K = 3.2 * 10^{-4}$ (1/wt %) and $a = 0.70 \pm 0.06$ for PEO. Error bars indicate 95% confidence interval. Where error bars are not visible, 95% confidence interval is within the symbol size. Comparison to literature KMHS values at 15 °C (where available) and 30 °C are presented over their stated valid molecular weight ranges (Table 2.3).[21–25]
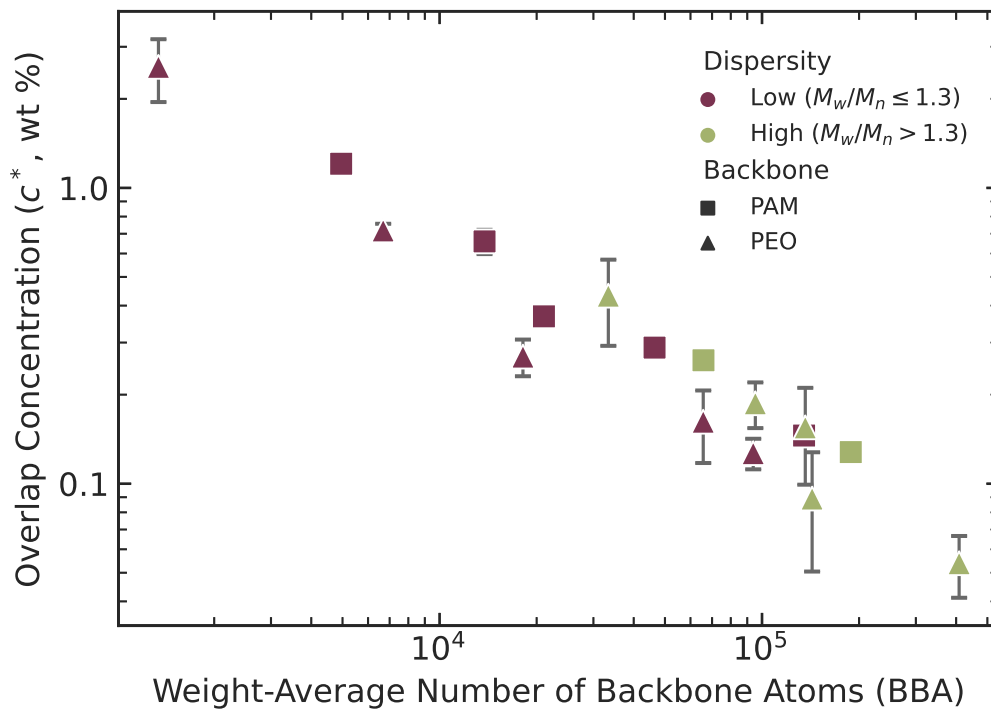
Figure 2.2: Overlap concentration (c^*, wt %) as a function of weight-average number of backbone atoms (BBA) for low dispersity PAM and low ($M_w/M_n \leq$ 1.3) and high ($M_w/M_n > 1.3$) dispersity PEO at 15 °C.

ber of backbone bonds was calculated by taking the weight-average molecular weight divided by the repeat unit molecular weight and multipled by the number of backbone bonds per repeat unit (Equation 2.2).

$$n_{w,backbone\ bonds} = M_w \frac{n_{backbone\ bonds\ per\ repeat\ unit}}{M_{repeat\ unit}} \tag{2.2}$$

Measurement of Degradation Using GPC

PAM and PEO samples with similar number of Kuhn steps were chosen for chain scission experiments—4M PAM, ($N_k \approx$ 9,000) and 1M PEO ($N_k \approx$ 9,000)—along with a high molecular weight PEO (6M PEO, Dow WSR301, $N_k \approx$ 55,000) also observed to undergo chain scission in turbulent flow (see Chapter 3). Samples of as-prepared solutions and aliquots taken after selected numbers of passes through a centrifugal pump were analyzed using gel permeation chro-

matography (GPC) with refractive index (RI) and multi-angle light scattering (MALLS) detectors. ASTRA software (Wyatt Technologies) was used to analyze the elution curves (Figure 2.3(a)) and evaluate the number- and weight-average molecular weights (M_n and M_w). The highly disperse 6M PEO presented a number of challenges: 1) the measured mass recovery of these samples was low ($\sim 50\%$), indicating loss of sample to the column, which precludes reliable molecular weight determination by GPC results, and 2) "spikes" in the 6M PEO chromatograms (red arrows in Figure 2.3(a)) indicated aggregates or particulates with higher signal than those reliably measurable in our instrument, despite injecting the filtered samples at very low concentrations.

Ratios of measured molecular weight ($M_{w,i}$) to starting molecular weight ($M_{w,0}$) were calculated at pass $i = 1$, 5, 10, and 20 for two different concentrations ($c/c^* = 0.19$ and 0.38) (Figure 2.3(b)). Thus, there are two symbols for each sample at each number of passes. Where only one symbol is visible, $M_{w,i}$ were indistinguishable for the two concentrations. By inspection of the GPC traces and analysis through ASTRA of the corresponding refractive index measurements, very little change occurs in the first pass for all samples but 6M PEO at $c/c^* = 0.38$. Accordingly, those five values of $M_{w,1}/M_{w,0} \approx 1$. Likewise, by inspection, there is no significant change in the GPC traces of 1M PEO for up to 20 passes for both concentrations (middle of Figure 2.3(a)); so $M_{w,i}/M_{w,0} \approx 1$ for all i for 1M PEO. The first sample to show significant reduction of M_w is 6M PEO: $M_{w,5}/M_{w,0} \approx 0.65$ for both concentrations tested, and the GPC traces show a decrease in the population of the longest chains (those that elute within 19 minutes). Note that 1M PEO does not contain such long chains in its distribution. After 10 passes, degradation becomes measurable in 4M PAM and continues for 6M PEO; both 4M PAM and 6M PEO show small further
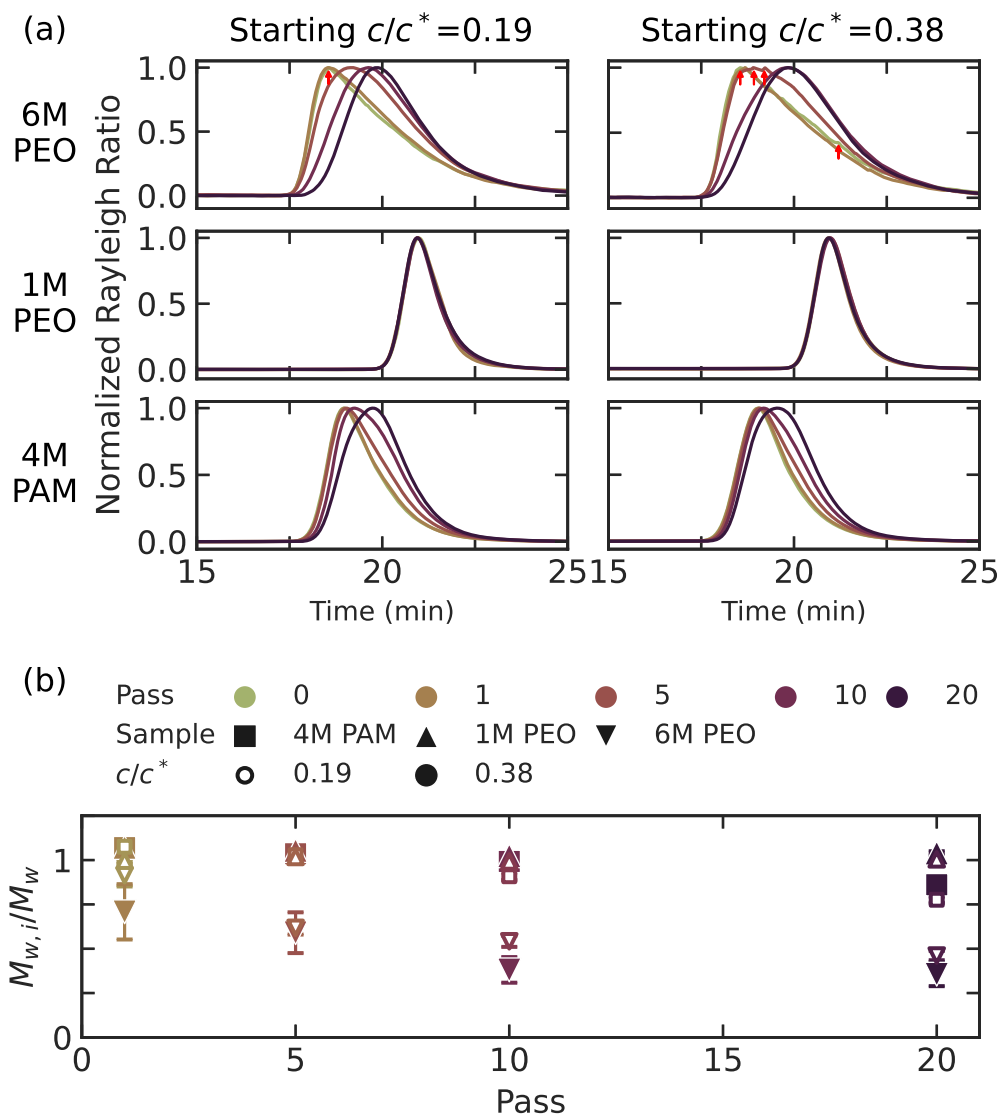
Figure 2.3: (a) Normalized Rayleigh Ratio as a function of aqueous gel permeation chromatography elution time (min) for samples with starting molecular weights and backbones of 4M PAM, 1M PEO, and 6M PEO, after 0, 1, 5, 10, and 20 passes through a pump at a concentration of c/c* of 0.19 (left) and 0.38 (right). (b) Ratio of measured weight-average molecular weight M_w ($M_{w,i}$) at pass $i = 1, 5, 10,$ and 20 to starting M_w ($M_{w,0}$) as a function of pass for samples shown in (a). Error bars represent the statistical standard deviation from propagation of uncertainty of weight-average molecular weight as determined in ASTRA GPC software. Where error bars are not visible, standard deviation is within symbol size. Reported ratios for 6M PEO samples should be treated as estimates (see text for details).

shift in M_w from 10 to 20 passes.

Measurement of Degradation using Extensional Rheology

Normalized diameter (D/D_0) was measured by image analysis of high-speed videos of dripping-onto-substrate extensional rheometry experiments and the critical time was evaluated from $D(t)/D_0$ as described in Appendix A (Figure 2.4). The inertio-capillary regime (times less than the critical time) appeared very similar across samples, and is consistent with water-only observations (Figure 2.5). The duration of the elastocapillary (EC) regime differed among samples, with the longest observable EC regime seen in the as-prepared 6M PEO solution at the higher concentr ation (c/c* = 0.38), and the shortest EC regime seen in the 1M PEO solutions at the lower concentration (c/c* = 0.19).
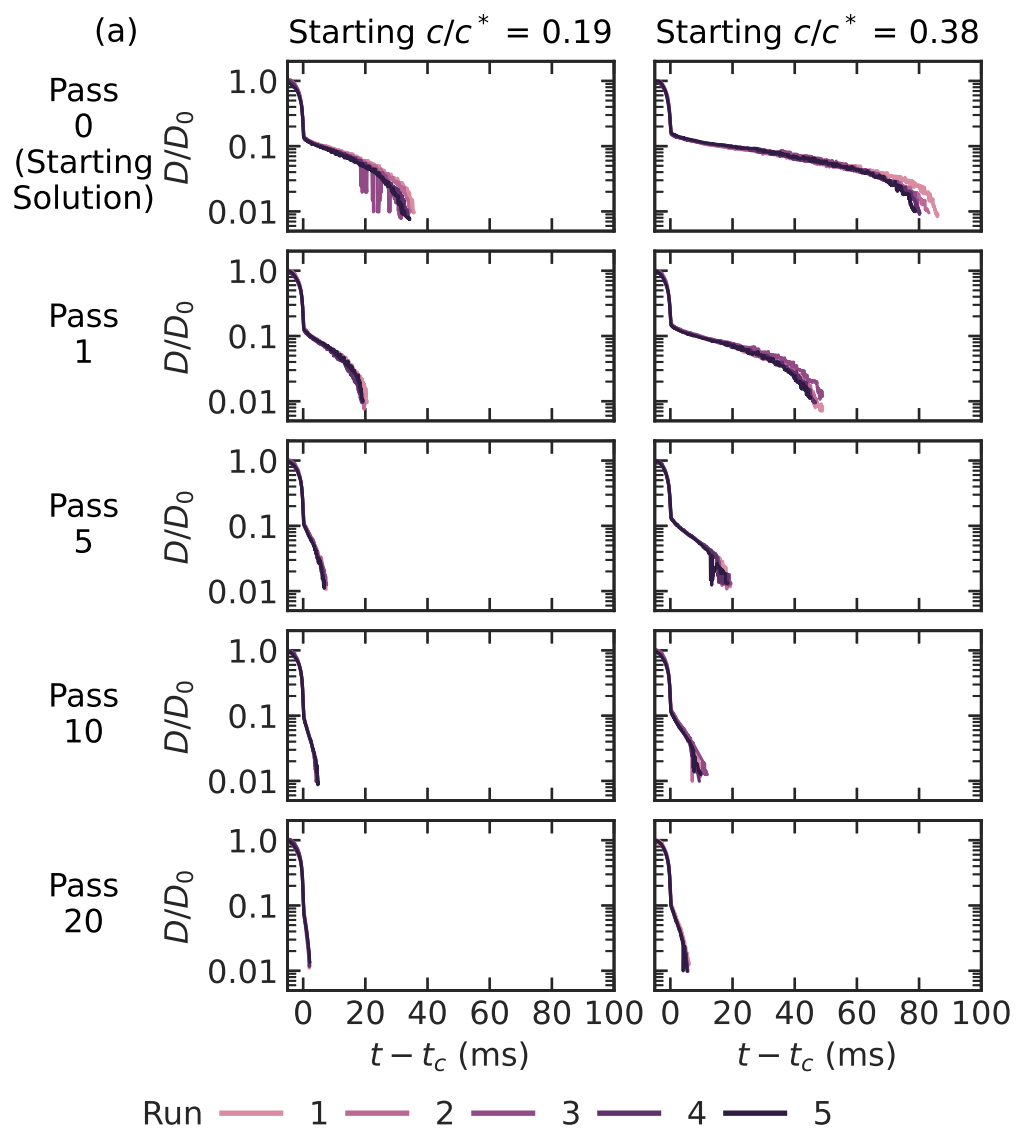
(a) 6M PEO, $c/c^* = 0.19$ and $c/c^* = 0.38$
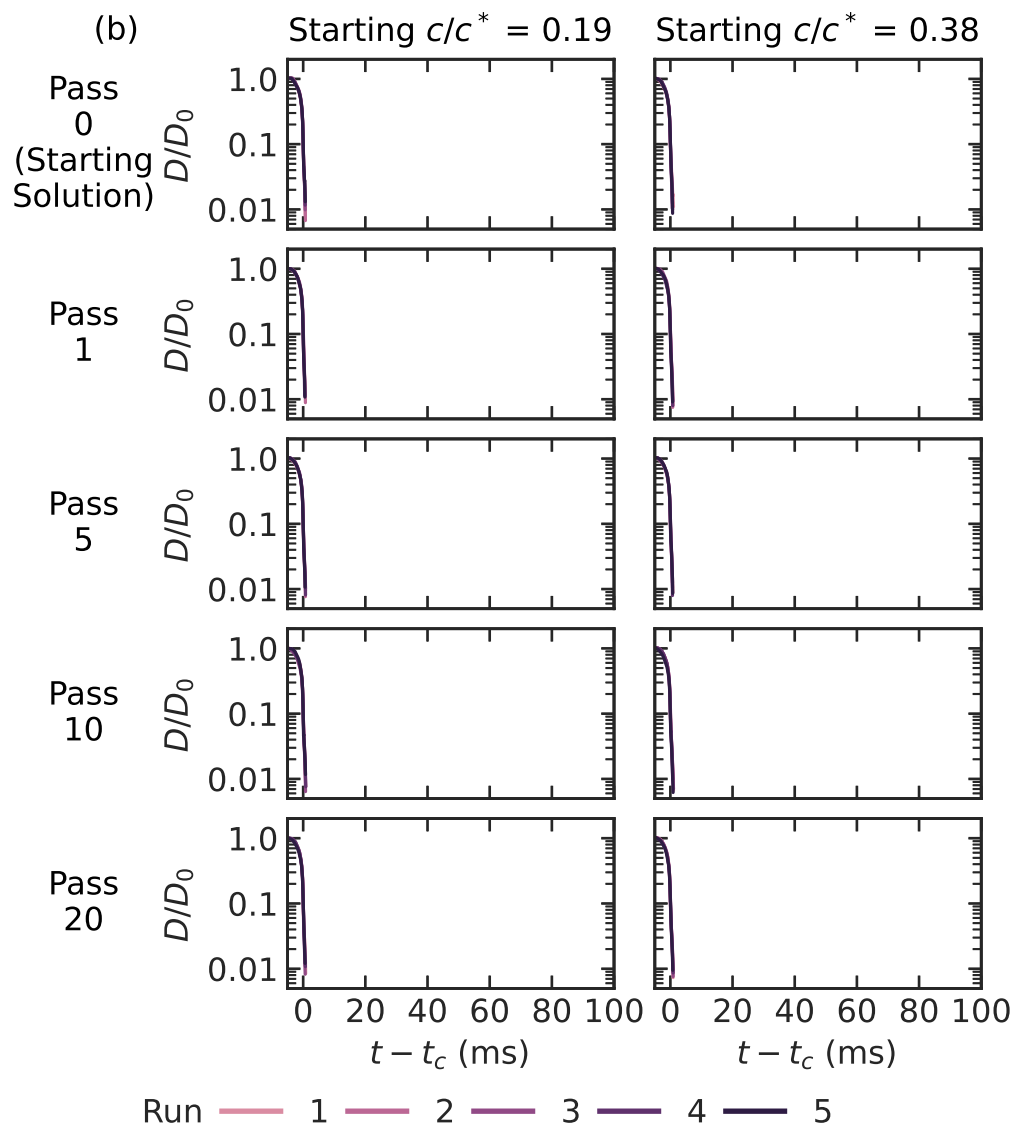
(b) 1M PEO, $c/c^* = 0.19$ and $c/c^* = 0.38$
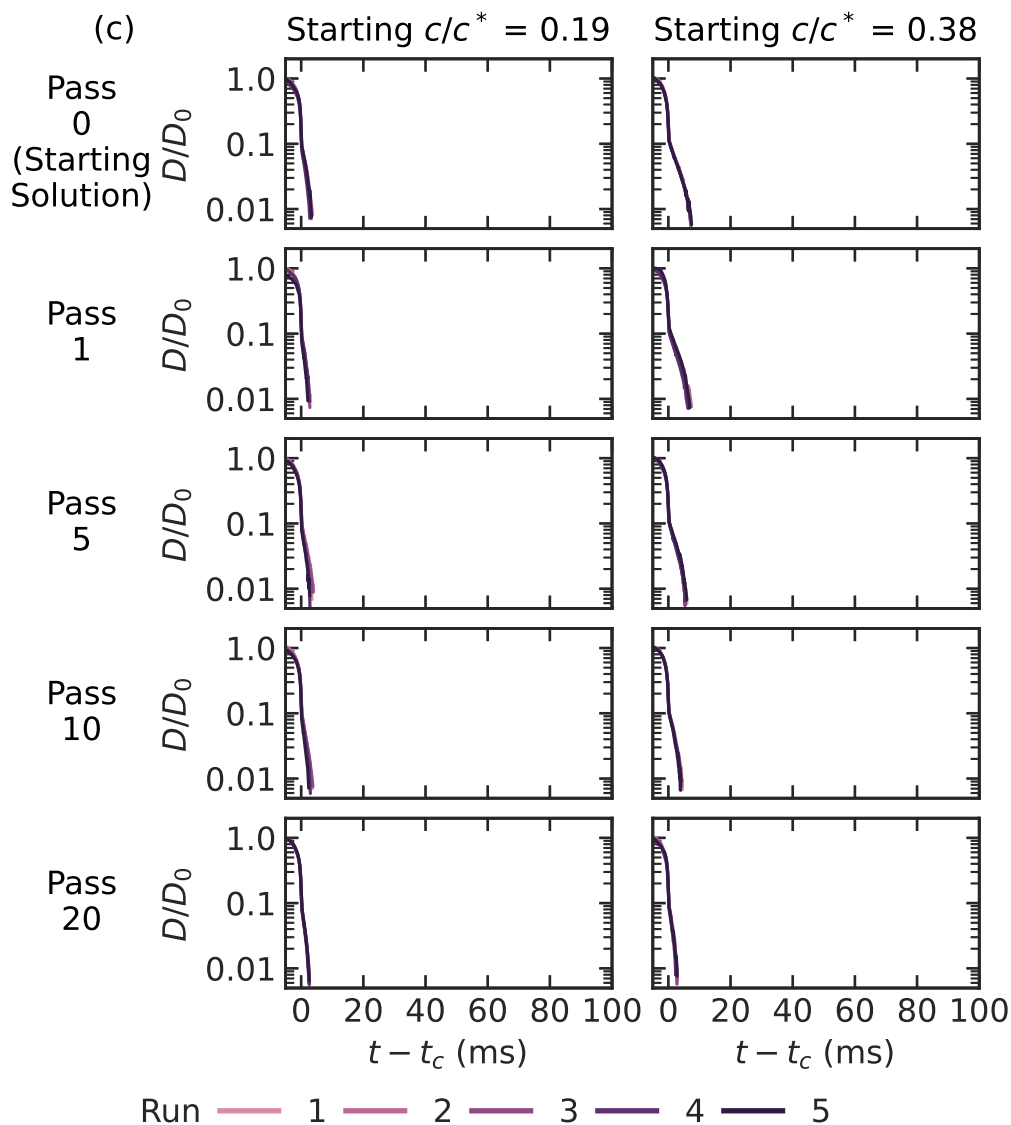
(c) 4M PAM, $c/c^* = 0.19$ and $c/c^* = 0.38$

Figure 2.4: Normalized diameter (D/D_0) of the liquid bridge measured during dripping-onto-substrate extensional rheometry as a function of the time past the critical time (t_c) of transition into the elastocapillary regime (ms), varying solution concentration relative to overlap concentration and number of passes through a pump. The samples' as-prepared molecular weight and backbone were (a) 6M PEO, (b) 1M PEO, and (c) 4M PAM. For each backbone-molecular weight combination, the solutions' reduced concentrations were c/c^* = 0.19 (left) and 0.38 (right).
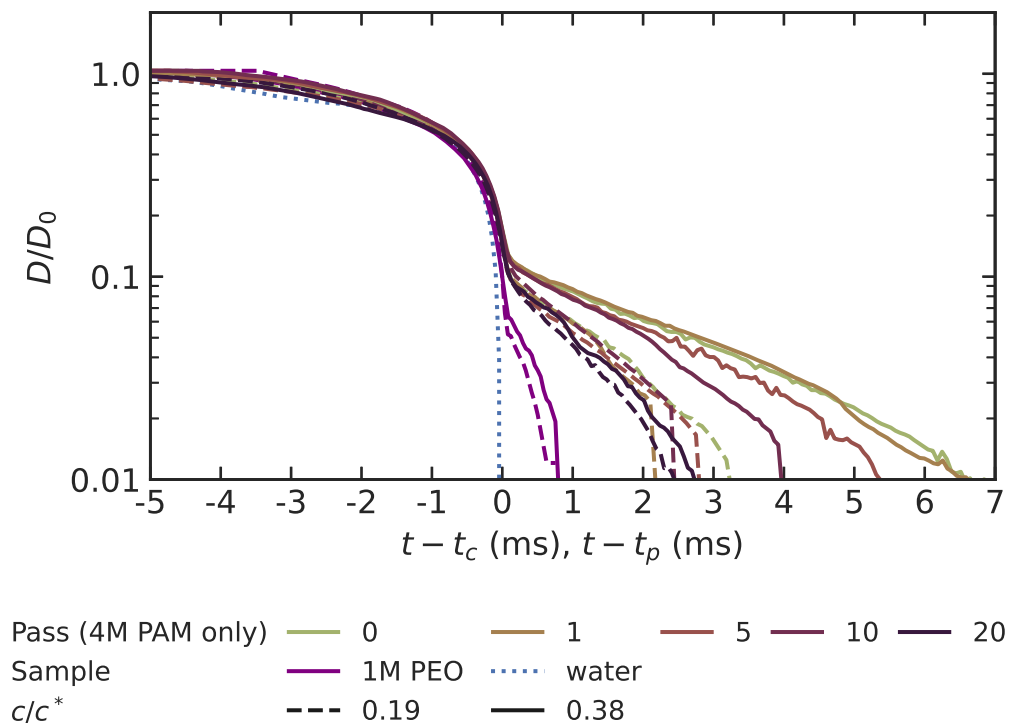
Figure 2.5: Normalized diameter (D/D_0) of the liquid bridge measured during dripping-onto-substrate extensional rheometry as a function of the time (ms) prior to the critical time (t_c) for polymeric samples, 4M PAM (averaged over runs and plotted for each pass) and 1M PEO (averaged over all runs and passes, purple), or pinchoff time (t_p) of the thread of deionized water (averaged over five runs, blue dotted). As-prepared concentrations for 4M PAM and 1M PEO samples were $c/c* = 0.19$ (dashed) and 0.38 (solid).

Focusing first on the 4M PAM solutions, both the slope of the normalized diameter as a function of time and the EC duration are observed to decrease with successive pass through the pump (Figure 2.5), corresponding to the degradation in molecular weight measured by GPC (Figure 2.3). In contrast, solutions of 1M PEO demonstrate little difference in slope and duration of EC regime with pass number (Figure 2.4(b)), corresponding to the unchanged GPC trace observed for 1M PEO (Figure 2.3).

Fits to the normalized diameter in the elastocapillary regime as described in Appendix A were used to determine the extensional relaxation time (λ_E) for

each specimen (Figure 2.6(a)). The relaxation time of the 6M PEO solutions was observed to rapidly drop with pass number for both concentrations. The relaxation time of the 4M PAM solutions was observed to decrease with pass number and converge to a similar value for both concentrations and the lower concentration 6M PEO solution.

Empirically, Robert Learsch observed a power-law dependence of λ_E on M_w (g/mol) and concentration (c, wt %): $\lambda_E \sim M_w^{K_M} c^{K_c}$. Using PAM solutions having M_w in the range 2.3-6.7 Mg/mol (characterized by GPC) and c in the range 0.01-1 wt %, the exponents were found to be $K_{M,PAM} = 3.5$ and $K_{c,PAM} = 0.82$. Using PEO solutions having M_w in the range 0.5-7.3 Mg/mol (characterized by GPC) and c in the range 0.006-2 wt %, the exponents were found to be $K_{M,PEO} = 2.5$ and $K_{c,PEO} = 0.89$. Discussion of the meaning of the molecular weight and concentration exponents is planned to be in the thesis of Robert Learsch.

By using the empirical power-law relationship for λ_E, I define an effective molecular weight for a given solution as the calculated molecular weight corresponding to the measured relaxation time and concentration. I evaluated the ratio of effective molecular weight at pass i to the starting effective molecular weight ($M_{eff,i}/M_{eff,0}$, dimensionless) for given concentration using Equation 2.3.

$$\frac{M_{eff,i}}{M_{eff,0}} = \left(\frac{\lambda_{E,i}}{\lambda_{E,0}}\right)^{1/K_M} \tag{2.3}$$

For solutions of 4M PAM and 6M PEO that were characterized by both GPC and DoSER, $M_{eff,i}/M_{eff,0}$ correlated with $M_{w,i}/M_{w,0}$ found via GPC, with a correlation of 0.96 (Figure 2.6(c)).

Additional measurements of D/D_0 were performed for solutions undergoing pumping with as-prepared molecular weights and backbones of 6.7M PAM
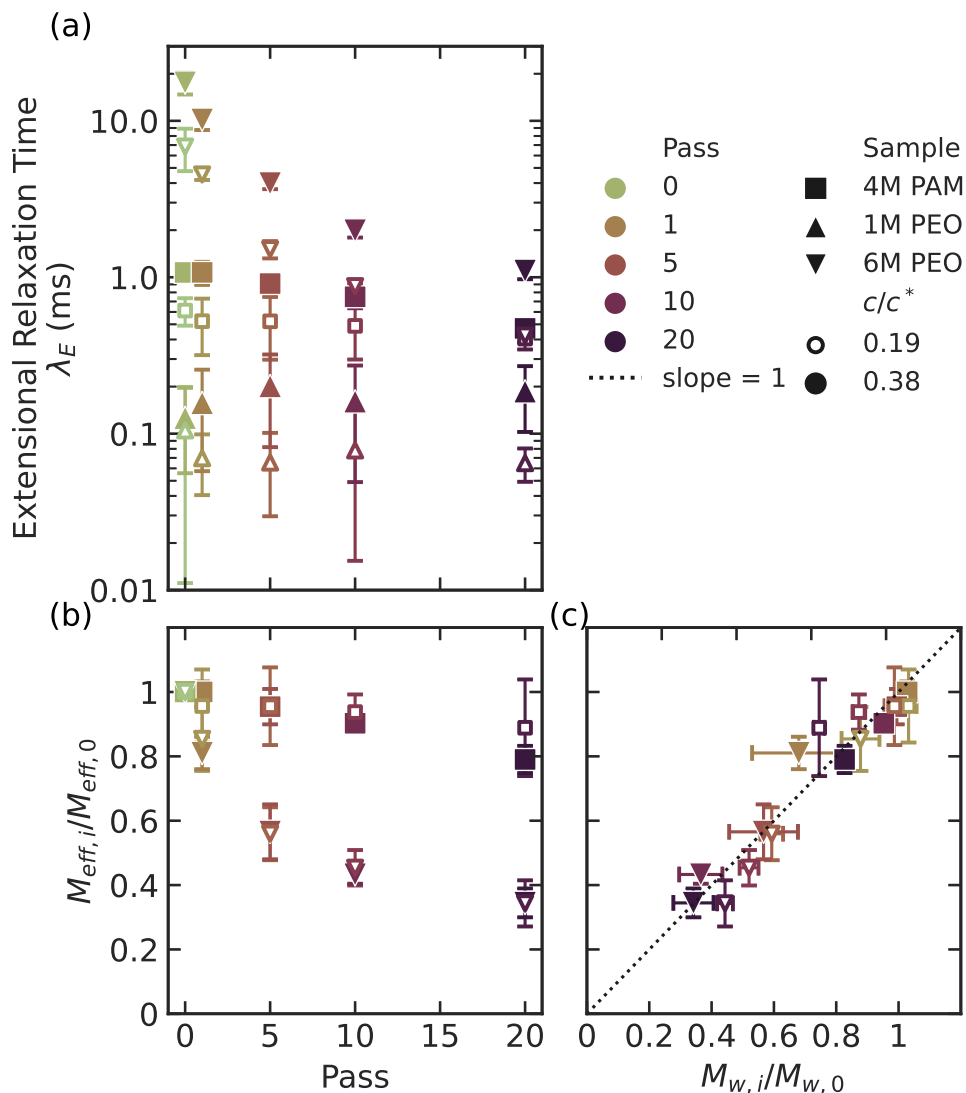
Figure 2.6: Changes with passes through a pump of sample solutions with as-prepared molecular weight and backbone of 4M PAM, 1M PEO, 6M PEO at as-prepared reduced concentrations of c/c* = 0.19 and 0.38. (a) Extensional relaxation time (λ_E, ms) as a function of passes. (b) Ratio of effective molecular weight of degraded samples to initial effective molecular weight as a function of pass ($M_{eff,i}/M_{eff,0}$), given observed extensional relaxation time from (a) using Equation 2.3, assuming a constant total concentration of the solution. (c) Effective molecular weight ratio ($M_{eff,i}/M_{eff,0}$) from (b) versus measured molecular weight ratio $M_{w,i}/M_{w,0}$ from GPC measurements (Figure 2.3). Dotted line with slope of 1 to guide the eye. In all plots, vertical error bars represent 95% confidence intervals, representing run-to-run variation in DoSER measurements (fitting errors are substantially smaller). Horizontal error bars in (c) represent the statistical standard deviation from propagation of uncertainty of weight-average molecular weight as determined in ASTRA GPC software. In each case, where error bars are not visible, the corresponding interval is within symbol size.

(a) Starting $c/c^* = 0.16$

Pass 0 (Starting Solution)

Pass 10

Pass 20

$t - t_c$ (ms)

Run —— 1 —— 2 —— 3 —— 4 —— 5
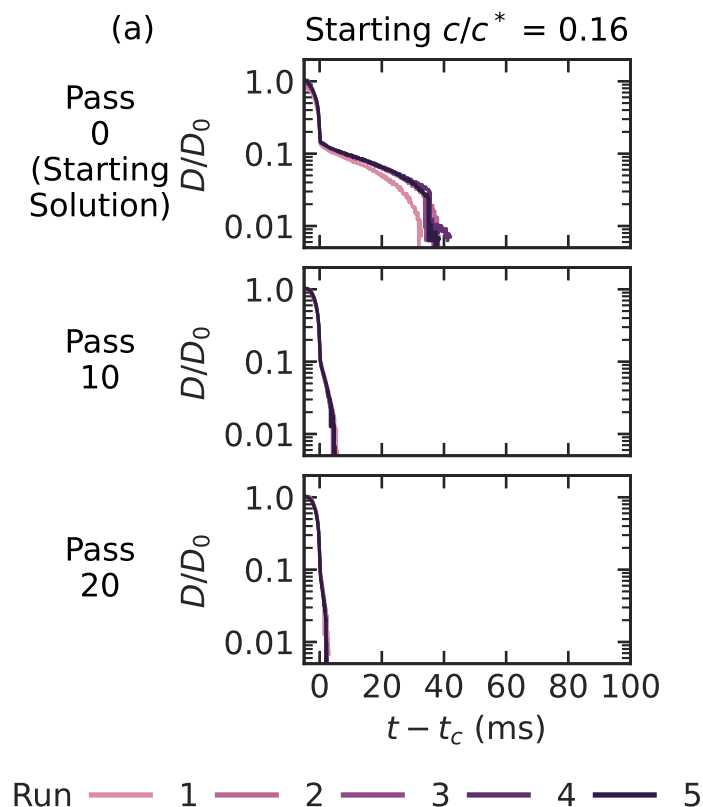
(a) 6M PEO, $c/c^* = 0.16$

(substantially longer than 4M PAM above) and 6M PEO (same PEO as above), with as-prepared reduced concentration of 0.16, lower than the 0.19 above (Figures 2.7 and 2.8). Aliquots were collected and measured for the as-prepared solutions and after pass $i = 10$ and 20. Corresponding GPC measurements were attempted but were not included due to substantial issues with chromatogram spikes that thwarted our ability to meaningfully interpret the results.

As noted above, the inertio-capillary regime corresponded to that of water for all specimens. The elastocapillary behavior observed for 6M PEO at c/c*=0.16 was very similar to the same polymer at c/c*=0.19 (compare Figures 2.4a and 2.7a; open downward triangles from Figure 2.6(a) are repeated in Figure 2.8). The population of longer chains in 6.7M PAM correlate with greater decrease in λ_E at 10 and 20 passes compared to observations for 4M PAM (Figure 2.6).
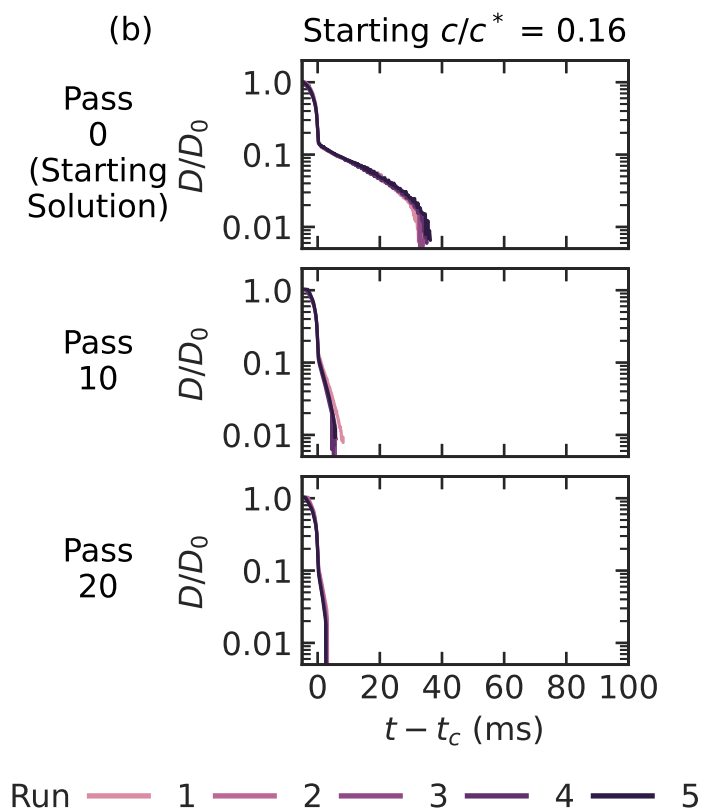
(b) 6.7M PAM, $c/c^* = 0.16$

Figure 2.7: Normalized diameter (D/D_0) of the liquid bridge measured during dripping-onto-substrate extensional rheometry as a function of the time past the critical time of transition into the elastocapillary regime (ms), varying solution concentration relative to overlap concentration and number of passes through a pump. The samples' as-prepared weight-average molecular weight and backbone were (a) 6.7M PAM and (b) 6M PEO. For each backbone-molecular weight combination, the as-prepared solution reduced concentration was c/c^* of 0.16.

The duration of the elastocapillary regime and the extensional relaxation times were similar for PAM and PEO of similar molecular weights, despite PEO's greater fully extended length ($\sim$190,000 BBA for 6.7M PAM and $\sim$410,000 BBA for 6M PEO) (Figure 2.4a). The two polymers degraded in extensional relaxation time similarly as a function of pass (Figure 2.8(a)). As a result, because of the smaller exponent relating relaxation time to effective molecular weight for PAM relative to PEO (compare the resulting exponent of (1/3.5) for PAM to (1/2.6) for PEO in Equation 2.3), the effective molecular weight stayed at a higher value for the 6.7M PAM compared to 6M PEO and reached a similar value to the 4M PAM after 20 passes (3.3M for 6.7M PAM, 3.1M for 4M PAM, 2M for 6M PEO) (Figure 2.8(b)).

2.4   Discussion

Role of Solvent Quality in Chain Scission

The solvent quality at 15 °C for deionized water of PAM appears to be slightly lower than that of PEO based on the measured intrinsic viscosities and the Kuhn-Mark-Houwink-Sakurada fits obtained, indicating that we should expect the PAM chains to be slightly less swollen; water is not as good a solvent for PAM as it is for PEO. As the literature results for PAM vary in their reported values for a, and little to no data are available for either backbone at our temperature and molecular weight range of interest, it is difficult to evaluate the validity of the fit values of a with direct literature comparisons; although our values are within the ranges found in the literature (Table 2.3). Using the relationships discussed in Chapter 1 for the relationship between the Flory exponent ν and a, $\nu = 0.54$ for PAM in water and 0.57 for PEO in water ($\nu = 0.5$ is a theta solvent and $\nu = 0.6$ is a good solvent).

Overlap concentrations of PAM and low and high dispersity PEO as a func-
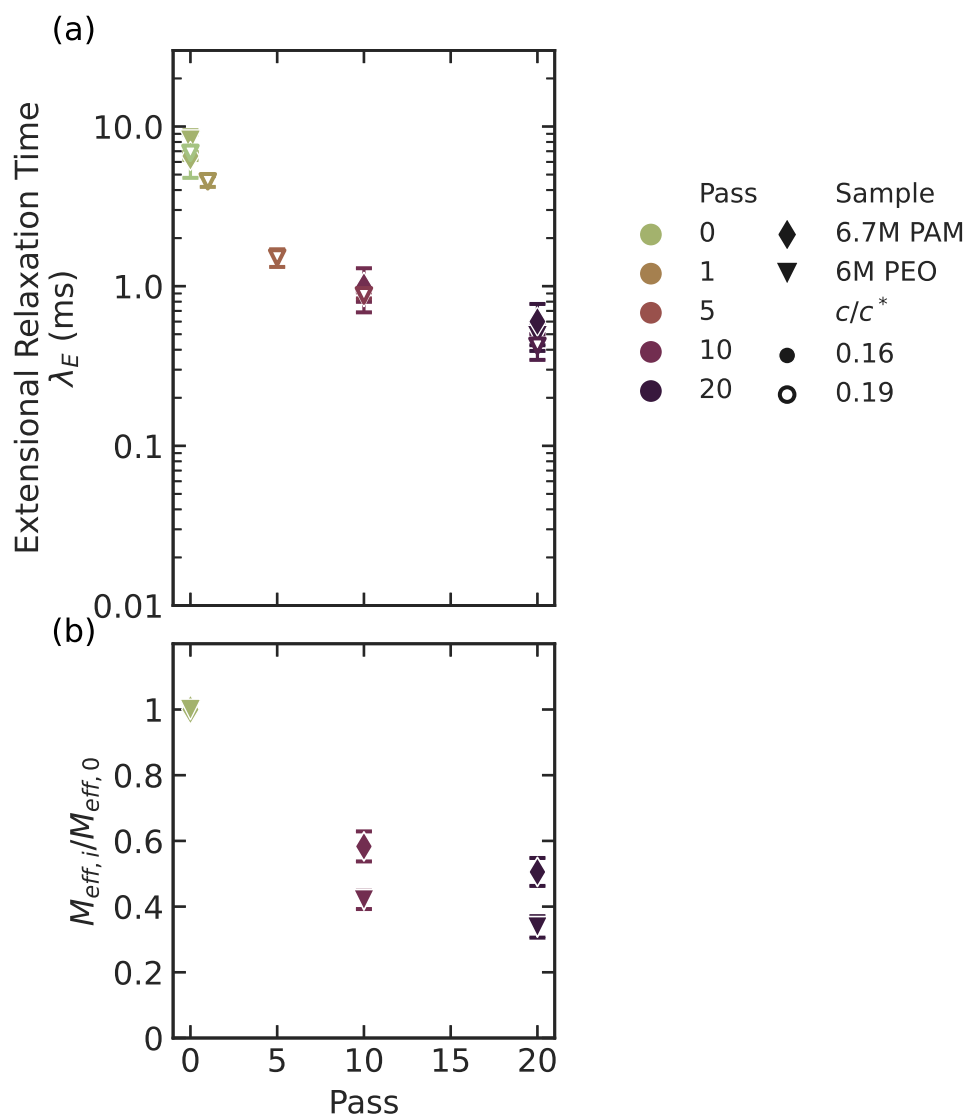
Figure 2.8: Changes with passes through a pump of sample solutions with as-prepared molecular weight and backbone of 6.7M PAM and 6M PEO at an as-prepared reduced concentration of c/c* = 0.16. (a) Extensional relaxation time (λ_E, ms) as a function of passes (open downward triangles are for 6M PEO at $c/c^* = 0.19$, repeated from Figure 2.6(a)). (b) Ratio of effective molecular weight of degraded samples to initial effective molecular weight ($M_{eff,i}/M_{eff,0}$) as a function of pass, given observed extensional relaxation time from (a) using Equation 2.3, assuming a constant concentration of the solution. Vertical error bars represent 95% confidence intervals representing run-to-run variation in DoSER measurements (fitting errors are substantially smaller). Where error bars are not visible, the interval is within symbol size.

tion of weight-average backbone atoms appear to fall along similar curves (Figure 2.2). Normalizing overlap behavior using the weight-average rather than number-average is supported by literature as a method of reducing dependence on dispersity.[26] Using backbone atoms allows comparison of the two backbones on the basis of length, removing the differences in molecular weight due to PAM's side groups. Matching PAM and PEO samples on the basis of Kuhn steps also led to similar overlap concentrations—the 4M PAM and 1M PEO used in the chain scission experiments both had overlap concentrations of 0.16 wt %.

The extensional results presented here for undegraded solutions of long PAM and PEO below their respective overlap concentrations agree with literature discussions of different dilution regimes for shear versus extension[45,46]—even below c^*, the extensional relaxation time demonstrates concentration dependence, indicating interchain interaction in extension even in the dilute regime for shear. I observed similar extensional relaxation times for the PAM and PEO at close molecular weights (6.7M and 6M respectively), despite PAM's fewer backbone atoms per molecular weight and the measured lower solvent quality. When comparing similar equilibrium dimensions, the 4M PAM and 1M PEO have matched Kuhn steps and overlap concentrations, yet the 4M PAM solutions demonstrated relaxation times of 6-8 times that of the 1M PEO at the same concentrations (and reduced concentrations). The combination of these results point towards a picture that the extensional behavior observed in capillary-breakup rheometry is not primarily a function of the equilibrium or shear dimensions of the polymer, but rather the dimensions of the extended chain, both in length and diameter. Dinic and Sharma proposed that differences in chain packing, flexibility, and extensibility all contribute to the observed differences in capillary-breakup behavior of hydroxyethyl cellulose

(a semi-flexible polysaccharide) compared to PEO.[45] In this work, PAM and PEO are much more similar in each of those proposed parameters due to their similar nature as flexible, synthetic polymers, despite some difference in solvent quality; yet the changes in behavior are still apparent and further support that the drag force on the extended backbone is important to understanding extensional behavior.[45] The role of solvent quality in extension is discussed further in Chapter 4 for polycyclooctadiene in hydrocarbon solvents.

In chain scission experiments, poorer solvent quality has been shown to result in more degradation.[38,50–52] Here, the effects of water as poorer solvent for PAM are coupled with differences in drag due to side groups. The combination of these factors is discussed in "Chain Scission Thresholds" below.

Characterizing Chain Scission

Gel permeation chromatography (GPC) has been the primary method of characterizing chain scission in prior studies because of its ability to capture the distribution of molecular weights generated in chain scission events. Researchers have sought equivalents for GPC measurements—for example, Nguyen, et al. proposed using birefringence to characterize molecular weight distributions of extending polymers during flow, but faced obstacles due to peak spreading and noise.[53] Additional methods of probing the molecular weight post-scission are advantageous for scenarios where GPC alone may not be an accurate method of characterizing the sample, such as in associative polymers or with backbones with solubility and aggregation issues.

High molecular weight PEO posed challenges for GPC characterization in this study. I observed low mass recovery ($\sim$ 50 % or less) and increased column pressure pointed towards loss of material to the column, which I expect resulted in unreliable molecular weight distributions. Material staying in the

column can damage the instrument due to increased need for higher pressures and can contaminate future measurements, making running high molecular weight PEO through the instrument undesirable. Additionally, even at very low concentrations and with use of a 0.45 μm syringe filter, the light scattering chromatogram had high signal "spikes" that were reduced, but not eliminated, with lowering injected concentration, which indicated highly scattering inclusions. Lowering the concentration, however, diminished the differential refractive index signal available for analysis, contributing to uncertainty in molecular weight estimates.

Combining the more reliable measurements from GPC of 4M PAM with the estimates of the 6M PEO results, I compared the GPC measured molecular weights to effective molecular weights estimated from the extensional relaxation time results (Figure 2.6(c)). The ratios of effective molecular weight and measured weight-average molecular weight to their respective starting values were highly correlated (correlation 0.96; a correlation of 1 would indicate a perfectly 1:1 linear relationship), indicating that we can use our relaxation time estimates of effective molecular weight as a reliable estimator of the molecular weight degradation that has occurred in the solution.

Utilizing extensional rheology as our primary tool for assessing chain scission misses out on the detailed molecular weight distribution, but particularly where GPC is not a reliable measuring device, it is a relatively easy and consistent way of revealing how much a solution has degraded. Extensional behavior is also of particular interest for our applications—as discussed in detail in Chapter 1, the extensional properties of the solution control drag reduction, drop impact, and drop size—and so measuring that behavior directly characterizes the most directly relevant effects of chain scission.

Chain Scission Thresholds

The 6M PEO, in comparison with both the 4M and the 6.7M PAM samples, underwent substantially more degradation during pumping as observed through the change in effective molecular weight (see Figures 2.6 and 2.8). The 1M PEO samples ($\sim$68,000 BBA), which had approximately the sample number of Kuhn steps and overlap concentration as the 4M PAM ($\sim$120,000 BBA), did not undergo statistically significant degradation as measured by either GPC or extensional relaxation time. These features indicated that what determined extensional potency and the potential for chain scission was not the pervaded volume at equilibrium (indicated by c/c*).

After 20 passes, the 6M PEO solutions prepared at c/c^* at 0.16 and 0.19 and all the observed PAM solutions degraded to extensional relaxation times in the range of 0.4 – 0.6 ms (average 0.48 ms $\pm$ 0.21 ms). Although long PEO started off as a more potent extensional rheological modifier, the rapid degradation of the PEO led to similar values of PAM and PEO extensional relaxation time after scission events. Convergence to similar relaxation times indicated that one backbone was not inherently more resilient under the conditions inside the pump in the frame of post-scission extensional behavior.

The convergence of relaxation times may also indicate the extensional rate experienced during pumping—if the rate of extension inside the pump exceeds the ability of the polymer chains to relax the tension, scission may occur.[34] If the extensional rate causing scission goes like $\dot{\epsilon} \sim 1/\lambda_{E,i\to\infty}$, then we expect the maximum extensional rate in this pump is order 1500-2500 1/s.

Assuming that both backbones experience similar extensional rates in the pump, the effective extended length after scission can be looked at as a measure of the relative drag force on each backbone, based on the turbulent drag

force arguments of Vanapalli et al.[29] After 20 passes, both the 6.7M and 4M PAM reached effective molecular weights of approximately 3M as determined from extensional relaxation time; 6M PEO degraded to approximately 2M. These effective molecular weights are equivalent to 85,000 BBA for PAM and 140,000 BBA for PEO. The result is that while the PAM's molecular weight is larger post-scission, its fully extended length is shorter than the degraded PEO. Because PEO's reported force for scission is lower than PAM,[29] a shorter length for PAM post-pumping implies that the forces on the PAM chain exceed those on the PEO chains at similar extensional rates. The lower solvent quality for PAM and the increased diameter from the side groups may both be contributing to the increased force on the backbone from the surrounding fluid during pumping. The effects of backbone identity on drag reduction and chain scission in turbulent flow is discussed further in Chapter 3.

Degradation experiments by Hojin Kim and extensional measurements by Robert Learsch using a terpyridene-ended telechelic PAM (TPAM) with nickel ions as a water-soluble megasupramolecule demonstrated corresponding behavior. A 0.1 wt% solution of 800 kg/mol TPAM without nickel had an extensional relaxation time of 0.2 ms, below the threshold extensional relaxation time determined in these experiments, while adding one nickel for every two terpyridene end-groups led to a relaxation time of 4.5 ms, above the threshold where degradation was experienced by the homopolymer PAM and PEO. After 20 passes through the same pump, the TPAM-nickel solution did not change in molecular weight as measured by GPC.[54]

2.5 Conclusion

Looking at post-scission polymer lengths measured through both extension and GPC, PAM is not inherently more resistant to mechanical scission than

PEO, even if its backbone itself can withstand a higher force.[29] Indeed, PAM degraded to smaller number of backbone atoms (i.e., shorter fully extended lengths) compared to the PEO samples after 20 passes. After scission, however, PAM and PEO's similar extensional relaxation times mean that they have similar potency in the applications of interest—mist control, drag reduction, and droplet impact. Due to the additional issues with PEO—relative vulnerability to chemical degradation due to light and heat, aggregation issues during dissolution and in GPC measurements—PAM becomes a more attractive backbone option because it can comparably perform in extension after scission, despite a smaller effective length post-degradation.

By looking at the extensional properties of polymers pre- and post-scission instead of molecular weight alone, our understanding of additives moves to be more backbone-agnostic. Rather than constraining choices of polymer and concentration to homopolymer solutions previously studied by the literature, or requiring that the exact extension rates inside the equipment are known, these results suggest a design process and engineering criteria for an associative polymer additive. First, one could run a generic polymer solution through the rigors expected of the final solution (a worst-case scenario pump, for example) to characterize the maximum extensional relaxation time that survives. After knowing the maximum that survives, the target extensional relaxation time for a disassociated unimer at the desired concentration should be a safety margin below that maximum, such that the unimer backbone itself will not break in the flow. Thus, if designed to meet this target, the resulting associative additive should survive until their opportunity to act on their intended flows— as rheological modifiers in pipeline flows, mists, and droplets.

References

[1]   W. Wirth, S. Storpb, and W. Jacobsenb. "Mechanisms Controlling Leaf Retention of Agricultural Spray Solutions". In: *Pesticide Science* 33.4 (1991), pp. 411–420.

[2]   V. Bergeron et al. "Controlling Droplet Deposition with Polymer Additives". In: *Nature* 405.6788 (June 2000), pp. 772–775. ISSN: 0028-0836, 1476-4687. DOI: 10.1038/35015525. URL: http://www.nature.com/articles/35015525 (visited on 08/05/2020).

[3]   T. Holmes, E. Nielsen, and L. Lee. "Managing Groundwater Contamination In Rural Areas". In: (), p. 9.

[4]   R. Peshin and A. K. Dhawan, eds. *Integrated Pest Management: Dissemination and Impact*. Dordrecht: Springer, 2009. 1 p. ISBN: 978-1-4020-8991-6.

[5]   *USGS FS-122-96: Pesticides in Public Supply Wells of Washington State*. URL: https://wa.water.usgs.gov/pubs/fs/fs122-96/ (visited on 03/24/2022).

[6]   A. S. Felsot et al. "Agrochemical Spray Drift; Assessment and Mitigation—A Review*". In: *Journal of Environmental Science and Health, Part B* 46.1 (Dec. 30, 2010), pp. 1–23. ISSN: 0360-1234, 1532-4109. DOI: 10.1080/03601234.2010.515161. URL: http://www.tandfonline.com/doi/abs/10.1080/03601234.2010.515161 (visited on 03/24/2022).

[7]   R. W. Lewis et al. "Polymeric Drift Control Adjuvants for Agricultural Spraying". In: *Macromolecular Chemistry and Physics* 217.20 (Oct. 2016), pp. 2223–2242. ISSN: 10221352. DOI: 10.1002/macp.201600139. URL: https://onlinelibrary.wiley.com/doi/10.1002/macp.201600139 (visited on 03/23/2022).

[8]   E. Hilz. "Spray Drift Review: The Extent to Which a Formulation Can Contribute to Spray Drift Reduction". In: *Crop Protection* (2013), p. 9.

[9]   M. Xu et al. "Quantifying the Effect of Extensional Rheology on the Retention of Agricultural Sprays". In: *Physics of Fluids* 33.3 (Mar. 1, 2021), p. 032107. ISSN: 1070-6631, 1089-7666. DOI: 10.1063/5.0038391. URL: https://aip.scitation.org/doi/10.1063/5.0038391 (visited on 03/15/2021).

[10] Y. Yeong, J. Burton, and E. Loth. "Drop Impact and Rebound Dynamics on an Inclined Superhydrophobic Surface". In: *Langmuir* 30 (2014), pp. 12027–12038. DOI: 10.1021/la502500z.

[11] V. Tirtaatmadja, G. H. McKinley, and J. J. Cooper-White. "Drop Formation and Breakup of Low Viscosity Elastic Fluids: Effects of Molecular Weight and Concentration". In: *Physics of Fluids* 18.4 (Apr. 2006),

p. 043101. ISSN: 1070-6631, 1089-7666. DOI: 10.1063/1.2190469. URL: http://aip.scitation.org/doi/10.1063/1.2190469 (visited on 08/14/2017).

[12]   Y. Song et al. "The Use of Folate/Zinc Supramolecular Hydrogels to Increase Droplet Deposition on *Chenopodium Album* L. Leaves". In: *ACS Sustainable Chemistry & Engineering* 8.34 (Aug. 31, 2020), pp. 12911–12919. ISSN: 2168-0485, 2168-0485. DOI: 10.1021/acssuschemeng.0c03396. URL: https://pubs.acs.org/doi/10.1021/acssuschemeng.0c03396 (visited on 09/17/2020).

[13]   M. Song et al. "Controlling Liquid Splash on Superhydrophobic Surfaces by a Vesicle Surfactant". In: *Science Advances* 3.3 (Mar. 2017), e1602188. ISSN: 2375-2548. DOI: 10.1126/sciadv.1602188. URL: https://advances.sciencemag.org/lookup/doi/10.1126/sciadv.1602188 (visited on 09/17/2020).

[14]   M. I. Smith and V. Bertola. "Effect of Polymer Additives on the Wetting of Impacting Droplets". In: *Physical Review Letters* 104.15 (Apr. 15, 2010). ISSN: 0031-9007, 1079-7114. DOI: 10.1103/PhysRevLett.104.154502. URL: https://link.aps.org/doi/10.1103/PhysRevLett.104.154502 (visited on 08/05/2020).

[15]   R. P. Mun, J. A. Byars, and D. V. Boger. "The Effects of Polymer Concentration and Molecular Weight on the Breakup of Laminar Capillary Jets". In: (1998), p. 13.

[16]   B. Keshavarz et al. "Studying the Effects of Elongational Properties on Atomization of Weakly Viscoelastic Solutions Using Rayleigh Ohnesorge Jetting Extensional Rheometry (ROJER)". In: *Journal of Non-Newtonian Fluid Mechanics* 222 (Aug. 2015), pp. 171–189. ISSN: 03770257. DOI: 10.1016/j.jnnfm.2014.11.004. URL: http://linkinghub.elsevier.com/retrieve/pii/S0377025714002055 (visited on 01/06/2017).

[17]   P. S. Virk. "Drag Reduction Fundamentals". In: *AIChE Journal* 21.4 (July 1975), pp. 625–656.

[18]   S. A. Vanapalli, M. T. Islam, and M. J. Solomon. "Scission-Induced Bounds on Maximum Polymer Drag Reduction in Turbulent Flow". In: *Physics of Fluids* 17.9 (2005), p. 095108. ISSN: 10706631. DOI: 10.1063/1.2042489. URL: http://scitation.aip.org/content/aip/journal/pof2/17/9/10.1063/1.2042489 (visited on 05/05/2016).

[19]   A. Somervaille, G. Betts, and C. F. I. Grains Research and Development Corporation (Australia). *Adjuvants: Oils, Surfactants and Other Additives for Farm Chemicals*. Kingston, ACT: Grains Research & Development Corporation, 2011. ISBN: 978-1-921779-32-9.

[20] H. Zhu et al. "Effects of Polymer Composition and Viscosity on Droplet Size of Recirculated Spray Solutions". In: *Journal of Agricultural Engineering Research* 67.1 (May 1997), pp. 35–45. ISSN: 00218634. DOI: `10.1006/jaer.1997.0151`. URL: `https://linkinghub.elsevier.com/retrieve/pii/S0021863497901517` (visited on 03/23/2022).

[21] v. W. Scholtan. "Molekulargewichtsbestimmung von Polyacrylamid mittels der Ultrazentrifuge". In: *Die Makromolekulare Chemie* 14.1 (1954), pp. 169–178. ISSN: 0025116X, 0025116X. DOI: `10.1002/macp.1954.020140113`. URL: `http://doi.wiley.com/10.1002/macp.1954.020140113` (visited on 02/04/2021).

[22] E. Collinson, F. S. Dainton, and G. S. McNaughton. "The Polymerization of Acrylamide in Aqueous Solution. Part 2.—The Effect of Ferric Perchlorate on the X- and \gamma-Ray Initiated Reaction". In: *Transactions of the Faraday Society* 53.0 (1957), pp. 489–498. ISSN: 0014-7672. DOI: `10.1039/TF9575300489`. URL: `http://dx.doi.org/10.1039/TF9575300489`.

[23] G. Misra and S. Bhattacharya. "Determination of the Molecular Weight of Polyacrylamide Fractions by Osmometry". In: *European Polymer Journal* 15.2 (Jan. 1979), pp. 125–128. ISSN: 00143057. DOI: `10.1016/0014-3057(79)90196-4`. URL: `https://linkinghub.elsevier.com/retrieve/pii/0014305779901964` (visited on 02/04/2021).

[24] P. Gregory and M. B. Huglin. "Viscosity of Aqueous and Alkaline Solutions of Poly(Ethy1ene Oxide)". In: *Die Makromolekulare Chemie* 187.7 (July 1986), pp. 1745–1755. ISSN: 0025116X, 0025116X. DOI: `10.1002/macp.1986.021870718`. URL: `http://doi.wiley.com/10.1002/macp.1986.021870718` (visited on 02/03/2021).

[25] F. E. Bailey, J. L. Kucera, and L. G. Imhof. "Molecular Weight Relations of Poly(Ethylene Oxide)". In: *Journal of Polymer Science* 32.125 (Nov. 1958), pp. 517–518. ISSN: 00223832, 15426238. DOI: `10.1002/pol.1958.1203212522`. URL: `http://doi.wiley.com/10.1002/pol.1958.1203212522` (visited on 02/04/2021).

[26] M. Bohdanecký, V. Petrus, and B. Sedláček. "Estimation of the Characteristic Ratio of Polyacrylamide in Water and in a Mixed Theta-solvent". In: *Die Makromolekulare Chemie* 184.10 (Oct. 1983), pp. 2061–2073. ISSN: 0025116X, 0025116X. DOI: `10.1002/macp.1983.021841011`. URL: `http://doi.wiley.com/10.1002/macp.1983.021841011` (visited on 02/04/2021).

[27] Chemical Retrieval on the Web. *Characteristic Ratio*. Polymer Database. Mar. 31, 2022. URL: `http://polymerdatabase.com/polymer%20physics/C%20Table%20.html` (visited on 03/31/2022).

[28] M. Rubinstein and R. H. Colby. *Polymer Physics*. Oxford ; New York: Oxford University Press, 2003. 440 pp. ISBN: 978-0-19-852059-7.

[29] S. A. Vanapalli, S. L. Ceccio, and M. J. Solomon. "Universal Scaling for Polymer Chain Scission in Turbulence". In: *Proceedings of the National Academy of Sciences* 103.45 (Nov. 7, 2006), pp. 16660–16665. ISSN: 0027-8424, 1091-6490. DOI: `10.1073/pnas.0607933103`. URL: `http://www.pnas.org/cgi/doi/10.1073/pnas.0607933103` (visited on 09/11/2016).

[30] R. Crooks and D. V. Boger. "Influence of Fluid Elasticity on Drops Impacting on Dry Surfaces". In: *Journal of Rheology* 44.4 (July 2000), pp. 973–996. ISSN: 0148-6055, 1520-8516. DOI: `10.1122/1.551123`. URL: `http://sor.scitation.org/doi/10.1122/1.551123` (visited on 08/05/2020).

[31] V. Bertola. "An Experimental Study of Bouncing Leidenfrost Drops: Comparison between Newtonian and Viscoelastic Liquids". In: *International Journal of Heat and Mass Transfer* 52.7-8 (Mar. 2009), pp. 1786–1793. ISSN: 00179310. DOI: `10.1016/j.ijheatmasstransfer.2008.09.028`. URL: `https://linkinghub.elsevier.com/retrieve/pii/S0017931008005875` (visited on 08/06/2020).

[32] V. Bertola. "Effect of Polymer Concentration on the Dynamics of Dilute Polymer Solution Drops Impacting on Heated Surfaces in the Leidenfrost Regime". In: *Experimental Thermal and Fluid Science* 52 (Jan. 2014), pp. 259–269. ISSN: 08941777. DOI: `10.1016/j.expthermflusci.2013.09.019`. URL: `https://linkinghub.elsevier.com/retrieve/pii/S0894177713002306` (visited on 09/02/2020).

[33] A. Keller and J. A. Odell. "The Extensibility of Macromolecules in Solution; A New Focus for Macromolecular Science". In: *Colloid & Polymer Science* 263.3 (Mar. 1985), pp. 181–201. ISSN: 0303-402X, 1435-1536. DOI: `10.1007/BF01415506`. URL: `http://link.springer.com/10.1007/BF01415506` (visited on 04/06/2022).

[34] T. Q. Nguyen and H.-H. Kausch. "Chain Scission in Transient Extensional Flow Kinetics and Molecular Weight Dependence". In: *Journal of non-newtonian fluid mechanics* 30.2-3 (1988), pp. 125–140. URL: `http://www.sciencedirect.com/science/article/pii/0377025788850201` (visited on 09/11/2016).

[35] H. G. Sim, B. Khomami, and R. Sureshkumar. "Flow–Induced Chain Scission in Dilute Polymer Solutions: Algorithm Development and Results for Scission Dynamics in Elongational Flow". In: *Journal of Rheology* 51.6 (2007), p. 1223. ISSN: 01486055. DOI: `10.1122/1.2789945`. URL: `http://scitation.aip.org/content/sor/journal/jor2/51/6/10.1122/1.2789945` (visited on 08/29/2016).

[36]   J. Dinic et al. "Extensional Relaxation Times of Dilute, Aqueous Polymer Solutions". In: *ACS Macro Letters* 4.7 (July 21, 2015), pp. 804–808. ISSN: 2161-1653, 2161-1653. DOI: `10.1021/acsmacrolett.5b00393`. URL: `http://pubs.acs.org/doi/abs/10.1021/acsmacrolett.5b00393` (visited on 03/17/2016).

[37]   P. Nghe, P. Tabeling, and A. Ajdari. "Flow-Induced Polymer Degradation Probed by a High Throughput Microfluidic Set-Up". In: *Journal of Non-Newtonian Fluid Mechanics* 165.7 (2010), pp. 313–322. URL: `http://www.sciencedirect.com/science/article/pii/S037702571000008X` (visited on 09/13/2016).

[38]   A. Dupas et al. "Mechanical Degradation Onset of Polyethylene Oxide Used as a Hydrosoluble Model Polymer for Enhanced Oil Recovery". In: *Oil & Gas Science and Technology – Revue d'IFP Energies nouvelles* 67.6 (Nov. 2012), pp. 931–940. ISSN: 1294-4475, 1953-8189. DOI: `10.2516/ogst/2012028`. URL: `http://ogst.ifpenergiesnouvelles.fr/10.2516/ogst/2012028` (visited on 01/15/2019).

[39]   K. Brakstad and C. Rosenkilde. "Modelling Viscosity and Mechanical Degradation of Polyacrylamide Solutions in Porous Media". In: *All Days*. SPE Improved Oil Recovery Conference. Tulsa, Oklahoma, USA: SPE, Apr. 11, 2016, SPE-179593–MS. DOI: `10.2118/179593-MS`. URL: `https://onepetro.org/SPEIOR/proceedings/16IOR/All-16IOR/Tulsa,%20Oklahoma,%20USA/187343` (visited on 03/23/2022).

[40]   S. L. Anna and G. H. McKinley. "Elasto-Capillary Thinning and Breakup of Model Elastic Liquids". In: *Journal of Rheology* 45.1 (2001), p. 115. ISSN: 01486055. DOI: `10.1122/1.1332389`. URL: `http://scitation.aip.org/content/sor/journal/jor2/45/1/10.1122/1.1332389` (visited on 03/22/2016).

[41]   J. Dinic, M. Biagioli, and V. Sharma. "Pinch-off Dynamics and Extensional Relaxation Times of Intrinsically Semi-Dilute Polymer Solutions Characterized by Dripping-onto-Substrate Rheometry". In: *Journal of Polymer Science Part B: Polymer Physics* 55.22 (Nov. 15, 2017), pp. 1692–1704. ISSN: 08876266. DOI: `10.1002/polb.24388`. URL: `http://doi.wiley.com/10.1002/polb.24388` (visited on 03/05/2020).

[42]   J. Dinic, L. N. Jimenez, and V. Sharma. "Pinch-off Dynamics and Dripping-onto-Substrate (DoS) Rheometry of Complex Fluids". In: *Lab on a Chip* 17.3 (2017), pp. 460–473. ISSN: 1473-0197, 1473-0189. DOI: `10.1039/C6LC01155A`. URL: `http://xlink.rsc.org/?DOI=C6LC01155A` (visited on 02/10/2020).

[43]   E. Greiciunas et al. "Design and Operation of a Rayleigh Ohnesorge Jetting Extensional Rheometer (ROJER) to Study Extensional Properties of Low Viscosity Polymer Solutions". In: *Journal of Rheology* 61.3 (May 2017), pp. 467–476. ISSN: 0148-6055, 1520-8516. DOI: `10.1122/1.`

4979099. URL: http://sor.scitation.org/doi/10.1122/1.4979099 (visited on 03/31/2022).

[44] J. Dinic and V. Sharma. "Macromolecular Relaxation, Strain, and Extensibility Determine Elastocapillary Thinning and Extensional Viscosity of Polymer Solutions". In: *Proceedings of the National Academy of Sciences* 116.18 (Apr. 30, 2019), pp. 8766–8774. ISSN: 0027-8424, 1091-6490. DOI: 10.1073/pnas.1820277116. URL: http://www.pnas.org/lookup/doi/10.1073/pnas.1820277116 (visited on 05/05/2021).

[45] J. Dinic and V. Sharma. "Flexibility, Extensibility, and Ratio of Kuhn Length to Packing Length Govern the Pinching Dynamics, Coil-Stretch Transition, and Rheology of Polymer Solutions". In: *Macromolecules* 53.12 (June 23, 2020), pp. 4821–4835. ISSN: 0024-9297, 1520-5835. DOI: 10.1021/acs.macromol.0c00076. URL: https://pubs.acs.org/doi/10.1021/acs.macromol.0c00076 (visited on 05/05/2021).

[46] C. Clasen et al. "How Dilute Are Dilute Solutions in Extensional Flows?" In: *Journal of Rheology* 50.6 (Nov. 2006), pp. 849–881. ISSN: 0148-6055, 1520-8516. DOI: 10.1122/1.2357595. URL: http://sor.scitation.org/doi/10.1122/1.2357595 (visited on 05/14/2021).

[47] B. Keshavarz and G. H. McKinley. "Micro-Scale Extensional Rheometry Using Hyperbolic Converging/Diverging Channels and Jet Breakup". In: *Biomicrofluidics* 10.4 (July 2016), p. 043502. ISSN: 1932-1058. DOI: 10.1063/1.4948235. URL: http://scitation.aip.org/content/aip/journal/bmf/10/4/10.1063/1.4948235 (visited on 10/14/2016).

[48] R. Learsch. "Investigation in Experimental Conditions and Automation of Dripping-onto-Substrate Rheology". American Chemical Society Spring Meeting (San Diego, CA). Mar. 23, 2022.

[49] S. A. Vanapalli. "Polymer Chain Scission in Extensional and Turbulent Flows and Implications for Friction Drag Technologies". University of Michigan, 2006. 219 pp.

[50] F. Rodriguez and C. Winding. "Mechanical Degradation of Dilute Polyisobutylene Solutions". In: *Industrial & Engineering Chemistry* 51.10 (Oct. 1959), pp. 1281–1284. ISSN: 0019-7866, 1541-5724. DOI: 10.1021/ie50598a034. URL: https://pubs.acs.org/doi/abs/10.1021/ie50598a034 (visited on 04/12/2022).

[51] Y. Minoura et al. "Degradation of Poly(Ethylene Oxide) by High-Speed Stirring". In: *Journal of Polymer Science Part A-2: Polymer Physics* 5.1 (Jan. 1967), pp. 125–142. ISSN: 04492978, 15429377. DOI: 10.1002/pol.1967.160050111. URL: https://onlinelibrary.wiley.com/doi/10.1002/pol.1967.160050111 (visited on 04/12/2022).

[52] R. E. Harrington and B. H. Zimm. "Degradation of Polymers by Controlled Hydrodynamic Shear [1]". In: *The Journal of Physical Chemistry* 69.1 (Jan. 1965), pp. 161–175. ISSN: 0022-3654, 1541-5740. DOI: 10.1021/j100885a025. URL: https://pubs.acs.org/doi/10.1021/j100885a025 (visited on 04/12/2022).

[53] T. Q. Nguyen, G. Yu, and H.-H. Kausch. "Birefringence of a Polystyrene Solution in Elongational Flow: Effects of Molecular Weight and Solvent Quality". In: *Macromolecules* 28.14 (July 1995), pp. 4851–4860. ISSN: 0024-9297, 1520-5835. DOI: 10.1021/ma00118a010. URL: http://pubs.acs.org/doi/abs/10.1021/ma00118a010 (visited on 09/13/2016).

[54] R. W. Learsch. "Long, Associative, Telechelic Poly(Acrylamide) under Shear and Extensional Flow". American Chemical Society Spring Meeting (San Diego, CA). Mar. 20, 2022.

Chapter 3

MEASUREMENTS OF DRAG REDUCTION AND EXTENSIONAL RHEOLOGY OF DEGRADING POLYMER SOLUTIONS

3.1 Introduction

In transporting fluids between locations (i.e., oil through long pipelines) or cycling fluids within a closed system (i.e., heat transfer fluids in a vehicle), substantial energy expenditure comes from pumping the fluid to overcome the friction (drag) experienced during turbulent flow. One method currently employed industrially to reduce that friction (such as in the Trans-Alaska pipeline)[1] is polymeric drag reduction, where a high molecular weight polymer additive in a fluid results in increased flow rates at the same pressure differential. Applications of polymeric drag reduction, however, are limited by mechanical chain scission of polymer backbones, which causes a decrease in the molecular weight of the polymer additive and thus a decrease in efficacy over time, particularly in high flow rate elements of flow, such as pumping (see Chapter 2 for further discussion of chain scission).[2–7] The Kornfield group has sought to develop end-associative polymeric additives to be scission-resistant (see Chapter 1 for discussion of megasupramolecules)—these megasupramolecular polymer systems have previously demonstrated drag reduction without degradation in fuel.[8] To intentionally design additives for new applications and fluids, such as water instead of fuel, we need to understand the underlying mechanisms of polymeric drag reduction; however, polymeric drag reduction couples two complex problems: polymer conformations under flow and turbulence.

History and Features of Polymeric Drag Reduction

The phenomenon of drag reduction was independently discovered by multiple individuals during World War II, including B.A. Toms and Karol Mysels, and published in the years following.[9–12] In the case of Toms, the study of drag reduction was a byproduct of trying to understand why polymer additives for lubricants were degrading under flow—characterizing degradation and chain scission has been a part of the drag reduction field since its inception.[11,12] Historically, the mechanism of turbulent polymeric drag reduction has been debated extensively, with most theories only fitting a subset of empirical observations.[13,14] Key features of polymeric drag reduction that theory seeks to explain include the onset, the velocity profile near the wall, the maximum drag reduction asymptote, and, more recently of interest, intermediate regimes of drag reduction. The onset of polymeric drag reduction is both a function of the flow conditions and the solution properties, and is typically experimentally characterized by the Reynolds number (either bulk Reynolds—$Re = \rho U D / \eta_{shear}$, where ρ is the density, U is the mean velocity, D is the length scale of the flow, and η_{shear} is the shear viscosity—or the friction Reynolds number—$Re_\tau = D\sqrt{\tau_w}/\eta_{shear}\sqrt{\rho}$, where τ_w is the wall shear stress) and the combination of concentration, polymer molecular weight, and backbone identity. In simulation work, those polymer properties relative to the fluid flow are bundled into the Weissenburg number ($Wi = \lambda\dot{\epsilon}$, where λ is the relaxation time of the polymer and $\dot{\epsilon}$ is the rate of strain on the polymer).[14] The near-wall mean velocity profile in the log-law region, as initially captured by Virk and coworkers, is seen in polymeric solutions in turbulent flow to transition from the Newtonian case (the Prandtl-Kármán law) to a maximum drag profile with increasing drag reduction.[15–19] That maximum drag profile is one reported characteristic of the maximum drag regime (MDR, also called the

maximum drag asymptote), a regime that appeared universal in which further raising the Reynolds number, the polymer molecular weight, or the concentration of polymer would not further increase the measured drag reduction.[17,18,20] Research after Virk has characterized two additional intermediate regimes of drag reduction—a low-extent drag reduction regime (LDR) and a high-extent drag reduction regime (HDR)—that have distinct mean velocity profiles and fluctuation characteristics, with an empirical transition around a percent drag reduction of 30-35 %.[14,21]

Experimentally, bulk measurements of drag reduction have been used since the 1940s to determine how much polymer additives can reduce friction. In last 25 years, particle image velocimetry (PIV), a technique in which particles sufficiently small to not disrupt the flow (but sufficiently large to track) are added to the fluid of interest and then observed using a high-speed camera, has become a powerful technique for looking at the microscale effects on turbulent structures corrersponding to bulk effects.[22,23] Degradation of polymers has limited the ability to use both macro and micro techniques to their full extent reproducibly. For example, in PIV, observations of turbulent flow may be assumed to be at quasi-steady state, to be able to average over a series of measurements to obtain a mean velocity profile. If the polymer is degrading within the viewing window, a mean velocity profile obtained via averaging becomes less meaningful. On the other hand, simulation has opened a window into the interaction of polymers with turbulent flow structures, uncovering details that would be smaller than the observable scale in experiments and without necessarily being constrained by degradation. Due to limited processing power, however, simulation cannot yet reach high Reynolds numbers $(Re_\tau > 100 - 1000)$ for sufficiently large domain sizes and long times with practical amounts of computing resources.[14]

The community studying drag reduction, as a result, is pushing the limits of these techniques to find opportunities for overlap between experiment and simulation, fill gaps in our collective knowledge, and evaluate potential theories. Recent simulation work has iterated through a number of hypotheses,[1,14,20,24] challenging our conceptions of the nature of drag reduction and its long established regimes. In relatively small simulation box sizes, turbulent drag reduction was observed to consist over time of bursts of active Newtonian turbulence followed by "hibernation," where the behavior mimicked that of MDR. By varying Wi, modulation between these two extremes was achieved.[1,25] Extension of these simulation techniques to larger box sizes revealed that what was appeared to be purely temporal on a small scale was instead a spatio-temporal phenomenon, in which hibernation was observed to only affect subdomains of flow, rather than the entire domain simultaneously.[20,26]

A relatively recent discovery in polymeric drag reduction is the regime of elasto-inertial turbulence (EIT). EIT can occur at lower Reynolds numbers than Newtonian turbulence, but sufficiently high Re that inertia cannot be neglected (unlike in elastic turbulence). In the presence of the elasticity from a polymer additive, EIT suppresses Newtonian turbulence and approaches the maximum drag asymptote as Re increases.[24] In addition to introduction of EIT as a potential mechanism for polymeric drag reduction, work examining MDR has also found that the behavior is not as universal as originally thought, exhibiting hibernation and relaminarization behavior at Reynolds numbers near the transition between laminar and turbulent flow, while demonstrating characteristics of EIT farther from transition.[19,20,26]

Scope

Because our primary applications of interest for megasupramolecular polymer additives are industrial scale, relevant Reynolds numbers are much higher than what is readily accessible in current simulation work. The scope of this chapter is to describe the design, construction, and characterization of a instrument for simultaneous measurement of polymeric drag reduction in sufficiently high Reynolds number pipe flow via particle image velocimetry and bulk flow rates. We monitored the degradation of an example polymer solution in different elements of the instrument and due to specific actions in our procedure. We acquired preliminary measurements of drag reduction as degradation occurred for two water-soluble polymer backbones, poly(ethylene oxide) (PEO) and polyacrylamide (PAM), while probing the extensional relaxation time of the initial and degraded solutions as a measure of how much chain scission had occurred. In the thesis work of Jacqueline Tawney, validation of particle image velocimetry and measurements of polymeric drag reduction with this instrument are planned, along with use of the measured velocity profile in resolvent analysis, a technique in which the Navier-Stokes equation can be broken down into forcing and response modes,[27,28] allowing insight into the underlying perturbation of turbulence by polymers.

This work describes an ongoing collaboration between members of the groups of Professor Julia Kornfield and Professor Beverley McKeon—detailed descriptions of contributions are documented in the Experimental Section.

3.2 Experimental Section

Materials

Polyethylene oxide acquired from Dow (Polyox WSR301). Polyacrylamide (PAM) was prepared by Hojin Kim. PAM synthetic details to be included in

Table 3.1: Molecular weights, dispersities, and sources for polyacrylamide (PAM) and poly(ethylene oxide) (PEO) samples.

Backbone	M_w (Mg/mol)	M_n (Mg/mol)	Đ	Sample Name	Source
PAM	6.70	5.00	1.3	6.7M PAM	HK
PEO	6.00	3.80	1.6	6M PEO	Dow WSR301

M_w: Weight-average molecular weight, M_n: Number-average molecular weight, Đ: Dispersity index (M_w/M_n),
PAM: Polyacrylamide, PEO: Poly(ethylene oxide),
HK: Hojin Kim
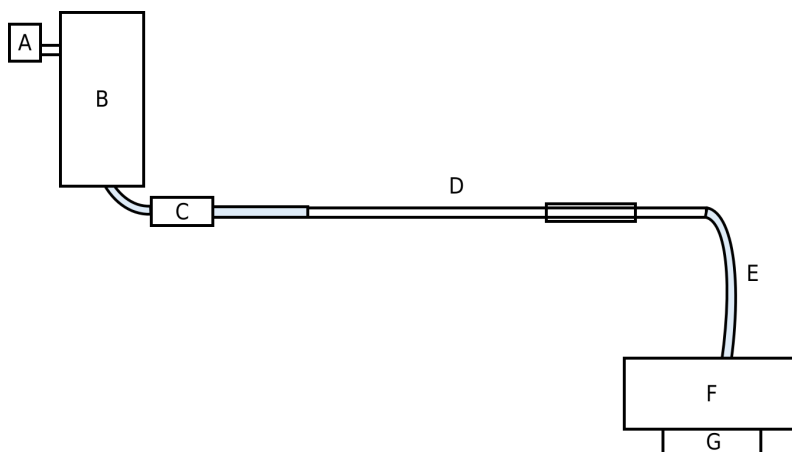
Figure 3.1: Schematic of drag reduction instrument.

the thesis of Hojin Kim. Table 3.1 includes number-average molecular weight (M_n), weight-average molecular weight (M_w), dispersity (Đ), and source for polymers used in this chapter.

Drag Reduction Instrument Construction

The instrument used in the drag reduction measurements described below was designed, constructed, and refined in collaboration with Dr. David Huynh, Dr. Ryan McMullen, and Jacqueline Tawney, members of Professor Beverley McKeon's group. Without the collaboration with Professor McKeon and her students, these experiments would not have been possible.

The drag reduction instrument consists of a reservoir tank (**B**, Figure 3.1)
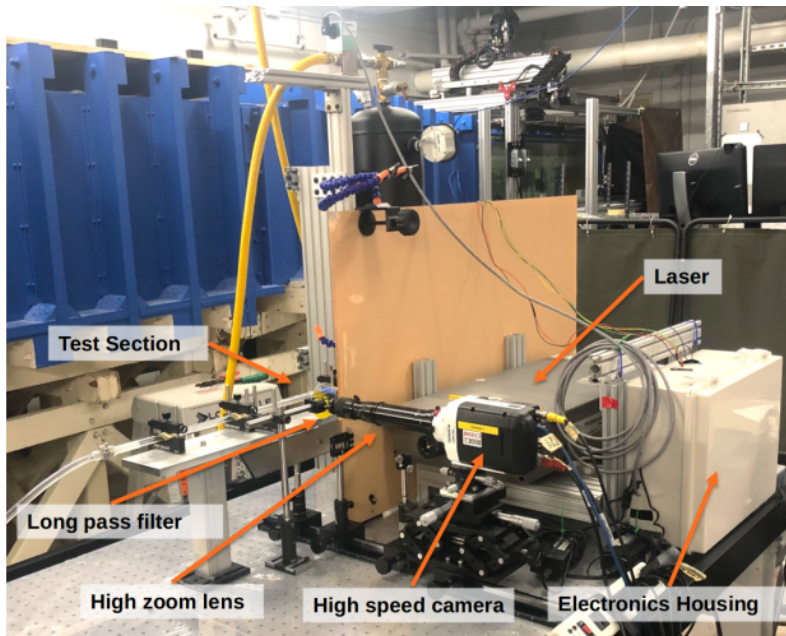
Figure 3.2: Photo of drag reduction instrument with optical components labeled. Image provided by Jacqueline Tawney, used with permission.

that can be pressurized using a pressure regulator (**A**, ProportionAir QB3), a ball-valve (**C**, DynaQuip 1AWH8) connected to the reservoir tank and to the quartz optical section (**D**) by flexible polytetrafluoroethylene tubing (**E**), and a receiving tank (**F**) on a scale (**G**) also connected to the quartz optical section by flexible tubing. The flexible tubing between the quartz optical section and the receiving tank can be exchanged to change the length of the total tube length for determination of the pressure differential not including the head leosses at the inlet and outlet. The two total lengths were 4.27 m ("short") and 5.89 m ("long"). For contraction experiments, the receiving tank is connected directly to the ball valve via a 16 cm segment of flexible tubing. The instrument was assembled by Dr. David Huynh and Dr. Ryan McMullen and adapted and validadated by Jacqueline Tawney.

The optical section of the instrument (test section in 3.2) is a long cylindrical quartz tube with a small section of square tubing with a cylindrical center
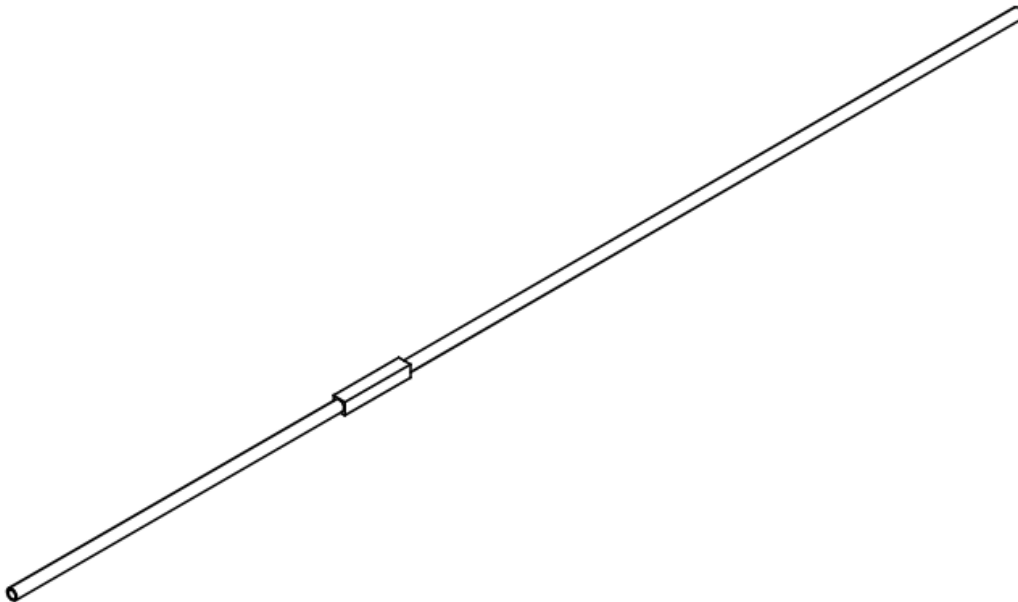
Figure 3.3: Isometric view of quartz optical section with cylindrical section for flow and rectangular segement for optical viewing

inserted into the center (Figure 3.3). I designed the final optical section in collaboration with Dr. David Huynh and Dr. Ryan McMullen, and the piece was constructed by PGB Optical, based on initial prototypes I built using commercially available quartz sections and optical glue.

To make repeated experiments practical and reproducible, I designed and installed a custom Arduino-operated system for operating the ball-valve and pressure regulator and for measuring the pressure at the regulator and the reservoir tank and the mass at the receiving tank. Jacqueline Tawney and I refined and rebuilt the custom system to be more robust. Jacqueline Tawney then enclosed all possible electrical components in a water-resistent enclosure for safety.

I programmed a LabVIEW graphical user interface to simultaneously record the mass measurements and issue commands to the Arduino-operated system to control each part of the instrument. The recorded mass measurements are

automatically saved to text files. Jacqueline Tawney then performed analysis in MATLAB to extract the steady-state mass flow rate for each experiment.

Particle image velocimetry measurements using this instrument are planned to be part of the thesis of Jacqueline Tawney.

Solution Preparation

As discussed above, long polymer chains are vulnerable to mechanical degradation. We sought to minimize degradation prior to running samples in the instrument.

Stock solutions of polymer in deionized water were prepared by adding solid polymer to a 2L glass vessel of deionized water with a stir bar creating a vortex to distribute the solid polymer throughout the volume of water and reduce clumping. After polymer was fully added, stirring was stopped to prevent high shear conditions at the bottom of the vessel. The glass vessel was placed on a roller at 30 rpm for 7-10 days at ambient temperature, 15 $\pm$ 1 °C. During rolling, the vessels were covered in aluminum foil to reduce chemical degradation of PEO due to light and ultraviolet radiation.

In the case of the PEO solutions, stock solutions were visually homogeneous before use. In the case of PAM stock solution, the initial stock solution had small flakes of undissolved polymer after over a week of rolling time. After the further dilution described below, polymer clumps were no longer observed.

Stock solutions were diluted to 0.0066 wt% (66 parts-per-million by weight) with deionized water in an opaque drum and rolled for 5 hours at 21 rpm. After rolling, diluted solutions were checked for visual inhomogeneities, and none were observed.

Solutions were used within two weeks of initial stock preparation.

Stock solutions were prepared by Red Lhota. Dilutions to concentrations used in the instrument were completed by Jacqueline Tawney.

The as-prepared 0.0066 wt % solutions were each split into two portions. In case of contraction measurement, one portion of a 6M PEO solution was used for the lower pressure experiment (15 psi, 0.10 MPa) and one portion was used for the higher pressure experiment (20 psi, 0.14 MPa). In the case of drag reduction experiments, one portion each of a 6M PEO solution and a 6.7M PAM solution were used for their own short-tube experiment, and one each was used for their own long-tube experiment. The two PEO solutions were each split into two 7.5 L portions; due to limited polymer availability, PAM solution was split into 4.43 L portions.

Degradation and Drag Reduction Measurements

The following procedures were performed by Jacqueline Tawney. Two related sets of experiments were performed, in addition to two additional samplings (loading and pushback, as discussed below). The first used only the reservoir tank, the ball-valve, a 16 cm segment of flexible tubing, and the receiving tank to measure the degradation as a function of pass due to the contraction from the reservoir tank into the ball valve and the expansion into the receiving tank (referred to below as a contraction experiment). The second used the complete system as described above with Figure 3.1 and measured the degradation and drag reduction as a function of pass from flow from the reservoir tank to the receiving tank.

After mixing and splitting the solutions as described above, a solution portion was loaded into an carboy. An initial sample of the solution added to the carboy was collected. The carboy was attached to the reservoir tank (**B** in Figure 3.1) by a quick-disconnect connector, while the reservoir tank was unpressur-

ized and open to the air, and the ball valve was closed. Fluid was allowed to run from the carboy into the tank through gravity-driven flow through the connection until all of the fluid was in the reservoir tank. In the loading sampling, an additional sample was collected by simulating gravity-driven flow through the quick-disconnect connector from the carboy into a sampling vessel.

After loading the initial fluid, a "pass" would proceed as follows. In a drag reduction, the reservoir tank would be pressurized to 5 psi (0.03 MPa) and the tube connecting the reservoir tank to the receiving tank (**F** in Figure 3.1) would be "primed" with a small amount of solution by opening the ball valve for 2.5 seconds to reduce vibration of the receiving tank from air blowing through prior to solution flow. In a contraction experiment, no priming step was used due to the shorter distance and lack of measurement of the receiving tank's mass. The reservoir tank would be pressurized to the trial pressure. After pressurization, the ball valve would be opened, and solution would flow into the receiving tank. In the case of the contraction experiments, all fluid was allowed to flow into the receiving tank before the ball valve was closed, and the total time of flow and the total mass of fluid remaining in the tank were used to estimate the mass flow rate. In the case of the drag reduction experiments, the mass of the receiving tank was measured as a function of time by the scale (**G** in Figure 3.1) and the ball valve was closed after a set duration (7.5 s for PEO short tests and 7 s for PEO long and all PAM tests). For the measurements of the 6M PEO solution in drag reduction, a second trial was performed by opening the valve again and measuring flow rate a second time at the same pressure. If any additional solution remained in the reservoir tank, it was pushed through at the testing pressure into the receiving tank. The reservoir tank would then be depressurized slowly back to atmospheric pressure.

After passes 1, 5, and 10, the fluid in the receiving tank was sampled. Then, to return the fluid back to the reservoir tank, the receiving tank was pressurized to 5 psi (0.03 MPa) and the ball valve opened ("pushback"). In the pushback sampling experiment, a small portion of the fluid returned to the reservoir tank after pass 1 of a contraction experiment was allowed to flow back into the receiving tank to be sampled.

The above "pass" and "pushback" procedure was repeated for 10 passes. When exceeding 10 passes, the solutions demonstrated too low of relaxation times to be reliably measured in DoSER (discussed in Chapter 1). The solution was then removed from the instrument and disposed of. The instrument was rinsed by loading ~8 L of deionized water and then allowing flow at 10 psi (0.07 MPa) followed by drying using air at 5-20 psi (0.03-0.14 MPa).

The pressure for the contraction experiments was chosen to mimic the range of flow rates previously achieved in prior drag reduction measurements in the instrument. At 15 psi (0.10 MPa), the mass flow rate was approximately 0.44 kg/s. At 20 psi (0.13 MPa), the mass flow rate was approximately 0.50 kg/s. To extract a measurement of the friction per unit length of tube, the pressure difference required to acheive similar flow rates through a 4.27 m ("short") and 5.89 m ("long") tube for the PEO at 0.0066 wt % on its first pass was determined by Jacqueline Tawney. At 40 psi for the short-tube and 43 psi for the-long tube experiments, the mass flow rates were approximately 0.52 kg/s and 0.50 kg/s respectively. Based on these results, the appropriate pressure difference for wall shear stress calculation was estimated to be 4 psi, which yields a Reynolds number based on the wall shear stress (Re_τ) of $1.8 * 10^3$. The 40 psi for short and 43 psi for long pressures were maintained for the 6.7M PAM solution for consistency.

Dripping-onto-Substrate Extensional Rheometry (DoSER)

A dripping-onto-substrate extensional rheometry (DoSER) instrument was constructed by Robert Learsch and Red Lhota consisting of a GSVitec MultiLED G8 with QT lamp head (12000 lumen light source, Figure 1.7**A**), a Harvard Elite 11 syringe pump on an adjustable track (solution delivery, **B**), Photron FASTCAM Nova S12 type 1000K-M-32GB (high-speed camera, **C**) equipped with an optical train as described below, and a custom holder for aluminum substrates (**D**). The optical train consisted of a Resolve4K 7:1 Zoom Video microscope lens, two rear projection lenses, a 1.0x objective lens, and a coupler, resulting in a resolution limit at full zoom of 3.5 µm (**E**). The camera was operated at 25,000 frames per second with a shutter speed of 150,000 Hz (i.e., 7 µs exposure). The light passes through a diffuser before reaching the measurement plane (**F**).

A syringe with a 22G blunt-tip stainless-steel needle (outer diameter 0.718 mm) was mounted to the syringe pump. The substrate was positioned at a height of 2.8 mm below the tip of the needle, corresponding to a height-to-needle-diameter ratio of 4 or a height-to-initial-droplet-diameter ratio of 1, which is within the optimal range for water solutions.[29] Ambient temperature was measured with each experiment and was in the range 15 ± 1 °C.

For each solution, DoSER was performed using the following procedure. An aliquot was slowly loaded into a syringe through a 22G stainless-steel blunt-tip needle. The syringe was attached to the syringe pump and the syringe pump was slowly advanced until solution was observed to drip from the needle, and then the needle tip was cleaned. A clean set of aluminum substrates was loaded onto the substrate holder and the first substrate was aligned below the needle tip. The light was turned on and the camera was focused and aligned with the needle tip. The substrate was then raised or lowered to the correct

Figure 1.7: Schematic of dripping-onto-substrate extensional rheometer (not to scale). (repeated from page 14)

height (as describe above) relative to the needle tip. A background video with a droplet-free needle and substrate was acquired. A drop was dispensed from the needle tip by the syringe pump at a rate of 0.02 mL/min, until the drop was nearly touching the substrate. The syringe pump was stopped prior to droplet-substrate contact. The events of droplet contact through liquid bridge formation and pinchoff were recorded (referred to as an experimental video or "run"). A clean substrate was then placed below the needle tip. Dispensing drops onto a clean substrate was repeated until five total runs were recorded. The videos were analyzed using the *dosertools* Python package, described in detail in Appendix A, to obtain the normalized diameter as function of time after the critical time (time of transition between solvent behavior and elasto-capillary response). The decay of the normalized diameter is used to evaluate the extensional relaxation time. In our experiments, run-to-run variation on the DoSER instrument was observed to be more significant than errors in

fitting–errors in measured relaxation times are thus quantified using the run-to-run variation. Solutions with relaxation times of 0.05 ms and lower were difficult to consistently characterize on our instrument.

Further discussions of DoSER theory and analysis are available in Chapter 1 and Appendix A respectively.

3.3   Results

Instrument Characterization

To characterize at what point in the solution's time in the instrument the degradation was occurring, we used dripping-onto-substrate extensional rheometry (DoSER) to measure the extensional relaxation time of samples before and after the loading, pushback, and tank-to-ball valve stages of the procedure. To determine extensional relaxation times, we first measured normalized diameter (D/D_0) by image analysis of high-speed videos of DoSER experiments as described in Appendix A, then fits to the normalized diameter in the elastocapillary regime as described in Appendix A were used to determine the extensional relaxation time (λ_E).

Loading the sample into the tank from the carboy resulted in a slight, but not statistically significant increase in the measured extensional relaxation time (Figure 3.4(a)). Pushback at low pressure from the destination tank back to the reservoir tank does not statistically signficantly change the measured extensional relxation time (Figure 3.4(b)).

To determine where degradation primarily occurs in the instrument, Jacqueline Tawney isolated the contraction from the reservoir tank into the ball valve and expansion back into the destination tank for collection (with minimal instital flexible tubing, 16 cm) and flowed a solution of 6M PEO at 0.0066 wt % in deionized water through the system at 15 and 20 psi (0.10 and 0.14
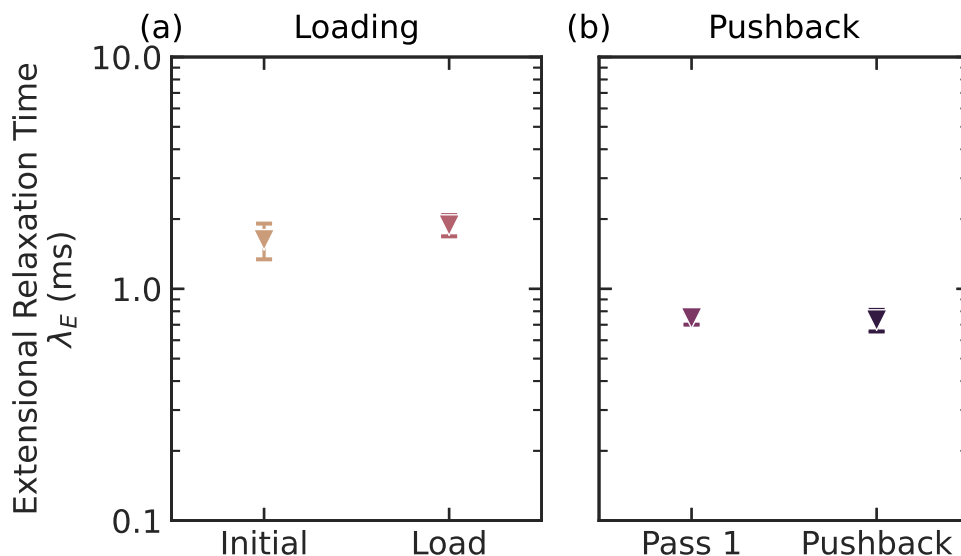
Figure 3.4: Extensional relaxation time (λ_E, ms) of 6M PEO at 0.0066 wt % in water (a) before and after loading from the carboy into the reservoir tank and (b) after a single pass at 15 psi (0.10 MPa) and after pushback from the receiving tank into the reservoir tank. Vertical error bars represent 95% confidence intervals. Where error bars are not visible, the corresponding interval is within symbol size.

MPa, respectively). The fluid achieved flow rates of approximately 0.43 kg/s at 15 psi and 0.50 kg/s at 20 psi, bounding typical flow rates for polymer solutions through the full drag reduction instrument. Aliquots of the initial solution, and of the fluid in the receiving tank after passes 1, 5, and 10, were collected and measured using DoSER (Figure 3.5(a)). Effective molecular weights were calculated from the measured extensional relaxation times as described in Chapter 2 using Equation 2.3 (Figure 3.5(b)). The flow through the contraction resulted in substantially decreased extensional relaxation time and thus effective molecular weight with repeated passes.

Turbulent Drag Reduction

Mass flow measurements were performed for solutions of both 6M PEO and 6.7M PAM at 0.0066 wt % in deionized water for both the short and long
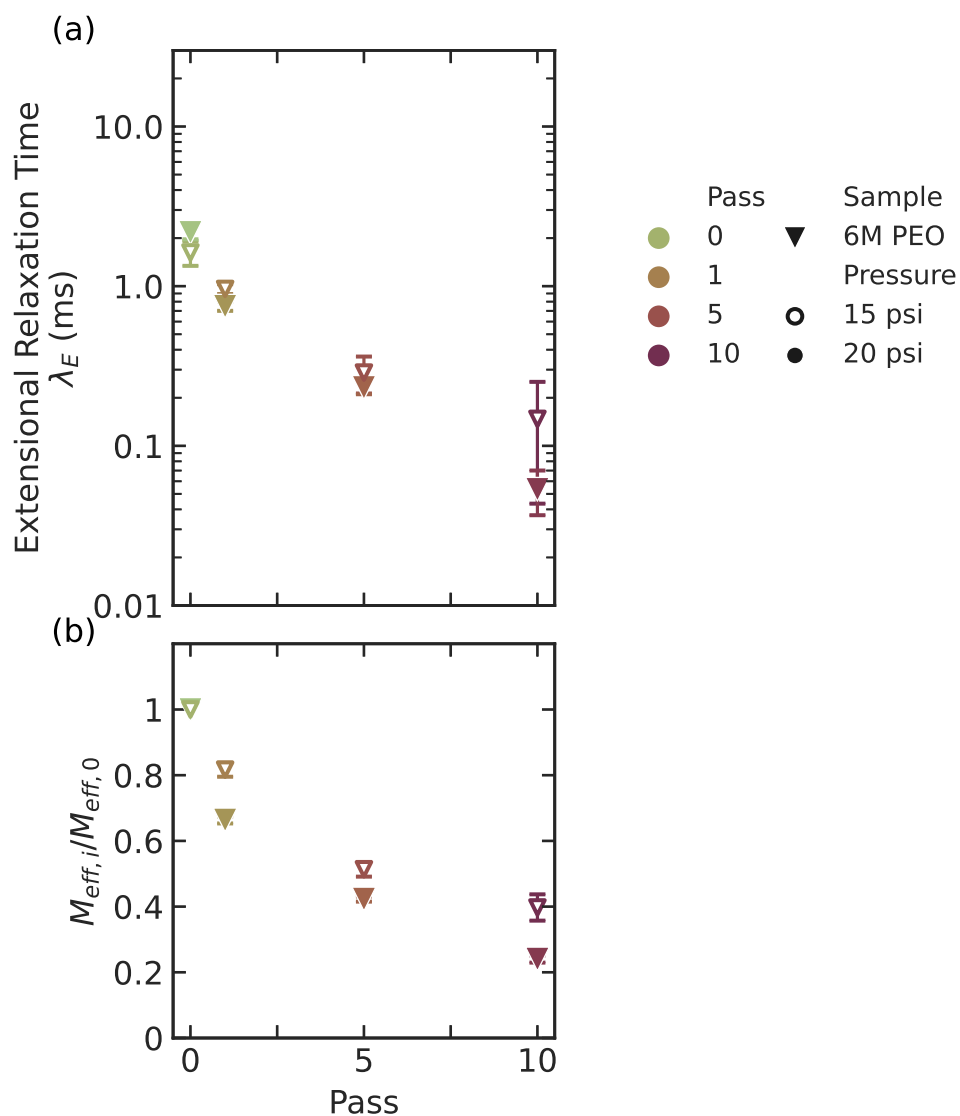
Figure 3.5: Changes with passes through the contraction-expansion of the drag reduction instrument for solutions with as-prepared molecular weight and backbone of 6M PEO at concentrations of 0.0066 wt %. (a) Extensional relaxation time (λ_E, ms) as a function of passes. (b) Ratio of effective molecular weight of degraded samples to initial effective molecular weight as a function of pass ($M_{eff,i}/M_{eff,0}$), given observed extensional relaxation time from (a) using Equation 2.3, assuming a constant total concentration of the solution. Vertical error bars represent 95% confidence intervals representing run-to-run variation in DoSER measurements (fitting errors are substantially smaller). Where error bars are not visible, the corresponding interval is within symbol size.

tubes. These measurements were used to calculate bulk Reynolds numbers for the flow (Figure 3.6(a)). Using a water flow rate at 40 psi through the short tube as our baseline (dashed lines in Figure 3.6(a), $\dot{m}_{water}$), the percent drag reduction (% DR) due to the polymer at each pass was defined using Equation 3.1, where $\dot{m}_{solution,i}$ is the mass flow measured for the solution after pass i (Figure 3.6(b)).

$$\% \ DR_i = \frac{\dot{m}_{solution,i} - \dot{m}_{water}}{\dot{m}_{water}} \tag{3.1}$$

Aliquots of the initial solution, and of the fluid in the reservoir tank after passes 1, 5, and 10, were collected and measured using DoSER (Figure 3.7(a)). Effective molecular weights were calculated from the measured extensional relaxation times as described in Chapter 2 using Equation 2.3 (Figure 3.7(b)).

Using the effective molecular weight ratios calculated from the extension relaxation times measured and multiplying by the known starting molecular weight, we compared the measured drag reduction to the effective molecular weight as the solutions decay. The PEO solutions are at a reduced concentration (weight concentration divided by overlap concentration, c/c^*) of 0.12; the PAM solutions are at c/c^* of 0.05.

3.4 Discussion

Drag Reduction Instrument Design

We considered a number of key features and constraints in the design of the instrument. On the fluid flow side, we sought to reach high Reynolds numbers in pipe flow that were largely unstudied in the literature at the intersection of polymeric drag reduction and particle image velocimetry (PIV), particularly those not reachable by current drag reduction simulation capabilities. Increasing Reynolds number, though, requires high pressures and large volumes of
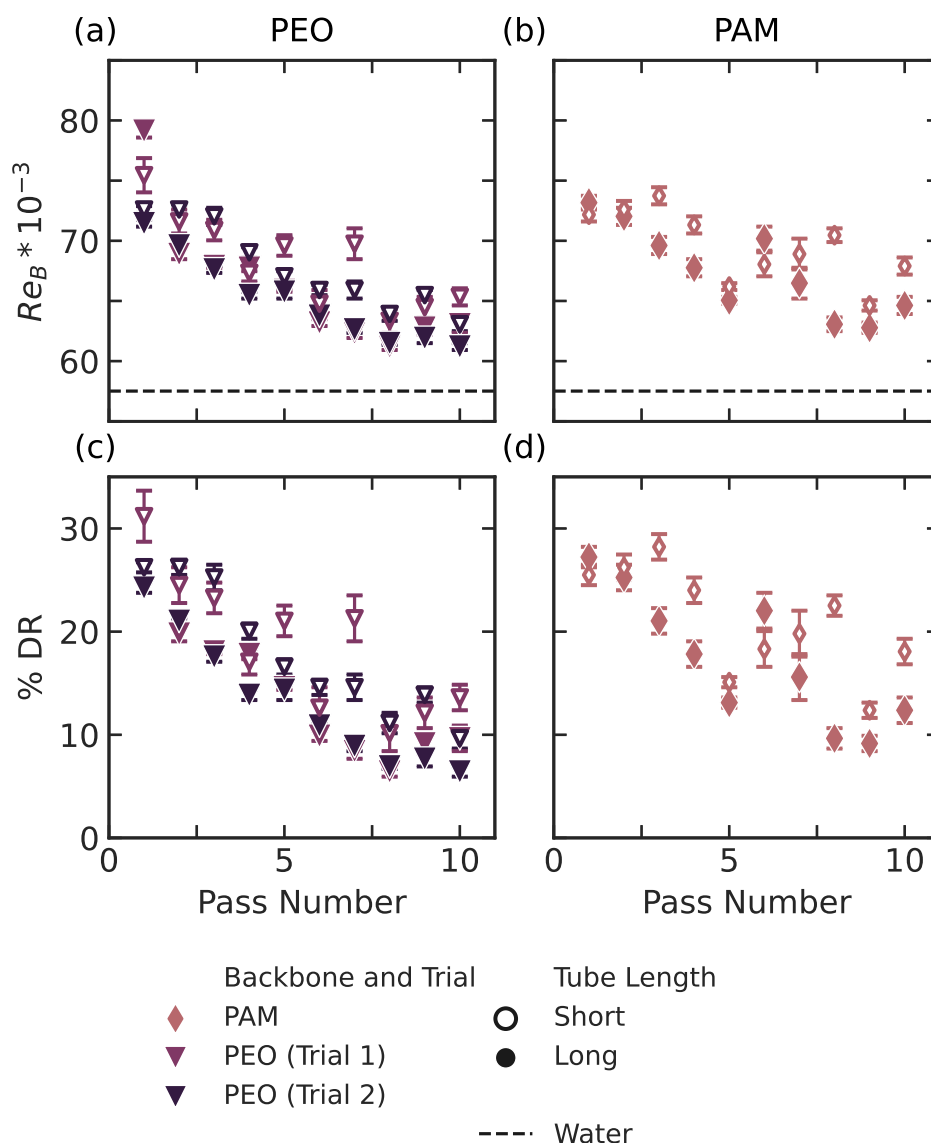
Figure 3.6: Changes with passes through the drag reduction instrument of sample solutions with as-prepared molecular weight and backbone of 6M PEO (two trials) and 6.7M PAM at as-prepared concentrations of 0.0066 wt %. (a) Bulk Reynolds number ($Re_B = 4\dot{m}/(\pi D \eta_{shear})$), where $\dot{m}$ is the mass flow rate, D is the tube diameter, and η_{shear} is the shear viscosity, approximately that of water) as a function of pass. Dashed line indicates the bulk Reynolds number for water in the short tube under the same conditions. (b) Calculated percent drag reduction as defined in Equation 3.1 as a function of pass. Vertical error bars represent 95% confidence intervals representing run-to-run variation in DoSER measurements (fitting errors are substantially smaller). Where error bars are not visible, the corresponding interval is within symbol size.
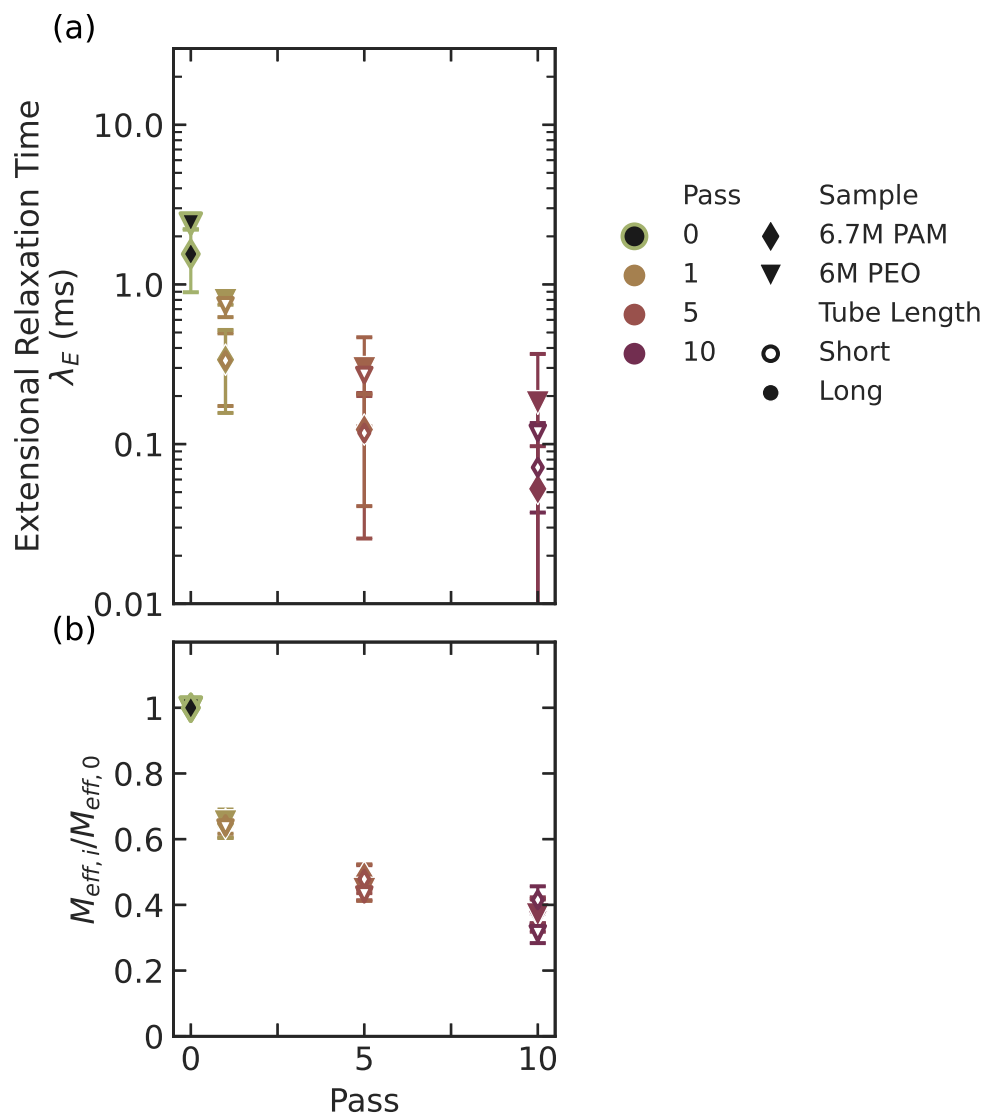
Figure 3.7: Changes with passes through the drag reduction instrument for solutions with as-prepared molecular weight and backbone of 6M PEO and 6.7M PAM at concentrations of 0.0066 wt %. (a) Extensional relaxation time (λ_E, ms) as a function of passes. (b) Ratio of effective molecular weight of degraded samples to initial effective molecular weight as a function of pass ($M_{eff,i}/M_{eff,0}$), given observed extensional relaxation time from (a) using Equation 2.3, assuming a constant total concentration of the solution. Vertical error bars represent 95% confidence intervals representing run-to-run variation in DoSER measurements (fitting errors are substantially smaller). Where error bars are not visible, the corresponding interval is within symbol size.
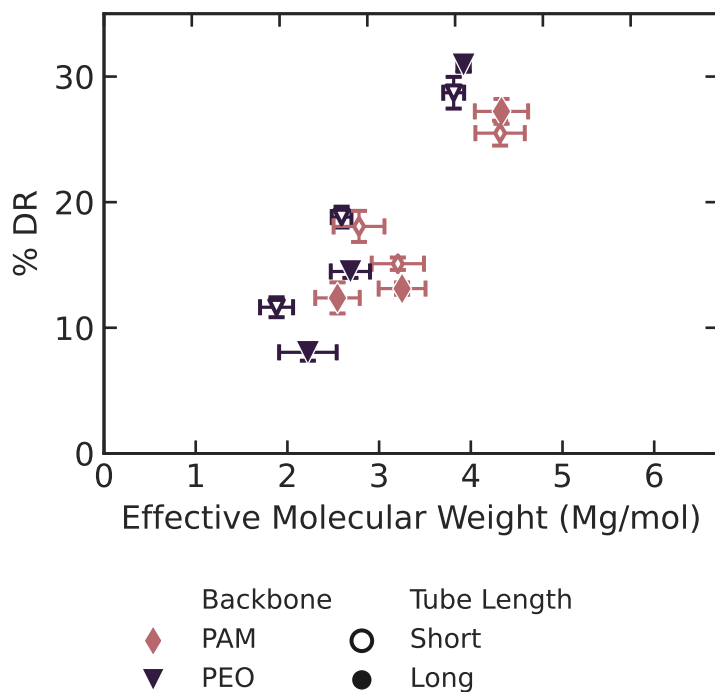
Figure 3.8: Percent drag reduction for solutions of 6M PEO (averaged over two trials) and 6.7M PAM after passes 1, 5, and 10 compared to water alone as a function of effective molecular weight (Mg/mol) calculated from extensional relaxation time measurements using Equation 2.3, assuming a constant total concentration of the solution. Vertical and horizontal error bars represent 95% confidence intervals on the respective measurements. Where error bars are not visible, the corresponding interval is within symbol size.

fluid. For safety reasons as well as equipment constraints, we were limited to 100 psi (0.69 MPa), 80 psi (0.55 MPa) with a safety margin. Because the instrument will eventually be used to test novel polymer additives, we were constrained to fluid volumes such that reasonable treat rates for polymeric drag reduction (50-100 ppm) will only require ∼1 g polymer per batch.

To enable optical access to observe pipe flow using PIV, we designed an optical section in quartz to meet the multiple needs of the experiments desired. For optical purposes, the viewing windows needs to be flat on at least two perpendicular sides: one for viewing with the camera, one for penetration of a laser

light sheet to create observable scattering of the fluorescent particles during PIV measurements. To establish a steady-state turbulent pipe flow, the tube must be sufficiently long and the inner wall must be circular throughout. For safety, the wall of the tube must be sufficiently thick to withstand pressures up to 100 psi (the upper end on the supply line and regulator). We met this set of constraints with the optical section depicted in Figure 3.3.

In addition to observations of the effects of polymeric drag reduction through PIV, we measure the mass flow of fluid through the instrument using a scale and use the steady-state rate of mass accumulation over time to determine the drag reduction relative to water alone. The tubing after the optical section and before the receiving tank can be exchanged to adjust the length and thus determine the pressure differential per length of tube (which is important to separate the effects of polymeric drag reduction from increased pressure loss in contraction and expansion due to polymers), which can be used to calculate the wall-shear-stress Reynolds number for comparison with PIV measurements. To keep the instrument tube lengths reasonable on a lab scale and with the pressure capabilities available, while still reaching the desired Reynolds numbers, our maximum total length is order 6 m.

For fair comparison of commericially available, traditional, long chain polymers with proposed end-associative polymers, we attempted to minimize potential degradation in the instrument. To avoid a known source of substantial degradation—pumping (see Chapter 2)—flow through the instrument occurs because of pressurization with air, rather than inducing additional highly extensional flow with a pump. To minimize contraction upon entering the tubing, a ball-valve was used as it permits the most open valve flow. Loading and pushback are both relatively gentle processes, the former done with only gravity-driven flow, the latter with relatively low air pressure. We still observe

substantial degradation of both poly(ethylene oxide) and polyacrylamide additives due to flow through the instrument, as discussed further below, but are able to ascribe it fully to the contraction-expansion flow.

Our instrument is able to reach bulk Reynolds numbers exceeding 50,000 for water at only 40 psi (0.28 MPa) (well below the upper limit of 80 psi), and we have observed drag reduction exceeding 30 % in preliminary polymeric drag reduction measurements, meeting our desired design criteria. Jacqueline Tawney is working towards full validation of the PIV measurements to establish canonical turbulent pipe flow and calibration of measurements close to the pipe wall to be able to observe polymer interactions with near-wall flow.

Localizing Degradation

Comparing the degradation for PEO at similar mass flow rates observed via decrease in extensional relaxation time of the solutions (and thus the effective molecular weight) in the contraction-expansion flow alone to the flow through the full drag reduction instrument indicates that the majority of degradation is happening in those elements, rather than in the pipe flow. The implication of these results is that during future particle image velocimetry (PIV) measurements, the portion of the flow observed in PIV will able to probe the polymer physics at a steady-state snapshot of degradation, rather than averaging over chains that are undergoing scission during turbulent flow in the optical section.

Degradation, however, does not appear to occur to a significant extent during loading or pushback of the fluid, isolating degradation observed to each full pressure pass. This information allows us to estimate the extension rates experienced in the contraction via the limiting extensional relaxation time after degradation ($\dot{\epsilon} \sim 1/\lambda_E$). At the flow rates for the drag reduction experiments, the extensional relaxation times reached by the PEO solutions in both the 15

psi contraction and drag reduction experiments were order 0.1 ms, implying that the contraction has extensional rates exceeding 10000 1/s.

Chain Scission and Drag Reduction

In agreement with the literature, we generally observed decreased drag reduction with degradation of the polymers in flow, with a relatively consistent decrease in mass flow rate with pass for the PEO solutions. The PAM solutions solutions, however, demonstrated an unusual increase in mass flow rate from pass 5 to 6 for both the short-tube and the long-tube experiments (Figure 3.6(b)). One potential cause could be the formation of polymer aggregates[7] in solution while the flow experiment was paused for sample collection after pass 5; however, a similar increase is not observed after pass 1 (where a sample was also collected), or in the PEO samples, which were more typically prone to aggregation in sample preparation. Another possible cause comes from the inherently coupled nature of the pipe flow and the contraction-expansion elements—because our pipe is lab-scale, not industrial scale, entrance and exit effects matter. In this instrument, drag reduction due to the polymers and the additional loss of pressure in the contraction and expansion steps due to the increased extensional viscosity are competing and the sum is observed via the mass flow rate. As degradation occurs, a tipping point may be reached where the PAM degrades enough to contribute less to the extensional flow in the contraction, yet still is an effective drag reducing agent, allowing for a net increase in the mass flow rate. Because of the limited amount of PAM available for this study, we were unable to repeat these results; further interrogation of whether this result is an artifact of our procedure or an indication of such a threshold is suggested for a future study. Both samples demonstrate decreasing extensional relaxation time with pass, and the percent of drag reduction appears

correlated (0.82) with the effective molecular weight calculated from those extensional relaxation times, even with two different reduced concentrations, as discussed below.

Comparing our two backbones, we might expect a priori that the 6M PEO would provide more drag reduction than the 6.7M PAM for two potential reasons. First, PEO has a longer effective length per unit mass than PAM due to the additional weight of PAM's side groups, leading to a higher extensibility.[14] Second, relatedly, PEO has a lower overlap concentration at equilibrium than PAM at similar molecular weights, indicating that at the a constant additive loading by mass chosen for comparison, PEO has a greater pervaded volume of solution when in its coil state. See Chapter 2 for a more extensive discussion of the differences between PEO and PAM in extensional flow and chain scission. Despite lower reduced concentration (c/c^* of 0.05 for PAM, 0.12 for PEO) and the shorter extended length (190,000 backbone atoms for PAM, 410,000 for PEO), PAM still demonstrated similar levels of drag reduction as a function of effective molecular weight of the backbone during degradation (Figure 3.8) and retained higher drag reduction after 10 passes of degradation. Additionally, in contrast to the results observed in chain scission in a pump (Chapter 2), we observed similar degradation in effective molecular weight for both PEO and PAM, where previously PAM degradation was less severe than that of PEO. The discrepancies in these results may point towards fundamentally different character of the flow in the pump used in Chapter 2 and through the contraction and expansion experienced here.

3.5   Conclusion

Through the combination of extensional rheology and bulk flow measurement, we were able to quantify both drag reduction and extensional relaxation times

of polymer solutions as they degraded, and monitor the relationship between the effective molecular weight and observed drag reduction relative to water.

Simultaneous particle image velocimetry and bulk flow measurements will allow for connection of the micro-scale effects of polymers on turbulent structures to the observed bulk drag reduction, and allow further evaluation of the theories developing on the mechanisms of turbulent drag reduction via simulations. Comparing the extensional properties of the solutions with their direct effects on drag reduction will inform better design of polymer additives and expansion of the design space of end-associative polymers tailored to maximize drag reduction and minimize permanent chain scission. Future studies have an opportunity to reveal at multiple length and energy scales the interactions of polymers and turbulence by partnering rheology and PIV with the theoretical framework of resolvent analysis.

References

[1] M. D. Graham. "Drag Reduction and the Dynamics of Turbulence in Simple and Complex Fluids". In: *Physics of Fluids* 26.10 (Oct. 2014), p. 101301. ISSN: 1070-6631, 1089-7666. DOI: 10.1063/1.4895780. URL: http://scitation.aip.org/content/aip/journal/pof2/26/10/10.1063/1.4895780 (visited on 03/17/2016).

[2] S. U. Choi, Y. I. Cho, and K. E. Kasza. "Degradation Effects of Dilute Polymer Solutions on Turbulent Friction and Heat Transfer Behavior". In: *Journal of Non-Newtonian Fluid Mechanics* 41.3 (Feb. 1992), pp. 289–307. ISSN: 03770257. DOI: 10.1016/0377-0257(92)87003-T. URL: https://linkinghub.elsevier.com/retrieve/pii/037702579287003T (visited on 11/19/2020).

[3] T. Moussa and C. Tiu. "Factors Affecting Polymer Degradation in Turbulent Pipe-Flow". In: *Chemical Engineering Science* 49.10 (May 1994), pp. 1681–1692. ISSN: 0009-2509. DOI: 10.1016/0009-2509(93)E0029-C.

[4] J. M. J. Den Toonder et al. "Degradation Effects of Dilute Polymer Solutions on Turbulent Drag Reduction in Pipe Flows". In: *Applied scientific research* 55.1 (1995), pp. 63–82. URL: http://link.springer.com/article/10.1007/BF00854224 (visited on 05/05/2016).

[5] V. N. Kalashnikov. "Degradation Accompanying Turbulent Drag Reduction by Polymer Additives". In: (2002), p. 18.

[6] M. W. Liberatore et al. "Turbulent Drag Reduction of Polyacrylamide Solutions: Effect of Degradation on Molecular Weight Distribution". In: (2004), p. 10.

[7] E. J. Soares. "Review of Mechanical Degradation and De-Aggregation of Drag Reducing Polymers in Turbulent Flows". In: *Journal of Non-Newtonian Fluid Mechanics* 276 (Feb. 2020), p. 104225. ISSN: 03770257. DOI: 10.1016/j.jnnfm.2019.104225. URL: https://linkinghub.elsevier.com/retrieve/pii/S0377025719304197 (visited on 11/19/2020).

[8] M.-H. Wei et al. "Megasupramolecules for Safer, Cleaner Fuel by End Association of Long Telechelic Polymers". In: *Science* 350.6256 (Oct. 2, 2015), pp. 72–75. ISSN: 0036-8075, 1095-9203. DOI: 10.1126/science.aab0642. URL: http://www.sciencemag.org/cgi/doi/10.1126/science.aab0642 (visited on 03/17/2016).

[9] M. D. Graham. "Drag Reduction in Turbulent Flow of Polymer Solutions". In: *Rheology Reviews* 2 (2004), pp. 143–170.

[10] "Some Distinctive Rheological Concepts and Phenomena". In: *Rheology Series*. Ed. by R. Tanner and K. Walters. Vol. 7. Elsevier, 1998, pp. 159–186. ISBN: 978-0-444-82945-0. DOI: 10.1016/S0169-3107(98)

80008-7. URL: https://linkinghub.elsevier.com/retrieve/pii/ S0169310798800087 (visited on 04/28/2022).

[11] B. A. Toms. "Some Observations on the Flow of Linear Polymer Solutions through Straight Tubes at Large Reynolds Numbers". In: *Proceedings of the International Congress on Rheology* II (1949), pp. 135–141.

[12] B. A. Toms. "On the Early Experiments on Drag Reduction by Polymers". In: *Physics of Fluids* 20.10 (1977), S3. ISSN: 00319171. DOI: 10. 1063/1.861757. URL: http://scitation.aip.org/content/aip/ journal/pof1/20/10/10.1063/1.861757 (visited on 03/18/2016).

[13] C. M. White and M. G. Mungal. "Mechanics and Prediction of Turbulent Drag Reduction with Polymer Additives". In: *Annual Review of Fluid Mechanics* 40.1 (Jan. 2008), pp. 235–256. ISSN: 0066-4189, 1545-4479. DOI: 10.1146/annurev.fluid.40.111406.102156. URL: http://www. annualreviews.org/doi/abs/10.1146/annurev.fluid.40.111406. 102156 (visited on 12/10/2015).

[14] L. Xi. "Turbulent Drag Reduction by Polymer Additives: Fundamentals and Recent Advances". In: *Physics of Fluids* 31.12 (Dec. 1, 2019), p. 121302. ISSN: 1070-6631, 1089-7666. DOI: 10.1063/1.5129619. URL: http://aip.scitation.org/doi/10.1063/1.5129619 (visited on 07/13/2021).

[15] P. Virk. "The Toms Phenomenon - Turbulent Pipe Flow of Dilute Polymer Solutions". Cambridge, MA: Massachusetts Institute of Technology, Nov. 1966. 454 pp. URL: https://dspace.mit.edu/bitstream/ handle/1721.1/15484/11163935-MIT.pdf?sequence=2 (visited on 07/07/2016).

[16] P. S. Virk et al. "The Toms Phenomenon: Turbulent Pipe Flow of Dilute Polymer Solutions". In: *Journal of Fluid Mechanics* 30.02 (1967), pp. 305–328. URL: http://journals.cambridge.org/abstract_ S0022112067001442 (visited on 03/17/2016).

[17] P. S. Virk, H. S. Mickley, and K. A. Smith. "The Ultimate Asymptote and Mean Flow Structure in Toms' Phenomenon". In: *Journal of Applied Mechanics* 37.2 (1970), p. 488. ISSN: 00218936. DOI: 10.1115/1.3408532. URL: http://AppliedMechanics.asmedigitalcollection.asme.org/ article.aspx?articleid=1399383 (visited on 08/18/2016).

[18] P. S. Virk. "Drag Reduction Fundamentals". In: *AIChE Journal* 21.4 (July 1975), pp. 625–656.

[19] C. M. White, Y. Dubief, and J. Klewicki. "Re-Examining the Logarithmic Dependence of the Mean Velocity Distribution in Polymer Drag Reduced Wall-Bounded Flow". In: *Physics of Fluids* 24.2 (Feb. 2012), p. 021701. ISSN: 1070-6631, 1089-7666. DOI: 10.1063/1.3681862. URL:

`http://aip.scitation.org/doi/10.1063/1.3681862` (visited on 09/27/2019).

[20] J. M. Lopez, G. H. Choueiri, and B. Hof. "Dynamics of Viscoelastic Pipe Flow at Low Reynolds Numbers in the Maximum Drag Reduction Limit". In: *Journal of Fluid Mechanics* 874 (Sept. 10, 2019), pp. 699–719. ISSN: 0022-1120, 1469-7645. DOI: `10.1017/jfm.2019.486`. URL: `https://www.cambridge.org/core/product/identifier/S0022112019004865/type/journal_article` (visited on 06/16/2020).

[21] M. D. Warholic, G. M. Schmidt, and T. J. Hanratty. "The Influence of a Drag-Reducing Surfactant on a Turbulent Velocity Field". In: *Journal of Fluid Mechanics* 388 (June 1999), pp. 1–20. ISSN: 1469-7645, 0022-1120. DOI: `10.1017/S0022112099004498`. URL: `https://www.cambridge.org/core/journals/journal-of-fluid-mechanics/article/abs/influence-of-a-dragreducing-surfactant-on-a-turbulent-velocity-field/61C146D81503049603D3C6A050C84F98` (visited on 04/28/2022).

[22] M. D. Warholic et al. "A Study with Particle-Image Velocimetry of the Influence of Drag-Reducing Polymers on the Structure of Turbulence". In: *Experiments in Fluids* 31.5 (Nov. 1, 2001), pp. 474–483. ISSN: 0723-4864, 1432-1114. DOI: `10.1007/s003480100288`. URL: `http://link.springer.com/10.1007/s003480100288` (visited on 04/29/2022).

[23] C. M. White, V. S. R. Somandepalli, and M. G. Mungal. "The Turbulence Structure of Drag-Reduced Boundary Layer Flow". In: *Experiments in Fluids* 36.1 (Jan. 1, 2004), pp. 62–69. ISSN: 0723-4864, 1432-1114. DOI: `10.1007/s00348-003-0630-0`. URL: `http://link.springer.com/10.1007/s00348-003-0630-0` (visited on 04/29/2022).

[24] D. Samanta et al. "Elasto-Inertial Turbulence". In: *Proceedings of the National Academy of Sciences* 110.26 (June 25, 2013), pp. 10557–10562. ISSN: 0027-8424, 1091-6490. DOI: `10.1073/pnas.1219666110`. URL: `http://www.pnas.org/cgi/doi/10.1073/pnas.1219666110` (visited on 08/26/2016).

[25] L. Xi and M. D. Graham. "Dynamics on the Laminar-Turbulent Boundary and the Origin of the Maximum Drag Reduction Asymptote". In: *Physical Review Letters* 108.2 (2012). DOI: `10.1103/PhysRevLett.108.028301`. URL: `http://link.aps.org/doi/10.1103/PhysRevLett.108.028301`.

[26] G. H. Choueiri, J. M. Lopez, and B. Hof. "Exceeding the Asymptotic Limit of Polymer Drag Reduction". In: *Physical Review Letters* 120.12 (Mar. 19, 2018). ISSN: 0031-9007, 1079-7114. DOI: `10.1103/PhysRevLett.120.124501`. URL: `https://link.aps.org/doi/10.1103/PhysRevLett.120.124501` (visited on 05/17/2019).

[27] B. J. McKeon and A. S. Sharma. "A Critical-Layer Framework for Turbulent Pipe Flow". In: *Journal of Fluid Mechanics* 658 (Sept. 2010), pp. 336–382. ISSN: 0022-1120, 1469-7645. DOI: `10.1017/S002211201000176X`. URL: `http://www.journals.cambridge.org/abstract_S002211201000176X` (visited on 03/17/2016).

[28] B. J. McKeon, A. S. Sharma, and I. Jacobi. "Experimental Manipulation of Wall Turbulence: A Systems Approacha)". In: *Physics of Fluids (1994-present)* 25.3 (2013), p. 031301. URL: `http://scitation.aip.org/content/aip/journal/pof2/25/3/10.1063/1.4793444` (visited on 08/09/2016).

[29] R. Learsch. "Investigation in Experimental Conditions and Automation of Dripping-onto-Substrate Rheology". American Chemical Society Spring Meeting (San Diego, CA). Mar. 23, 2022.

Chapter 4

EFFECTS OF SOLVENT QUALITY AND VISCOSITY ON THE BEHAVIOR OF END-ASSOCIATIVE POLYMERS

4.1   Introduction

Hydrocarbon fluids in vehicles, such as many fuels, lubricants, and heat transfer fluids, can pose hazards upon accidental release, particularly when in the form of sprays, where drops can evaporate and contribute to flammable gases in the presence of potential spark sources.[1,2] Using long polymer additives as mist control agents, preventing the formation of small droplets that readily evaporate and biasing droplet distributions towards larger droplets, has been known as a mechanism for preventing hydrocarbon fluid fires;[3–6] however, long polymers are subject to degradation due to high shear forces during pumping,[7–10] which occurs in transport to and use in a vehicle.

Prior work in the Kornfield group for preventing jet fuel fires utilized long end-associative telechelic polycyclooctadiene (PCOD) to act as megasupramolecular mist-control agents that survive pumping events by disassociating during what would be a chain scission event for a covalently bonded long polymer and reassociating afterward.[6,11,12] Much as in jet fuel, lubricant mists are a potential fire hazards, motivating adapting this polymer system for mist control in polyalphaolefin (PAO) lubricant and heat transfer fluid.

Using the megasupramolecular PCOD system in PAO presents a number of challenges due to differences in the solvent compared to jet fuel. Both the backbone and end-groups are less soluble in PAO than in jet fuel and other hydrocarbon solvents studied by our group; and PAO, like many other lubricants, is substantially more viscous than jet or diesel fuel. Effects of variations

in chemical structure of backbone and end-group on solubility is planned to be discussed in the thesis of Hojin Kim. Here, the effects of solvent quality and viscosity on non-associative and end-associative polymers are investigated using the backbone and end-group structures developed by Dr. Ming-Hsin Wei.[6,12] To inform engineering criteria for further development of additives for mist control in lubricant systems, this study integrates efects on shear and extensional flow. In collaboration with Dr. Jacob Temme at Army Research Laboratory, we examine the effects of a homopolymer and an end-associative polymer on spray breakup in relation to their effects on shear and extensional properties.

Relationship between Extensional Properties and Mist Control

High molecular weight polymeric additives have been proposed as mist-control agents (as known as anti-mist agents) over the past 50 years for hydrocarbon fluids as a route to suppressing highly flammable fine-droplet mists.[3,5,6] The effect of these polymers is two-fold—the average droplet size is increased[3,4,13,14] and, in particular, small satellite droplets are substantially suppressed.[10,15] The driving force for both of these effects is hypothesized to be the resistance of the polymer additive to the highly extensional flow during ligament pinchoff, which has been experimentally supported.[13,16] Imaging of sprays of viscoelastic fluids with sufficiently high resistance to extension (characterized as a high extensional relaxation time) demonstrates thin filaments connecting proto-drops to larger fluid formations, resulting in many would-be satellite droplets returning to the main drops.[10,15,16]

The improvement in mist control, however, is lost with degradation of the polymer due to mechanical chain scission (such as during pumping) as the efficacy is directly tied to the extensional properties and thus the molecular

weight.[10,13,17,18] See Chapter 1 for further description of the physics of polymeric mist control and Chapter 2 for measurements of how chain scission affects extensional properties.

Effects of Solvent Quality and Viscosity in Extension and Chain Scission

The body of literature on extension of chains contains multiple, contradicting discussions of the effects of solvent quality on extensional properties of polymer solutions, likely due to the complexity of interpreting polymer conformations under different flow conditions.[19] For example, the critical extension rate for observations of birefringence ($\dot{\epsilon}_c$), which is tied to the coil-stretch transition, was initially predicted to depend on the solvent quality dependent through the relationship between $\dot{\epsilon}_c$ and molecular weight (M), of the form $\dot{\epsilon}_c \sim M^{-3\nu}$, where ν is the Flory exponent (a measure of the solvent quality).[20] Follow-up experimental results showed universality of the molecular weight dependence regardless of solvent quality, i.e., $\dot{\epsilon}_c \sim M^{-1.5}$,[21] and the theory was revised to a dependence of the form $\dot{\epsilon}_c \sim M^{-(1+\nu)}$, which yields exponents in the range of -1.5 to -1.6 across the range of solvent qualities for flexible polymers from Θ solvent ($\nu = 0.5$) to good solvent ($\nu = 0.6$),[20,22] although literature results report a larger range of exponents.[20] Solvent viscosity, on the other hand, has a relatively clear role in extensional flow—increasing solvent viscosity increases extensional relaxation time, based on theory[23] and on experiments.[21]

Prior literature has demonstrated that chain scission increases with a poorer solvent in laminar and turbulent flow.[24,25] In a poorer solvent, the chains are more compact and thus from the above, we would expect that coil-stretch transition would occur at higher extensional rates (more difficult to stretch) and that the ratio of extended length to the coil size would be larger. If
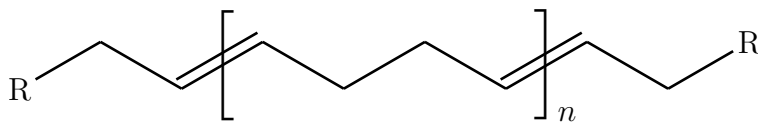
Scheme 4.1: Telechelic polycyclooctadiene (PCOD), end-groups R in Scheme 4.2.

increased chain scission is occurring, it implies that the extensional rate at scission is lower for the poor solvent, indicating that there is possibly increased drag from the solvent on the backbone occurring during the strong extension events or due to the poorer solubility. When designing potential additives, poor solvent quality thus imposes a limit on the molecular weight of the polymer additive.

In this study, I will simultaneously be considering the effects of solvent quality and viscosity on the behavior of the PCOD backbone in shear and extension, as well as the changes in association strength due to changing solvents.

4.2   Experimental Methods

Materials

Polycyclooctadiene samples prepared by Hojin Kim, utilizing the methods outlined in Appendix B using cyclooctadiene purified using zeolite molecular sieving. Decahydronaphthalene was acquired from Sigma-Aldrich. Polyalphaolefin compliant with MIL-PRF-87252E (BRAYCO 889 MIC) was acquired from QC Lubricants.

Telechelic polycyclooctadiene samples of the form in Scheme 4.1 were used in this study, where R groups are either a diacid group (Scheme 4.2(a), DA), a dibase group (Scheme 4.2(b), DB), or a C6 alkane chain (non-associative), as appropriate.

(a) R: Di-acid (DA) end-group

(b) R: Di-base (DB) end-group
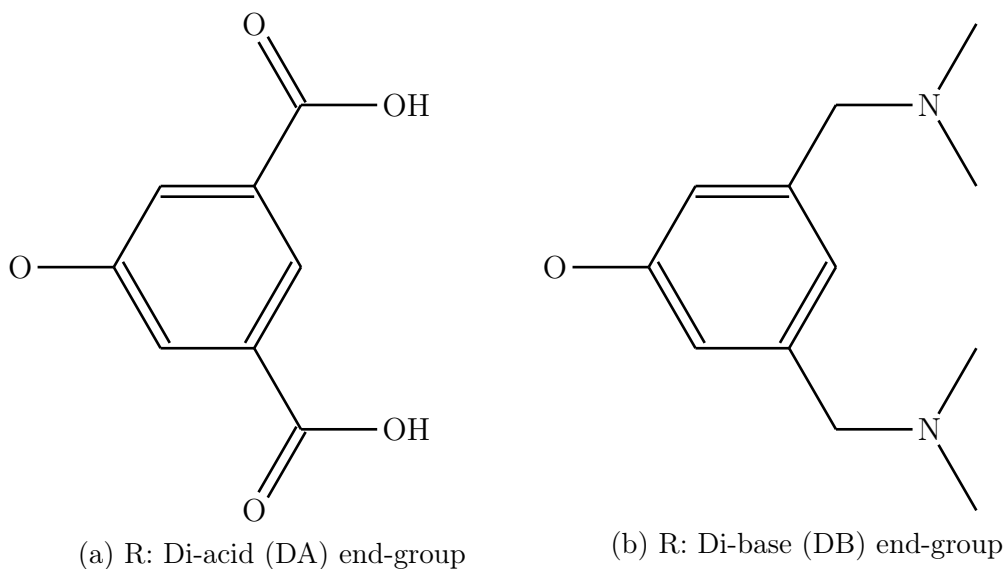
Scheme 4.2: Associative end-groups for telechelic polycyclooctadiene, "R" in Scheme 4.1.

Rheological Solution Preparation

To examine th eeffect of solvent quality and viscosity, three solvents were used. Of technological interest, PAO was selected as one of the three. As a partially unsaturated solvent that was known as a good solvent for polycyclooctadiene, decalin was selected as one of the solvents. To create a partially unsaturated solvent with shear viscosity at 15°C matched to PAO ($\sim$8.8±0.1 mPa-s at 15 °C), the third solvent was a mixture of decalin and 9.3 wt % 5 kg/mol polybutadiene.

Stock solutions in transparent glass vials were prepared by measuring a desired mass of solid polymer samples and adding to 5-10 mL, measuring the mass, of decahydronapthalene (decalin) or polyalphaolefin (PAO) as appropriate. For decalin stock solutions, 0.1 wt % butylated hydroxytoluene (BHT) was added as an anti-oxidant. For PAO samples, BHT was added at 5 times the polymer concentration. BHT acts as a solubilizer for when associative end-groups were present in addition to its anti-oxidant properties as discovered by Hojin Kim,[26] and was added to both the non-associative and associative solutions in PAO to

keep solvent viscosity and quality consistent between these samples. Solvent viscosity and extensional behavior of PAO alone was not substantially modified by the addition of 5 wt % of BHT. BHT was added to solvents prior to heating. Stock solutions were heated using two infrared (IR) lamps while rolling at 10 rotations per minute. Stock solutions were rolled under the IR heating until visibly homogeneous—3–5 days for samples in decalin and 5-10 days in PAO. After stock solutions preparation, dilutions were made by measuring out stock solution by mass into a separate vial and adding decalin or PAO until the desired PCOD concentration was reached. Diluted samples were rolled for at least 8 hours.

Shear rheological measurements were conducted at 15°C because the extensional measurements occur at ambient conditions (15 ± 1°C); however, solutions of high molecular weight PCOD in PAO were observed to precipitate out of solution after extended storage at these temperatures. In the case of PAO dilutions, all samples were heated with rolling until immediately prior to use for shear measurements (follow by 5 min at 15 °C after loading into the cone-and-plate geometry as a part of equilibration on the rheometer) or $\sim$30 minutes prior to use for extensional measurements, to avoid temperature inhomogeneties in the sample during an experiment.

For overlap concentration measurements, dilutions in decalin were first measured in shear, and then 9.3 wt % (measured relative to the decalin solvent only) of 5 kg/mol polybutadiene (Sigma-Aldrich), diluting the polymer concentration relative to the original solution. The resulting concentration of PCOD was used in intrinsic viscosity calculations. For solutions used in matched non-associative and associative shear and extensional measurements, stock solutions of non-associative and associative PCOD in decalin were measured to result in the correct polymer concentration after addition of the 9.3 wt %

5kg/mol polybutadiene, and then the polybutadiene was added. In both cases, dilutions were rolled overnight.

For the solutions of associative PCOD containing both diacid (DA) and dibase (DB) telechelic PCOD, separate stock solutions were prepared as described above, and measured aliquots of each stock solution were added to a vial to result in a DA:DB ratio within 1% of stoichiometry, and then these solutions were diluted with the appropriate solvent to the desired concentration.

Shear Rheological Measurements

Shear viscosity measurements were performed on an Anton Paar MCR 302 WESP rheometer using a cone-and-plate fixture of 50 mm diameter and 2.007° angle, with a truncation of 0.207 mm. Samples were loaded by depositing 1.1 mL of the sample on the center of the plate, lowering the cone to 0.217 mm, removing excess to create a flat edge, and then lowering to 0.207 mm to create a spherical edge condition. The plate was cooled to 15 $\pm$ 0.1 °C using a Peltier plate to regulate temperature and samples were allowed to thermally equilibrate and relax for 5 min after reaching 15 °C. Shear rate sweeps were performed from 1 to 100 1/s. The sample edge was examined to check for evidence of evaporation and none was observed.

Dripping-onto-Substrate Extensional Rheometry (DoSER)

A dripping-onto-substrate extensional rheometry (DoSER) instrument was constructed by Robert Learsch and Red Lhota consisting of a GSVitec MultiLED G8 with QT lamp head (12000 lumen light source, Figure 1.7**A**), a Harvard Elite 11 syringe pump on an adjustable track (solution delivery, **B**), Photron FASTCAM Nova S12 type 1000K-M-32GB (high-speed camera, **C**) equipped with an optical train as described below, and a custom holder for aluminum substrates (**D**). The optical train consisted of a Resolve4K 7:1 Zoom

Figure 1.7: Schematic of dripping-onto-substrate extensional rheometer (not to scale). (repeated from page 14)

Video microscope lens, two rear projection lenses, a 1.0x objective lens, and a coupler, resulting in a resolution limit at full zoom of 3.5 µm (**E**). The camera was operated at 25,000 frames per second with a shutter speed of 150,000 Hz (i.e., 7 µs exposure). The light passes through a diffuser before reaching the measurement plane (**F**).

A syringe with a 22G blunt-tip polytetrafluoroethylene needle (outer diameter 1.0 mm) was mounted to the syringe pump. The substrate was positioned at a height of 2.8 mm below the tip of the needle, corresponding to a height-to-needle-diameter ratio of 3 or a height-to-free-drop-diameter ratio of 1, which is within the optimal range for hydrocarbon solutions.[27] Ambient temperature was measured with each experiment and was in the range 15 ± 1 °C.

For each solution, DoSER was performed using the following procedure. An aliquot was slowly loaded into a syringe through a 22G polytetrafluoroethy-

lene blunt-tip needle. The syringe was attached to the syringe pump and the syringe pump was slowly advanced until solution was observed to drip from the needle, and then the needle tip was cleaned. A clean set of aluminum substrates was loaded onto the substrate holder and the first substrate was aligned below the needle tip. The light was turned on and the camera was focused and aligned with the needle tip. The substrate was then raised or lowered to the correct height (as describe above) relative to the needle tip. A drop was dispensed from the needle tip by the syringe pump at a rate of 0.02 mL/min, until the drop was nearly touching the substrate. The syringe pump was stopped prior to droplet-substrate contact. The events of droplet contact through liquid bridge formation and pinchoff were recorded (referred to as an experimental video or "run"). A background video was acquired after each run. A clean substrate was then placed below the needle tip. Dispensing drops onto a clean substrate was repeated until five total runs were recorded. The videos were analyzed using the *dosertools* Python package, described in detail in Appendix A, to obtain the normalized diameter as function of time after the critical time (time of transition between solvent behavior and elastocapillary response). The decay of the normalized diameter is used to evaluate the extensional relaxation time. In our experiments, run-to-run variation on the DoSER instrument was observed to be more significant than errors in fitting–errors in measured relaxation times are thus quantified using the run-to-run variation. Solutions with relaxation times of 0.05 ms and lower were difficult to consistently characterize on our instrument.

Further discussions of DoSER theory and analysis are available in Chapter 1 and Appendix A respectively.

Spray

Spray experiments and analysis were performed by Dr. Jacob Temme and coworkers at the Army Research Laboratory (ARL). Methods, data, and figures included with permission of ARL. Polymers and solutions for spray experiments presented in this chapter were prepared by Hojin Kim with concentrations based on measured rheological properties of preliminary solutions (Robert Learsch measured extension properties, I measured shear for these preliminary solutions).

The spray experiments were performed in an optically accessible atmospheric chamber. Two fields of view were observed using a Phantom SA-X2 high-speed camera paired with a Zeiss 50mm lens: the first from the nozzle tip to approximately 80 mm downstream and the second centered 30-35 mm downstream and 25 mm to the side of the orifice. In the first field of view, images were recorded at 10 kHz. The second field of view was imaged with high enough magnification to resolve features as small as 200 µm with recordings at 35 kHz. In each experiment, pressurized fluid at 120 psi (0.83 MPa) was released through a 5 mm orifice. Spray angle analysis was performed by MATLAB-based image analysis of spray videos (Figure 4.1), modified by ARL from Engine Combustion Tools.[28]

4.3   Results

Solvent Quality

Intrinsic viscosity as a function of weight-average molecular weight was measured for non-associative PCOD in three solvents: decalin, decalin with 9.3 wt % 5kg/mol polybutadiene added (9.3 wt % 5k PB decalin), and PAO (Figure 4.2). The intrinsic viscosity of 1Mg/mol PCOD in PAO was not measurable due to limited solubility. Logarithmic fits of the Kuhn-Mark-Houwink-
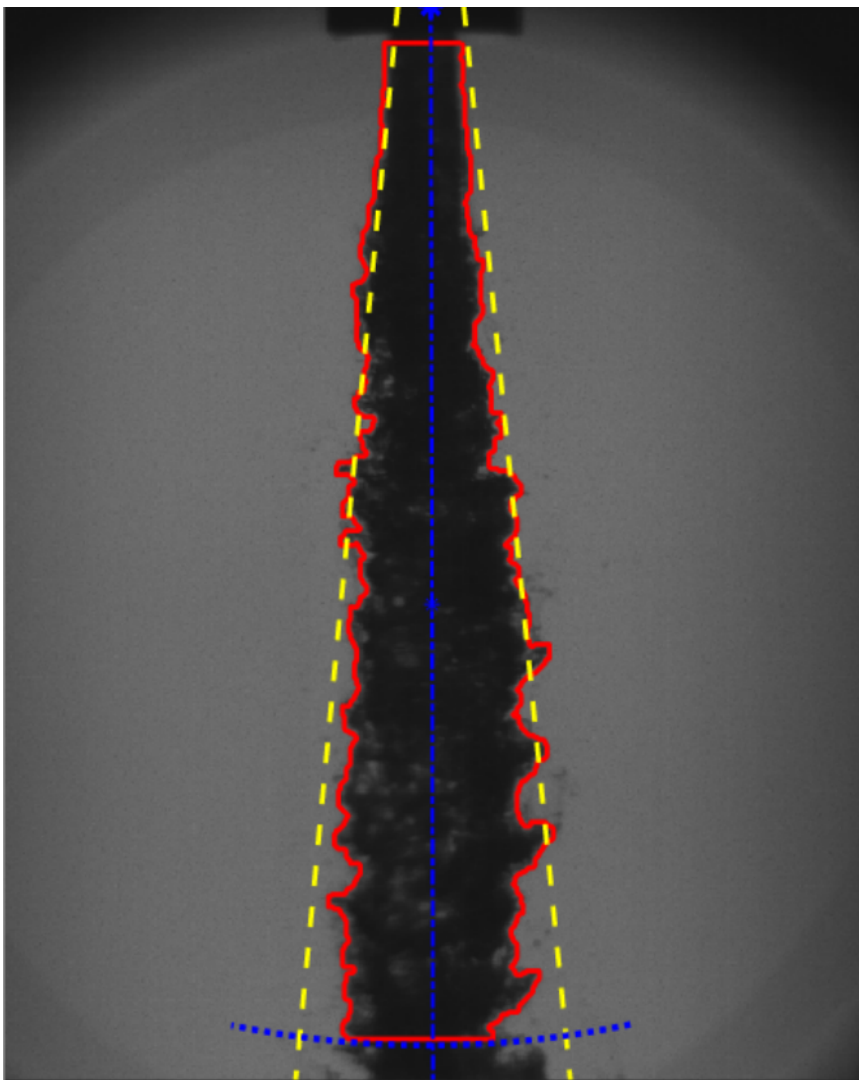
Figure 4.1: Example image for determination of spray angle. Red indicates edge of spray as determined by image analysis. Yellow indicates calculated spray angle.

Solvent	$K * 10^4$ (1/wt %)	a
decalin	5.5	0.66 ± 0.03
9.3 wt % 5k PB decalin	6.5	0.59 ± 0.02
PAO	1.3	0.68 ± 0.04

Table 4.1: Measured Kuhn-Mark-Houwink-Sakurada prefactor (K) and exponent (a) (Equation 1.2) for polycyclooctadiene in decalin, decalin with 9.3 wt % 5 kg/mol polybutadience added (9.3 wt % 5k PB decalin), and polyalphaolefin (PAO) at 15°C. ($a \pm$ one standard deviation, K standard deviations were less than 10^{-8})

Sakurada equation (Equation 1.2) to the measured data produced K and a that show PAO has the highest value of a among the three solvents (Table 4.1), although the values for decalin and PAO are within one standard deviation for the fit.

Recasting the intrinsic viscosity as overlap concentration using Equation 1.1, we observed much higher overlap concentrations for the same PCOD sample in PAO than in decalin (Figure 4.3). At the highest molecular weight in this study that was measurable in all three solvents, the overlap concentration in decalin is three times greater than in decalin.

Shear Viscosity of End-Associative Solutions

The effect of end-groups on the shear viscosity was measured for solutions of ~670 kg/mol PCOD in the three solvents of interest at three reduced concentrations ($c/c^* = 0.125, 0.25, 0.5$) where c^* denotes the overlap concentration of the corresponding non-associative polymer, 670 kg/mol non-associative PCOD in that solvent. Comparing solutions at matched c/c^* for the non-associative polymer corresponds to matching the volume pervaded by the polymer alone
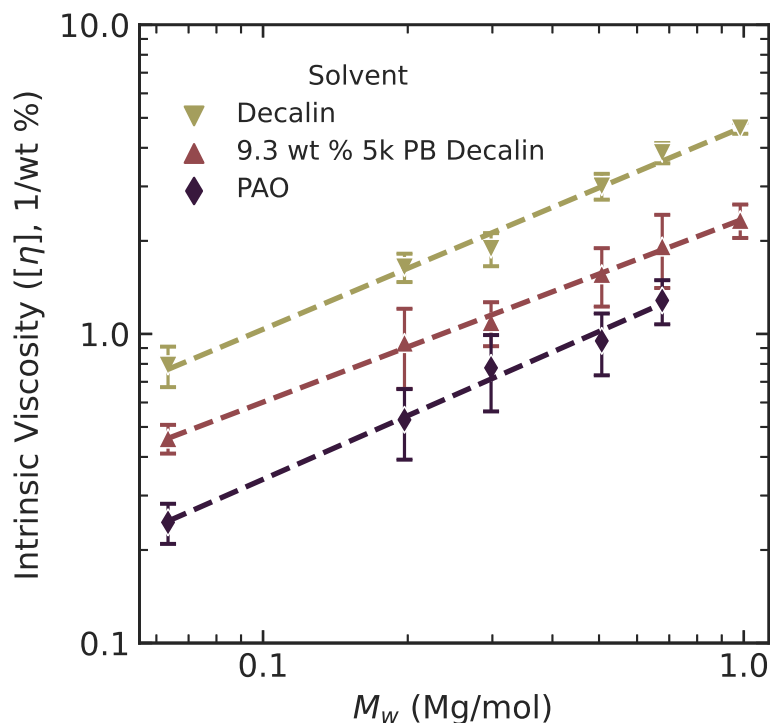
Figure 4.2: Intrinsic viscosity ([η], 1/wt%) of polycyclooctadiene as a function of weight-average molecular weight (M_w, Mg/mol) in decalin, decalin with 9.3 wt % 5kg/mol polybutadiene added (9.3 wt % 5k PB decalin), and polyalphaolefin (PAO). Dashed lines represent the Kuhn-Mark-Houwink-Sakurada (KMHS) equation (Equation 1.2) fits to the data for each solvent at 15°C. KMHS fits are found in Table 4.1

(without end-groups), which requires greater mass concentration for solvents in which the chain adopts a more compact conformation (670 kg/mol PCOD has a c^* of 0.2, 0.4, and 0.6 wt% for decalin, 9.3 wt % 5k PB decalin, and PAO, respectively). For each solvent and c/c^*, the specific viscosity of non-associative PCOD was compared to that of DA PCOD, DB PCOD, and a stoichiometric mixture of DA and DB PCOD (Figure 4.4).

For comparison with spray experiments described below, a separate batch of DA, DB, and 1:1 DA:DB 670 kg/mol solutions in PAO was prepared and characterized at concentrations of 0.05 wt % and 0.5 wt % (Figure 4.5).
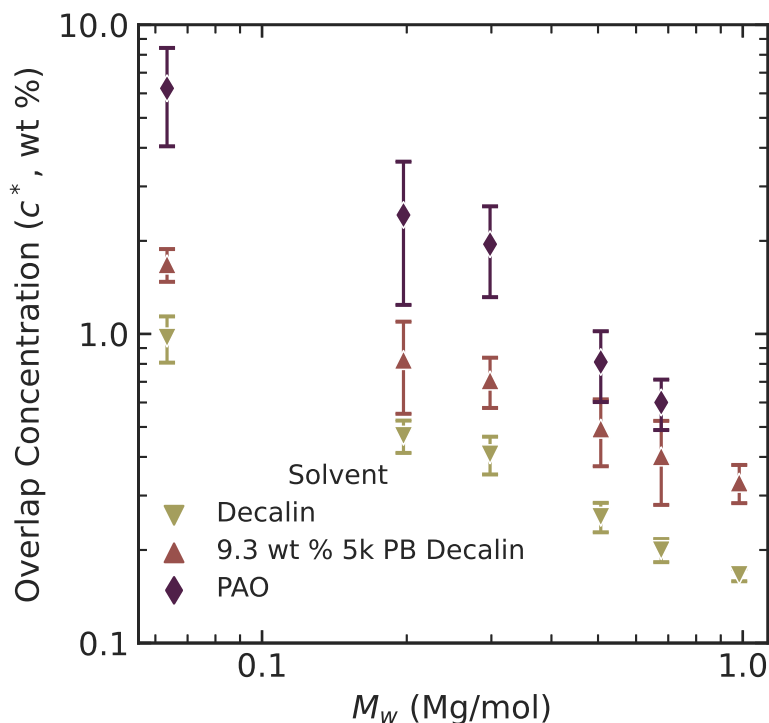
Figure 4.3: Overlap concentration (c^*, wt%) of polycyclooctadiene as a function of weight-average molecular weight (M_w, Mg/mol) in decalin, decalin with 9.3 wt % 5kg/mol polybutadiene added (9.3 wt % 5k PB decalin), and polyalphaolefin (PAO) at 15°C. Error bars indicate 95% confidence intervals.

Extensional Relaxation Time of End-Associative Solutions

Normalized diameter (D/D_0) was measured by image analysis of high-speed videos of dripping-onto-substrate extensional rheometry experiments as described in Appendix A. Fits to the normalized diameter in the elastocapillary regime as described in Appendix A were used to determine the extensional relaxation time (λ_E) for each of the solutions measured in the shear rheology in Figure 4.4, in addition to solutions at a $c/c^* = 1$ (Figure 4.6).

Extensional relaxation times of DA, DB, and 1:1 DA:DB 670 kg/mol PCOD in PAO from a separate batch of solutions were measured at additional concentrations (0.05 wt %, corresponding to spray measurements later in this work, and 0.5 wt %) by Robert Learsch—corresponding non-associative PCOD measure-
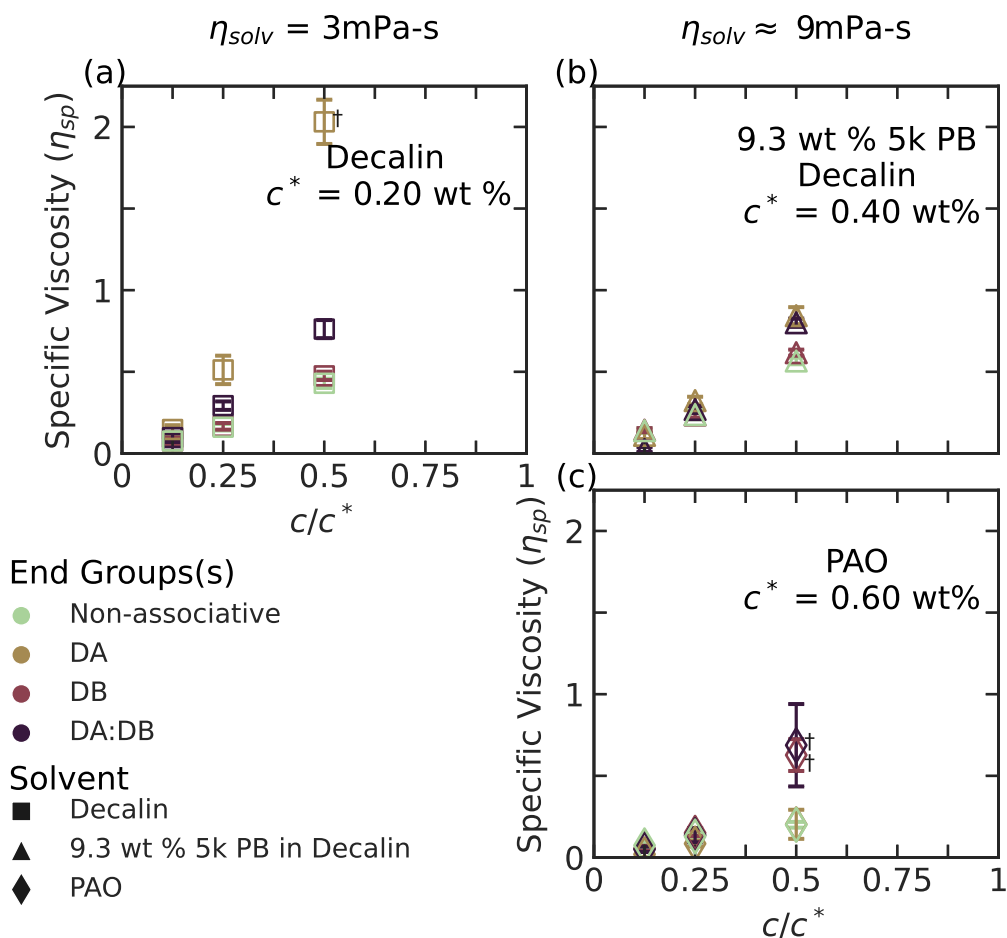
Figure 4.4: Specific viscosity (η_{sp}) averaged over low shear rates as a function of reduced concentration (c/c^*) and presence of end-groups for telechelic 670 kg/mol polycyclooctadiene dissolved in (a) decalin, (b) decalin with 9.3 wt % 5kg/mol polybutadiene added (9.3 wt % 5k PB decalin), and (c) polyalphaolefin (PAO) at 15°C. Error bars indicate 95% confidence intervals. Where error bars are not visible, the corresponding interval is within symbol size. † indicates samples in which shear-thinning was observed.
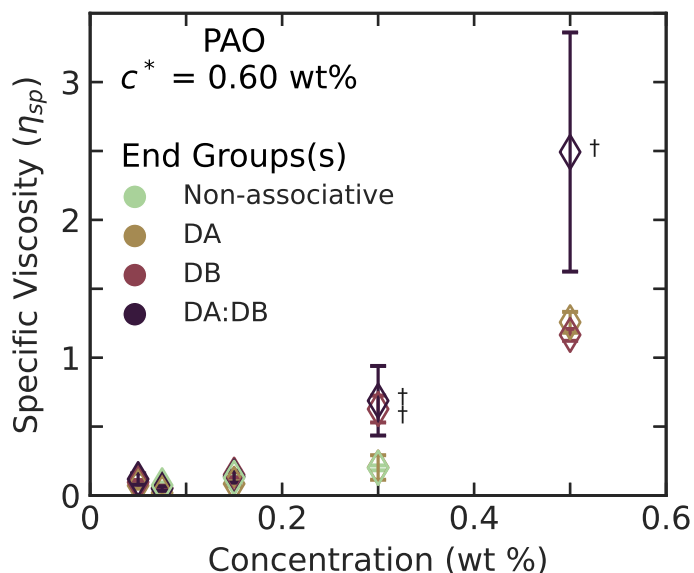
Figure 4.5: Specific viscosity (η_{sp}) averaged over low shear rates as a function of concentration (wt %) and presence of end-groups for telechelic 670 kg/mol polycyclooctadiene dissolved in polyalphaolefin (PAO) at 15°C. Measurements at 0.05 wt % and 0.5 wt % performed with a separate batch of solutions. Error bars indicate 95% confidence intervals. Where error bars are not visible, the corresponding interval is within symbol size. † indicates samples in which shear-thinning was observed.

ments at the same molecular weight and concentrations were not performed (Figure 4.7).

Comparing Sprays with and without Polymer Additives

Measurements and analysis of sprays performed at Army Research Laboratory (ARL) by Dr. Jacob Temme and coworkers.

The spray of polyalphaolefin (PAO) with no additives (left, Figure 4.8) was observed to spread intermittently during instabilities in the observed time period, kicking out thin ligaments that broke up into small droplets down to the resolution limit (200 µm). Adding non-associative 1Mg/mol polycyclooctadiene (PCOD) to PAO modified the spray angle, ligament structure, and droplet formation. Solutions of 0.05 wt % 1 Mg/mol PCOD in PAO (center Figure
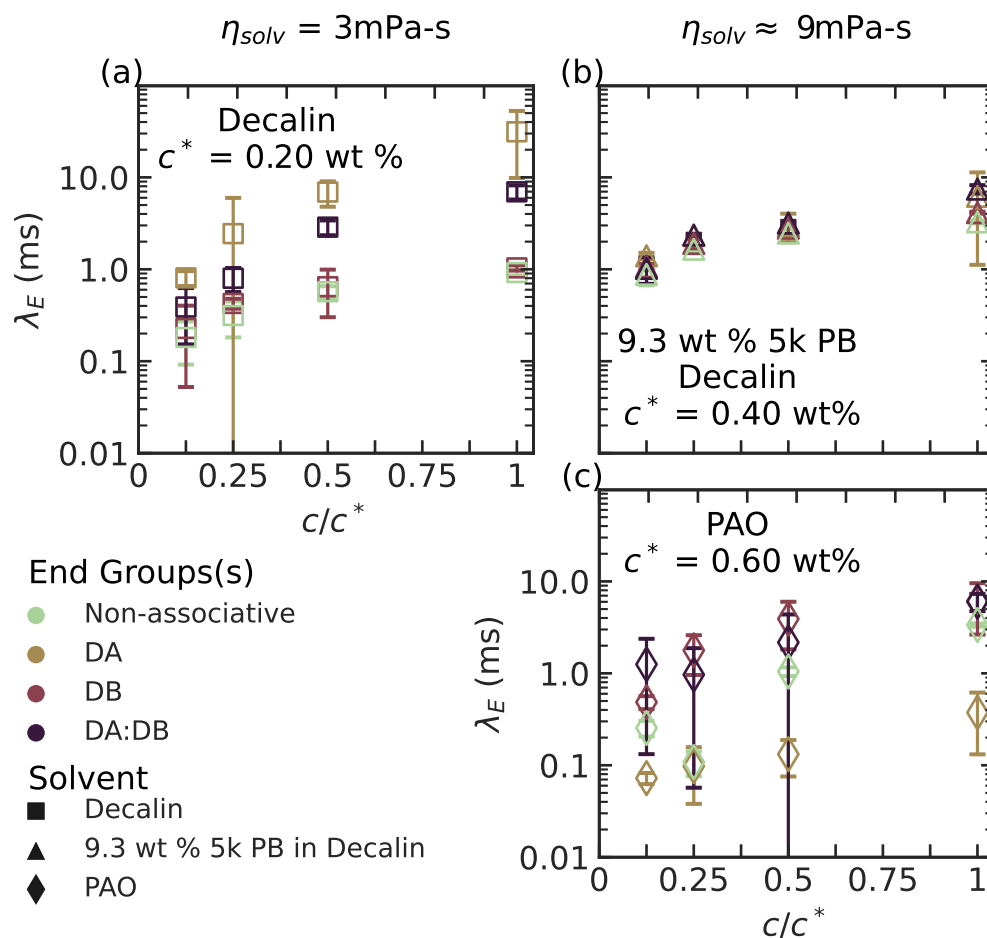
Figure 4.6: Extensional relaxation time (λ_E, ms) as a function of reduced concentration (c/c^*) and presence of end-groups for telechelic 670 kg/mol polycyclooctadiene dissolved in (a) decalin, (b) decalin with 9.3 wt % 5kg/mol polybutadiene added (9.3 wt % 5k PB decalin), and (c) polyalphaolefin (PAO) at 15°C. Error bars indicate 95% confidence intervals representing run-to-run variation in DoSER measurements (fitting errors are substantially smaller). Where error bars are not visible, the corresponding interval is within symbol size.
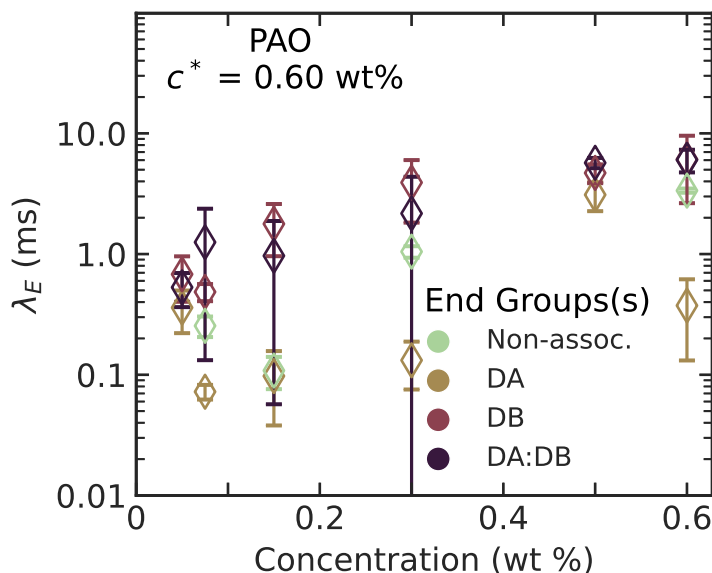
Figure 4.7: Extensional relaxation time (λ_E, ms) as a function of concentration (wt %) and presence of end-groups for telechelic 670 kg/mol polycyclooctadiene dissolved in polyalphaolefin at 15°C. Measurements at 0.05 wt % and 0.5 wt % performed with a separate batch of solutions by Robert Learsch. Error bars indicate 95% confidence intervals representing run-to-run variation in DoSER measurements (fitting errors are substantially smaller). Where error bars are not visible, the corresponding interval is within symbol size.

4.8) demonstrated some instabilities and spreading, though less dramatic than the PAO alone. The ligaments formed were thicker and produced few observable droplets. Solutions of 0.1 wt 1 Mg/mol % PCOD in PAO further modified spreading and increased ligament size, leading to large attached ligaments that stayed close to the main body of the jet.

Quantitative measurement of the spray angle as a function of time demonstrated significant differences between PAO with and without the non-associative additive. PAO with no additives experienced frequent large spray angle events, while adding 0.05 wt % 1 Mg/mol PCOD reduced the amplitude of those events, and 0.01 wt % 1 Mg/mol PCOD suppressed them in the time period observed (Figure 4.9). Averaging over the period observed showed that 0.05 wt% reduced the spray angle by nearly 50 % (Table 4.2). Spray angle is related

PAO   0.05 wt% pCOD   0.1 wt% pCOD
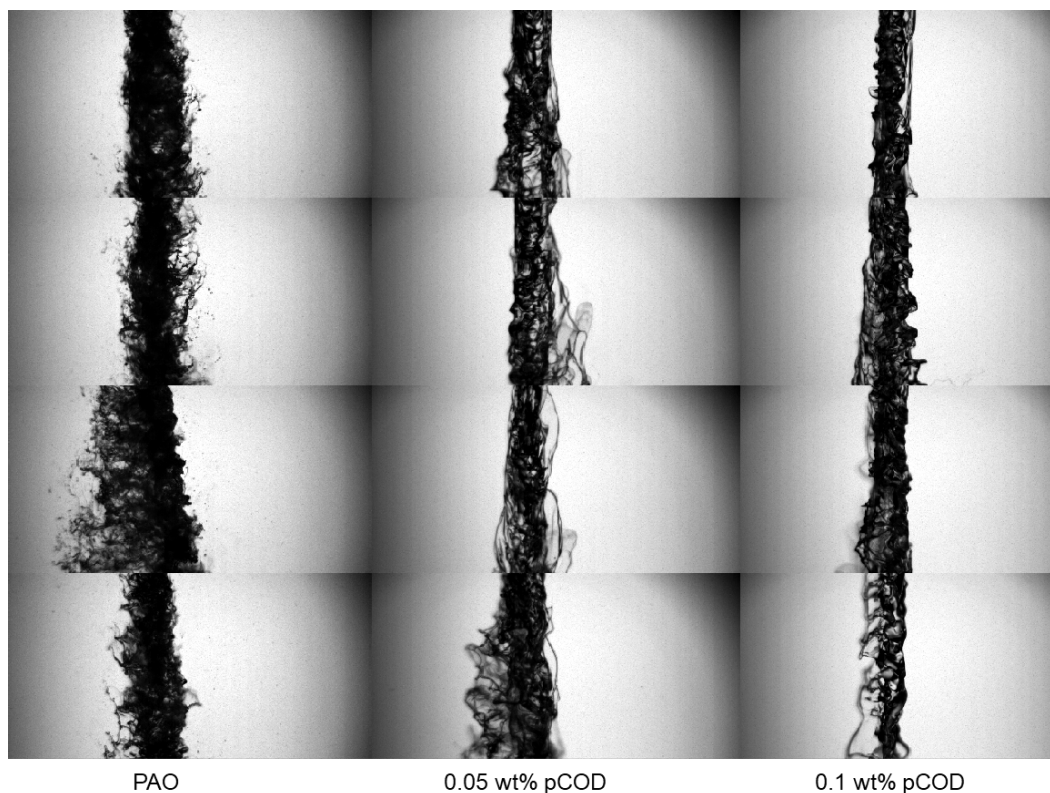
Figure 4.8: Representative spray images 30-35 mm downstream of the orifice for (left to right) PAO, 0.05 wt % 1 Mg/mol PCOD in PAO, 0.1 wt % 1 Mg/mol PCOD in PAO at ambient temperature. Images produced and provided by Dr. Jacob Temme, ARL.

to ignitability—a larger spray angle increases likelihood that a potential spark source will be in range for ignition.

As seen in the representative images in Figure 4.8, the addition of PCOD largely suppressed the formation of droplets in the range resolvable by the camera and optical setup used in these experiments ($> 200 \mu m$). As a result, average droplet diameter was only determinable for the PAO with no additive (Table 4.3). Ligament diameter can act a proxy for expected diameter size—as ligaments detach from the spray, their pinchoff will create droplets of similar diameter (described in Chapter 1). Average ligament diameter increased 30 % with the addition of 0.05 wt % 1 Mg/mol PCOD and 85 % with the addition of 0.1 wt % 1 Mg/mol PCOD (Table 4.3). The formation of ligaments or filaments
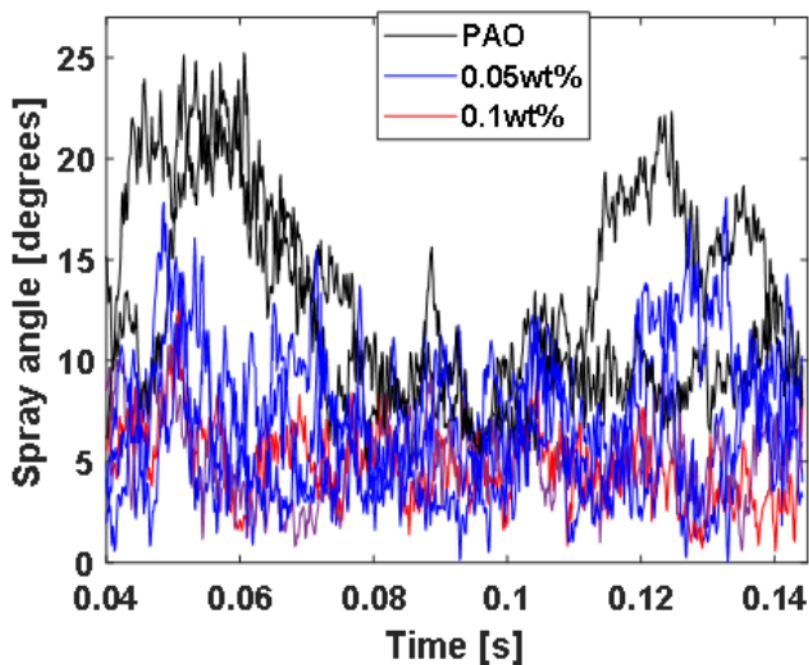
Figure 4.9: Spray angle as a function of time for PAO (black), 0.05 wt %
1 Mg/mol PCOD in PAO (blue), 0.1 wt % 1 Mg/mol PCOD in PAO (red).
Figure produced and provided by Dr. Jacob Temme, ARL.

Table 4.2: Average measured spray angle observed in quasi-steady state jetting
of PAO fluids. Values are ± one standard deviation. Processing performed by
Dr. Jacob Temme, ARL.

Fluid	Average Quasi-Steady State Spray Angle [degrees]
PAO	12.6 ± 0.2
0.05 wt % 1 Mg/mol PCOD in PAO	6.7 ± 0.1
0.1 wt % 1 Mg/mol PCOD in PAO	5.1 ± 0.1

PAO: Polyalphaolefin,
PCOD: Polycyclooctadiene

has been previously tied to ignition suppression, even at concentrations lower
than full droplet suppression.[3]

Adding associative PCOD (specifically 0.03, 0.05, and 0.1 wt % of 1:1 DA:DB

Table 4.3: Average droplet diameter and ligament diameter observed in jetting of PAO fluids. Image analysis performed by Dr. Jacob Temme, ARL.

Fluid	Average Droplet Diameter [μm]	Average Ligament Thickness [μm]
PAO	230	260
0.05 wt % 1 Mg/mol PCOD in PAO	-	340
0.1 wt % 1 Mg/mol PCOD in PAO	-	480

PAO: polyalphaolefin,
PCOD: 1 Mg/mol polycyclooctadiene

PAO   0.03 wt% DA:DB   0.05 wt% DA:DB   0.1 wt% DA:DB
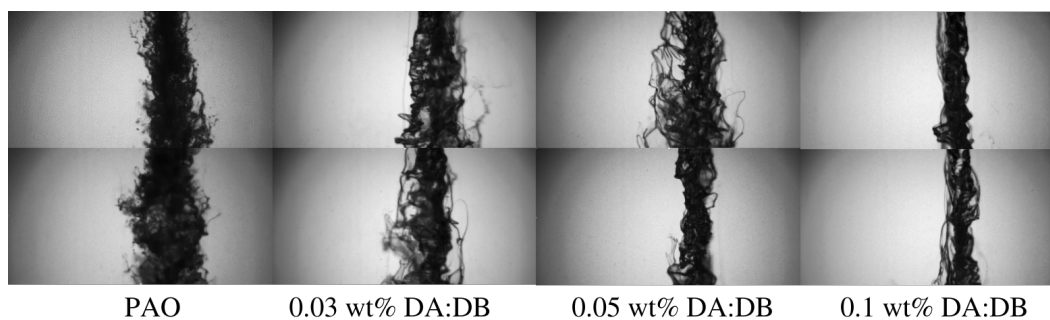
Figure 4.10: Representative spray images 30-35 mm downstream of the orifice for (left to right) PAO, 0.03 wt % DA:DB 670 kg/mol PCOD in PAO, 0.05 wt % DA:DB 670 kg/mol PCOD in PAO, 0.1 wt % DA:DB PCOD 670 kg/mol in PAO. Images produced and provided by Dr. Jacob Temme, ARL.

670 kg/mol PCOD) to PAO had a similar effect as the non-associative (but longer backbone) PCOD. As concentration of polymer additive increased, spray angle decreased, droplet formation was suppressed, and ligament diameter increased (Figure 4.10).

4.4 Discussion

Role of Solvent Quality and Viscosity for Non-associative PCOD in Shear and Extension

The measured solvent quality of PCOD in PAO using the Kuhn-Mark-Houwink-Sakurada exponent yields a Flory exponent (ν) of 0.56, implying PAO is a

better solvent for PCOD than decalin ($\nu = 0.55$) and the 9.3 wt % 5 kg/mol PB decalin ($\nu = 0.53$) (see discussion of the Kuhn-Mark-Houwink-Sakurada equation and the relationship to the Flory exponent in Chapter 1); however, we repeatedly observed solubility issues in PAO, including observations of inhomogeneties forming in solutions stored at 15 °C and lack of sufficient solubility of 1 Mg/mol PCOD to perform intrinsic viscosity measurements. Additionally, the higher overlap concentrations in PAO (and correspondingly the lower intrinsic viscosities) imply a highly compacted coil size compared to decalin. The poor solubility for PCOD in PAO compared to decalin implies that the maximum unimer molecular weight that can survive chain scission will be lower in PAO compared to decalin or jet fuel, motivating further study of these polymers under pumping conditions and adaptation of the backbone to be more soluble.

Our initial hypothesis was that adding low molecular weight PB to decalin would either keep the PCOD solvent quality constant or increase solvent quality relative to decalin alone, based on the similarity between polybutadiene and the PCOD backbone. The exponent and the overlap concentrations for 9.3 wt % 5 kg/mol PB decalin, however, indicate that it is a worse solvent than decalin.

Looking at the shear specific viscosity results (i.e., measuring increase over solvent viscosity), despite matched reduced concentrations (c/c^*), the specific viscosity of non-associative PCOD in decalin statistically significantly exceeds that of PAO at $c/c^* = 0.5$, and the specific viscosity of 9.3 wt % 5 kg/mol PB decalin is further increased over decalin. The relatively lower specific viscosity of the PAO at the same expected pervaded volume of the chains in solution suggests that at finite concentrations, PCOD in PAO is even further collapsed than what is anticipated by matching expected pervaded volumes with c/c^* and thus not contributing as expected to the shear viscosity.

Because PCOD is much less soluble in PAO, particularly as temperature decreases, we must view the extension results as a transient measurement of the properties—because the temperature history was similar among the samples (kept above solubility temperature until removed from heat from equilibration to ambient temperature 30 minutes before measurement), we are still able to compare the effects of concentration and association among PAO samples, as well as assess qualitative differences compared to decalin and decalin with 9.3 wt % 5kg/mol PB.

Comparing extensional relaxation times, one pair of datapoints stands out as either subject to concern over solubility or over sample labeling. Despite having a higher shear viscosity, the $c/c^* = 0.25$ sample of non-associative PCOD in PAO was measured to have a lower extensional relaxation time than the $c/c^* = 0.125$ sample. Two explanations reasonably fit these two points: if the higher concentration sample experienced PCOD precipitating out of solution before measurement (observed in a previous solubility study) or if the syringes containing the two samples were switched prior to measurement due to human error. Due to very limited material available, these measurements were not repeated.

Looking at the matched shear viscosity samples (decalin with 9.3 wt % 5kg/mol PB and PAO), the non-associative PCOD in PAO demonstrated lower relaxation times than the viscosity-matched decalin at concentrations below overlap. Additionally, despite having nearly three times the solvent viscosity, the relaxation times for PCOD in PAO below overlap are substantially less than three times that of decalin, even though the Zimm relationship for relaxation times of dilute solutions predicts a linear relationship between relaxation time and solvent viscosity.[29] These results are in line with the observed specific viscosities, and might suggest that the PCOD chains in PAO are not interacting

as strongly with the flow as the polymers in better solvent. However, comparing the decalin with and without the short polybutadiene added, we see an outsized increase in extensional relaxation time relative to their ratio of solvent viscosities, suggesting that a lower solvent quality might be increasing the relaxation time, contradicting that conclusion about the chains in PAO. One hypothesis to explain both results is that the poor solubility of PCOD in PAO resulted in polymer coils that are not stretching, acting more like semi-flexible polymers; while the decalin with polybutadiene still allows the chains to stretch. This hypothesis is in line with chain scission measurements in the literature that point towards increased chain scission in poorer (but still fully soluble) solvent[25]—the chains in poorer solvent resist extension more, leading to higher extensional relaxation times and chain scission at lower extension rates. These contradictory results suggest further interogation of the role of solvent quality in extension of dilute solutions, while controlling for solvent viscosity effects.

Role of Association in Shear and Extension

DA PCOD in decalin is highly self-associative (see Chapter 5 for further discussion of DA self-association and network formation). At low temperatures, the self-association has previously been shown to result in higher specific viscosities than pairwise association due to network formation.[30] In both shear and extension, DA in decalin demonstrated the highest measured specific viscosity and extensional relaxation time, shear thinning at $c/c^* = 0.5$, and high variance in extensional measurements, evidence of large megasupramolecular formations and possible network formation and disruption. In contrast, the shear and extensional measurements demonstrated significantly reduced effect of DA alone compared to DA:DB in PAO, implying the network self-association

of DA is suppressed in PAO.

On the other hand, DB in decalin is not self-associative, and has similar shear and extensional properties to non-associative PCOD, while DA:DB paired shows evidence of association in both shear and extension in decalin, in line with prior studies.[30] Surprisingly, in PAO, DB demonstrated similar shear viscosity and extensional relaxation time as DA:DB, implying that some kind of self-association directly between DB end-groups or indirectly via the BHT additive may be occurring for DB PCOD samples in PAO.

Changing Behavior in Spray

Even at small amounts of polymer additive ($\leq$0.05 wt %), both non-associative and associative, the spray behavior of PAO under the typical accidental release conditions substantially changed. By decreasing the spray angle and suppressing small droplets, the spray would be less likely to ignite in an accident. Additional PCOD (i.e., 0.1 wt % compared to 0.05 wt %) led to thicker ligaments and substantially modified spray behavior, which could overshoot the desired properties—we want to suppress small droplets, but not interfere with the flow through pumps inside the vehicle, or in the case of using an additive in fuel, still allow the fuel to ignite under the high-pressure conditions in an engine. Keeping the polymer additive content low is also desirable for use in the field—standards for lubricants and fuels require minimal additions of solids and increasing concentration can cause solubility issues.

4.5   Conclusion

Adding associative polycyclooctadiene to polyalphaolefin accomplishes our goal of controlling the droplet formation of a spray under simulated accidental release of a hydrocarbon lubricant using a pumping-tolerant additive. The increase in extensional relaxation time of the polymer solution is correlated with

the increased ligament diameter and suppression of small droplets. Even in a solvent for which this additive was not designed, the end-groups are shown to associate via increased shear viscosity and extensional relaxation time.

While DA:DB PCOD acted as a functional mist-control agent around room temperature in PAO, two directions of improvement are suggested by this work. First, PCOD has relatively low solubility in PAO, particularly as temperature decreases, which leads to collapsed coils and high overlap concentrations, leading to lower extensional performance per unit mass of polymer. Tailoring the backbone of the polymer to be better suited to PAO would likely improve performance of the additive to allow further decrease in the application concentration and assist in meeting standards that require solubility at low temperatures. Second, the DA:DB association was not as strong in PAO as in decalin, and more dramatic behavior changes per unit mass of polymer added could come from creating longer megasupramolecules and thus higher extensional relaxation time with larger association strength. Work on alternate associative groups could accomplish two tasks: lower additive loading for the same effect and eliminate the need for the excess of BHT added to solubilize the end groups. Further discussion of the optimization of additives for PAO will appear in the thesis of Hojin Kim.

References

[1] L. Yuan. "Ignition of Hydraulic Fluid Sprays by Open Flames and Hot Surfaces". In: *Journal of Loss Prevention in the Process Industries* 19.4 (July 2006), pp. 353–361. ISSN: 09504230. DOI: 10.1016/j.jlp.2005.09.001. URL: http://linkinghub.elsevier.com/retrieve/pii/S095042300500166X (visited on 12/21/2018).

[2] S. Gant. *Generation of Flammable Mists from High Flashpoint Fluids: Literature Review*. Research Report RR980. Derbyshire: Health and Safety Executive, 2013.

[3] K. K. Chao et al. "Antimisting Action of Polymeric Additives in Jet Fuels". In: *AIChE Journal* 30.1 (Jan. 1984), pp. 111–120. ISSN: 0001-1541, 1547-5905. DOI: 10.1002/aic.690300116. URL: http://doi.wiley.com/10.1002/aic.690300116 (visited on 03/23/2016).

[4] R. S. Marano et al. "Polymer Additives as Mist Suppressants in Metalworking Fluids Part I: Laboratory and Plant Studies - Straight Mineral Oil Fluids". In: *S.A.E. Transactions* 104 (Section 5 1995), pp. 136–146.

[5] G. H. McKinley and T. Sridhar. "Filament-Stretching Rheometry of Complex Fluids". In: *Annual Review of Fluid Mechanics* 34.1 (2002), pp. 375–415. URL: http://www.annualreviews.org/doi/abs/10.1146/annurev.fluid.34.083001.125207 (visited on 03/23/2016).

[6] M.-H. Wei et al. "Megasupramolecules for Safer, Cleaner Fuel by End Association of Long Telechelic Polymers". In: *Science* 350.6256 (Oct. 2, 2015), pp. 72–75. ISSN: 0036-8075, 1095-9203. DOI: 10.1126/science.aab0642. URL: http://www.sciencemag.org/cgi/doi/10.1126/science.aab0642 (visited on 03/17/2016).

[7] P. S. Virk. "Drag Reduction Fundamentals". In: *AIChE Journal* 21.4 (July 1975), pp. 625–656.

[8] S. A. Vanapalli, M. T. Islam, and M. J. Solomon. "Scission-Induced Bounds on Maximum Polymer Drag Reduction in Turbulent Flow". In: *Physics of Fluids* 17.9 (2005), p. 095108. ISSN: 10706631. DOI: 10.1063/1.2042489. URL: http://scitation.aip.org/content/aip/journal/pof2/17/9/10.1063/1.2042489 (visited on 05/05/2016).

[9] A. Somervaille, G. Betts, and C. F. I. Grains Research and Development Corporation (Australia). *Adjuvants: Oils, Surfactants and Other Additives for Farm Chemicals*. Kingston, ACT: Grains Research & Development Corporation, 2011. ISBN: 978-1-921779-32-9.

[10] R. W. Lewis et al. "Polymeric Drift Control Adjuvants for Agricultural Spraying". In: *Macromolecular Chemistry and Physics* 217.20 (Oct. 2016), pp. 2223–2242. ISSN: 10221352. DOI: 10.1002/macp.201600139.

URL: `https : / / onlinelibrary . wiley . com / doi / 10 . 1002 / macp . 201600139` (visited on 03/23/2022).

[11] R. L. A. David. "Associative Polymers as Antimisting Agents and Other Functional Materials via Thiol-Ene Coupling". Pasadena, California: California Institute of Technology, Mar. 7, 2008. 189 pp. URL: `http : / / thesis.library.caltech.edu/2173/`.

[12] M.-H. Wei. "Synthesis and Potency of Long End-Associative Polymers for Mist Control". Pasadena, California: California Institute of Technology, 2014.

[13] B. Keshavarz et al. "Studying the Effects of Elongational Properties on Atomization of Weakly Viscoelastic Solutions Using Rayleigh Ohnesorge Jetting Extensional Rheometry (ROJER)". In: *Journal of Non-Newtonian Fluid Mechanics* 222 (Aug. 2015), pp. 171–189. ISSN: 03770257. DOI: `10 . 1016 / j . jnnfm . 2014 . 11 . 004`. URL: `http : //linkinghub . elsevier.com/retrieve/pii/S0377025714002055` (visited on 01/06/2017).

[14] S. Kooij et al. "What Determines the Drop Size in Sprays?" In: *Physical Review X* 8.3 (July 20, 2018). ISSN: 2160-3308. DOI: `10.1103/PhysRevX . 8.031019`. URL: `https://link.aps.org/doi/10.1103/PhysRevX.8. 031019` (visited on 06/11/2020).

[15] R. P. Mun, J. A. Byars, and D. V. Boger. "The Effects of Polymer Concentration and Molecular Weight on the Breakup of Laminar Capillary Jets". In: (1998), p. 13.

[16] B. Keshavarz et al. "Ligament Mediated Fragmentation of Viscoelastic Liquids". In: *Physical Review Letters* 117.15 (Oct. 7, 2016). ISSN: 0031-9007, 1079-7114. DOI: `10.1103/PhysRevLett.117.154502`. URL: `https: //link.aps.org/doi/10.1103/PhysRevLett.117.154502` (visited on 08/14/2017).

[17] J. Dinic and V. Sharma. "Macromolecular Relaxation, Strain, and Extensibility Determine Elastocapillary Thinning and Extensional Viscosity of Polymer Solutions". In: *Proceedings of the National Academy of Sciences* 116.18 (Apr. 30, 2019), pp. 8766–8774. ISSN: 0027-8424, 1091-6490. DOI: `10.1073/pnas.1820277116`. URL: `http://www.pnas.org/lookup/doi/ 10.1073/pnas.1820277116` (visited on 05/05/2021).

[18] V. Tirtaatmadja, G. H. McKinley, and J. J. Cooper-White. "Drop Formation and Breakup of Low Viscosity Elastic Fluids: Effects of Molecular Weight and Concentration". In: *Physics of Fluids* 18.4 (Apr. 2006), p. 043101. ISSN: 1070-6631, 1089-7666. DOI: `10.1063/1.2190469`. URL: `http : //aip . scitation . org/doi/10 . 1063/1 . 2190469` (visited on 08/14/2017).

[19]   C. M. Schroeder. "Single Polymer Dynamics for Molecular Rheology". In: *Journal of Rheology* 62.1 (Jan. 2018), pp. 371–403. ISSN: 0148-6055, 1520-8516. DOI: `10.1122/1.5013246`. URL: `http://sor.scitation.org/doi/10.1122/1.5013246` (visited on 01/06/2018).

[20]   T. Q. Nguyen, G. Yu, and H.-H. Kausch. "Birefringence of a Polystyrene Solution in Elongational Flow: Effects of Molecular Weight and Solvent Quality". In: *Macromolecules* 28.14 (July 1995), pp. 4851–4860. ISSN: 0024-9297, 1520-5835. DOI: `10.1021/ma00118a010`. URL: `http://pubs.acs.org/doi/abs/10.1021/ma00118a010` (visited on 09/13/2016).

[21]   A. Keller and J. A. Odell. "The Extensibility of Macromolecules in Solution; A New Focus for Macromolecular Science". In: *Colloid & Polymer Science* 263.3 (Mar. 1985), pp. 181–201. ISSN: 0303-402X, 1435-1536. DOI: `10.1007/BF01415506`. URL: `http://link.springer.com/10.1007/BF01415506` (visited on 04/06/2022).

[22]   Y. Rabin, F. S. Henyey, and R. K. Pathria. "Scaling Behavior of Dilute Polymer Solutions in Elongational Flows". In: *Physical Review Letters* 55.2 (July 8, 1985), pp. 201–203. ISSN: 0031-9007. DOI: `10.1103/PhysRevLett.55.201`. URL: `https://link.aps.org/doi/10.1103/PhysRevLett.55.201` (visited on 04/05/2022).

[23]   M. Doi and S. F. Edwards. *The Theory of Polymer Dynamics*. International Series of Monographs on Physics. Oxford: Clarendon press, 1986. ISBN: 978-0-19-852033-7.

[24]   T. Moussa, C. Tiu, and T. Sridhar. "Effect of Solvent on Polymer Degradation in Turbulent Flow". In: *Journal of Non-Newtonian Fluid Mechanics* 48 (1993), pp. 261–284.

[25]   A. Dupas et al. "Mechanical Degradation Onset of Polyethylene Oxide Used as a Hydrosoluble Model Polymer for Enhanced Oil Recovery". In: *Oil & Gas Science and Technology – Revue d'IFP Energies nouvelles* 67.6 (Nov. 2012), pp. 931–940. ISSN: 1294-4475, 1953-8189. DOI: `10.2516/ogst/2012028`. URL: `http://ogst.ifpenergiesnouvelles.fr/10.2516/ogst/2012028` (visited on 01/15/2019).

[26]   H. Kim. "Megasupramolecules in Extremely Non-Polar Solvents: What to Do When 3000+ Backbone Units Fail to Drag Two End-Groups into Solution". International Congress of Rheology. 2020.

[27]   R. Learsch. "Investigation in Experimental Conditions and Automation of Dripping-onto-Substrate Rheology". American Chemical Society Spring Meeting (San Diego, CA). Mar. 23, 2022.

[28]   S. N. Laboratories. *Engine Combustion Network Schlieren Processing Code*. Engine Combustion Network. 2011. URL: `https://www.sandia.gov/ecn/code.php` (visited on 05/06/2022).

[29] F. D. Giudice, S. J. Haward, and A. Q. Shen. "Relaxation Time of Dilute Polymer Solutions: A Microfluidic Approach". In: (), p. 12.

[30] B. Li. "Ring/Chain versus Network: Architecture Induced by Self- versus Pairwise- Association of Telechelic Polymers". Pasadena, California: California Institute of Technology, 2016. 244 pp.

Chapter 5

END-FUNCTIONALITY DETECTION THROUGH SHEAR RHEOLOGY

5.1 Introduction

End-functional polymers offer diverse opportunities, from responsive drug delivery vehicles to polymer compatibilizers.[1,2] Very long associative α,ω-telechelic polymers (>40,000 backbone atoms, bba) act as highly potent additives that resist degradation while conferring turbulent drag reduction and mist control.[3,4] In hydrocarbons, like most fuels and lubricants, long end-associative polymers could improve safety and energy efficiency.[3,5] To form multi-million molecular weight supramolecules at the low concentrations (i.e., <0.2 wt %) relevant to drag reduction and mist control,[3] the individual units must both be long and be successfully α,ω-functionalized, demanding end-group fidelity even at high molecular weights.[4] To produce hydrocarbon-soluble telechelic polymers of controlled molecular weights, our group has employed ring-opening metathesis polymerization (ROMP) of emph*cis*,*cis*-1,5-cyclooctadiene (COD). ROMP enables high fidelity installation of functional groups at both ends of growing chains by the use of di-functional chain-transfer agents (CTAs) and a two-step polymerization process.[5,6] Targeting long chains with low additive loading by mass points to ROMP monomers with all of the heavy atoms in the backbone (e.g., cyclobutene, cyclooctene, and cyclooctadiene). For comparison to other polymers that have been extensively studied and used in hydrocarbons, the mass of polymer per bba is 85 g/mol for polyhexylmethacrylate, 80 g/mol for poly(t-butyl-styrene), 29 g/mol for polyisobutylene, and a mere 13 g/mol for polycyclooctadiene (PCOD). Among the atom-efficient candidate

cycloolefins for ROMP, COD (Figure 5.1a) has the advantages of high ring strain paired with good hydrocarbon solubility in the final product.

Although ROMP of COD has been used previously to prepare a variety of telechelic PCODs,[5,7–10] high molecular weight telechelic polymers (>500 kg/mol) with high end group fidelity were often inaccessible due to COD's isomer, 4-vinylcyclohexene (VCH) (Figure 5.1b), historically a common contaminent in commercially available COD.[5,11,12] The pendant vinyl group of VCH acts as an undesired CTA during ROMP of COD, terminating a growing chain[5,11] and leaving a non-functional end. Separation of the isomers, VCH and COD, is difficult at a lab-scale because of their close boiling points (131 and 150 °C, respectively, at atmospheric pressure).[5,12] Repeated distillations can reduce VCH levels to approximately 1000 ppm, limiting the average degree of polymerization (DP) to $\sim$1000 (8000 backbone atoms).[5] To produce telechelic PCOD with > 40,000 bba (DP > 5000) requires less than one unintentional chain transfer per 50,000 monomers incorporated (< 20 ppm VCH), motivating removal of VCH and subsequent validation of end-groups post-polymerization.

As molecular weight increases, traditional methods of detecting end-group fidelity, like nuclear magnetic resonance (NMR), become less able to distinguish between di-telechelic, mono-telechelic, and non-functional polymers due to the small number of end-group atoms compared to the backbone.[13,14] In this work, we detect the relative extent of α,ω-functionalization by using shear rheology to characterize the polymers produced from COD where VCH was removed by two different methods—competitive hydroboration of VCH and COD, the route recommended by the literature,[5] and molecular sieving by a zeolite, ZSM-5 (Figure 5.1c).[15–17]
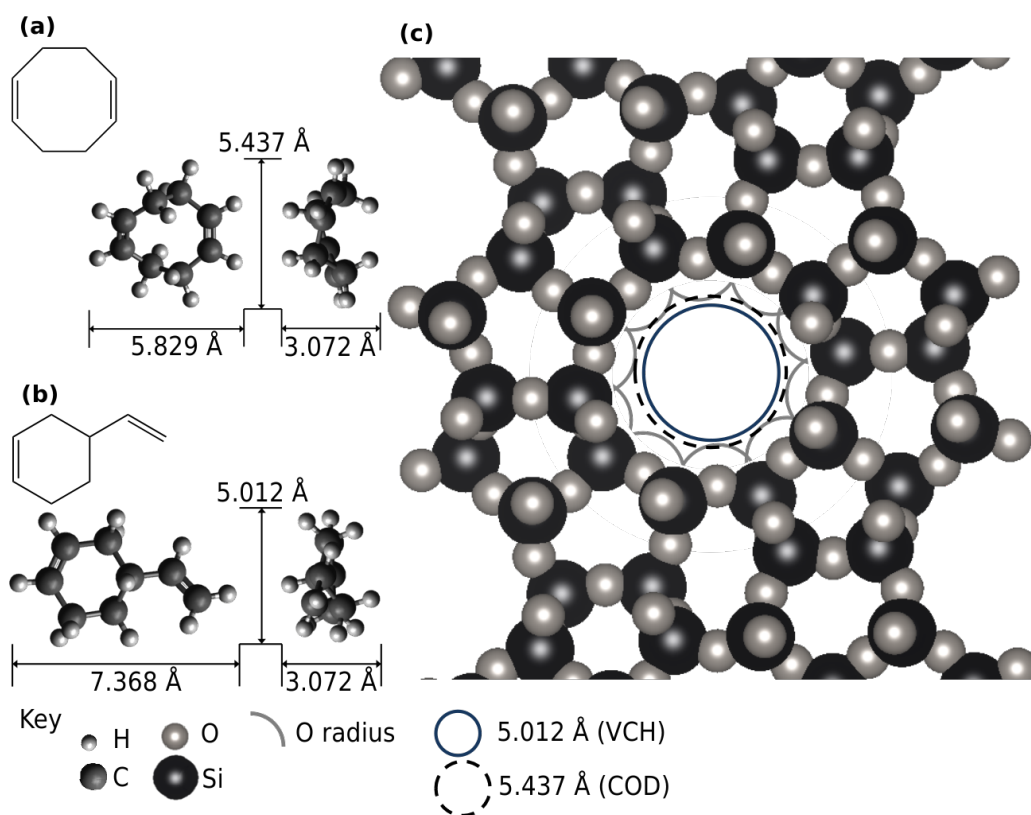
Figure 5.1: (a) Chemical structure and ball-and-stick model of cyclooctadiene (COD) demonstrating molecular dimensions of 5.437 Å by 5.829 Å by 3.072 Å. (b) Chemical structure and ball-and-stick model of 4-vinylcyclohexene (VCH) demonstrating molecular dimensions of 5.012 Å by 7.368 Å by 3.072 Å. COD and VCH ball-and-stick models optimized in Avogadro.[18,19] (c) Structure of a representative layer of ZSM-5, showing the opening of the straight channel pores, which are 5.4-5.6 Å wide.[20] Structure drawn in VESTA.[21] Gray arcs represent an oxygen radius of 1.52 Å,[20] black dashed circle represents a 5.437 Å diameter circle corresponding to the size of COD, blue solid circle represents a 5.012 Å diameter circle corresponding to the size of VCH.

5.2 Experimental Section

Treatment of COD and Synthesis of PCOD

Treatment of COD and synthesis of all PCOD samples were performed by Hojin Kim. See Appendix B.

PCOD Solutions in Decahydronaphthalene for Rheology

Solutions of PCOD in decahydronapthalene (decalin), a solvent with similar unsaturation to fuel with relatively low volatility and limited interference with hydrogen-bonding, were prepared for rheology by Hojin Kim. Approximately 10 ml of decahydronapthalene (mixture of *cis + trans*) was poured into a 20 ml glass vial with PTFE lined cap and the solvent weight was recorded. To this, 0.01 g of BHT and an appropriate amount of PCOD for the desired concentration were added with a stir bar. The head space was purged with argon, and the cap was sealed with parafilm. The mixture was stirred at 60°C for 4-12 hours and used for rheological experiments within 2 days.

Shear Rheological Measurements

Shear viscosity measurements were performed on an Anton Paar MCR 302 WESP rheometer using a cone-and-plate fixture of 50 mm diameter and 2.007° angle, with a truncation of 0.207 mm. Samples were loaded by depositing 1.1 mL of the sample on the center of the plate, lowering the cone to 0.217 mm, removing excess to create a flat edge, and then lowering to 0.207 mm to create a spherical edge condition. The plate was cooled to 0 ± 0.1 °C using a Peltier plate to regulate temperature and reduce volatility and samples were allowed to thermally equilibrate and relax for 5 min. Shear rate sweeps were performed from 0.1 1/s to 100 1/s for solutions with concentrations above 1 wt % and from 1 to 100 1/s for concentrations below 1 wt %. The sample edge was examined to check for evidence of evaporation and none was observed.

5.3 Results

Rheological Consequences of Monomer Purity for Low Molecular Weight Telechelic Polycyclooctadiene

The viscosities of non-associative and self-associative polymers made using hydroboration and molecular sieving methods were measured at concentrations of 1.2, 1.5, 2.0, and 2.5 wt% in decalin (Figures 5.3-5.2).

Gelation and gel fracture was observed for self-associative polymers at a molecular weight of 60 kg/mol at all concentrations from both purification methods and at a molecular weight of 200kg/mol at 2.5 wt% for polymers from hydroboration-treated COD and at 2.0 wt% and 2.5 wt% for polymers from zeolite-treated COD (noted by hollow symbols in Figure 5.2). Gel fracture was characterized by the sample ejecting from the gap between the cone and plate and moving on top of the cone, resulting in the appearance of significant shear thinning in the recorded viscosities. These results are in line with network formation previously observed for DA PCOD in decalin.[22]

The peak specific viscosities for non-associative polymers at the same molecular weight and concentration were not statistically significantly different across purification methods at 95% confidence (Figures 5.3 and 5.4). Enhancements in the viscosity of the self-associative polymer solutions compared to non-associative polymer solutions at 60 kg/mol were substantial, reaching over 100,000% the viscosity of the equivalent non-associative solution at 2.5 wt% (Figure 5.5). At 60 kg/mol, self-associative telechelic polymers from zeolite-treated COD (z, DA) demonstrated statistically significantly higher enchancement than self-associative telechelic polymers from hydroboration-treated COD (hb, DA) for concentrations of 1.2 wt%, 1.5 wt%, and 2.0 wt%. Enhancements in the viscosity of the self-associative polymer solutions compared to non-associative polymer solutions at 200 kg/mol were significant (Fig-

ure 5.6), but less than at 60 kg/mol, resulting in lower specific viscosities for solutions of self-associative polymers at 200 kg/mol than 60 kg/mol at the same concentration (Figures 5.3 and 5.4). At 200 kg/mol, self-associative telechelic polymers from zeolite-treated COD (z, DA) demonstrated statistically significantly higher enchancement than self-associative telechelic polymers from hydroboration-treated COD (hb, DA) for concentrations of 1.5 wt%, 2.0 wt%, and 2.5 wt%.

Rheological Consequences of End-groups at Low Concentration

The highest accessible molecular weight is of particular importance for enhancing rheological properties using a low polymer concentration of end-associative polymers.[3,4] Therefore, we compared solution viscosity at concentrations less than or equal to 0.15 wt% of the highest molecular weight telechelic polymers made from hydroboration- and zeolite-treated COD (M_w ∼200 kg/mol and ∼1000 kg/mol respectively, see Appendix B for details on molecular weights). No shear thinning or gelation was observed in the shear rate range tested for these samples. The enhancement of the shear viscosity relative to the solvent alone, i.e., the specific viscosity, was consistently greater for z, DA than hb, DA (Figure 5.7): ($\eta_{z,DA}/\eta_{hb,DA}$) is 260 % ± 50% at 0.15 wt% and 350% ± 27 % at 0.10 wt% when compared to the longest DA-ended telechelic polymer from hydroboration-treated COD. A subtle but significant feature was the similarity between the non-associative and self-associative counterparts obtained using hydroboration-treated COD—in contrast to the greater viscosity for z, DA than for its non-associative counterpart (Figure 5.8). In summary, z, DA demonstrated significant enhancement of shear viscosity at low concentrations compared to both hb, DA and non-associative PCOD of similiar molecular weight.
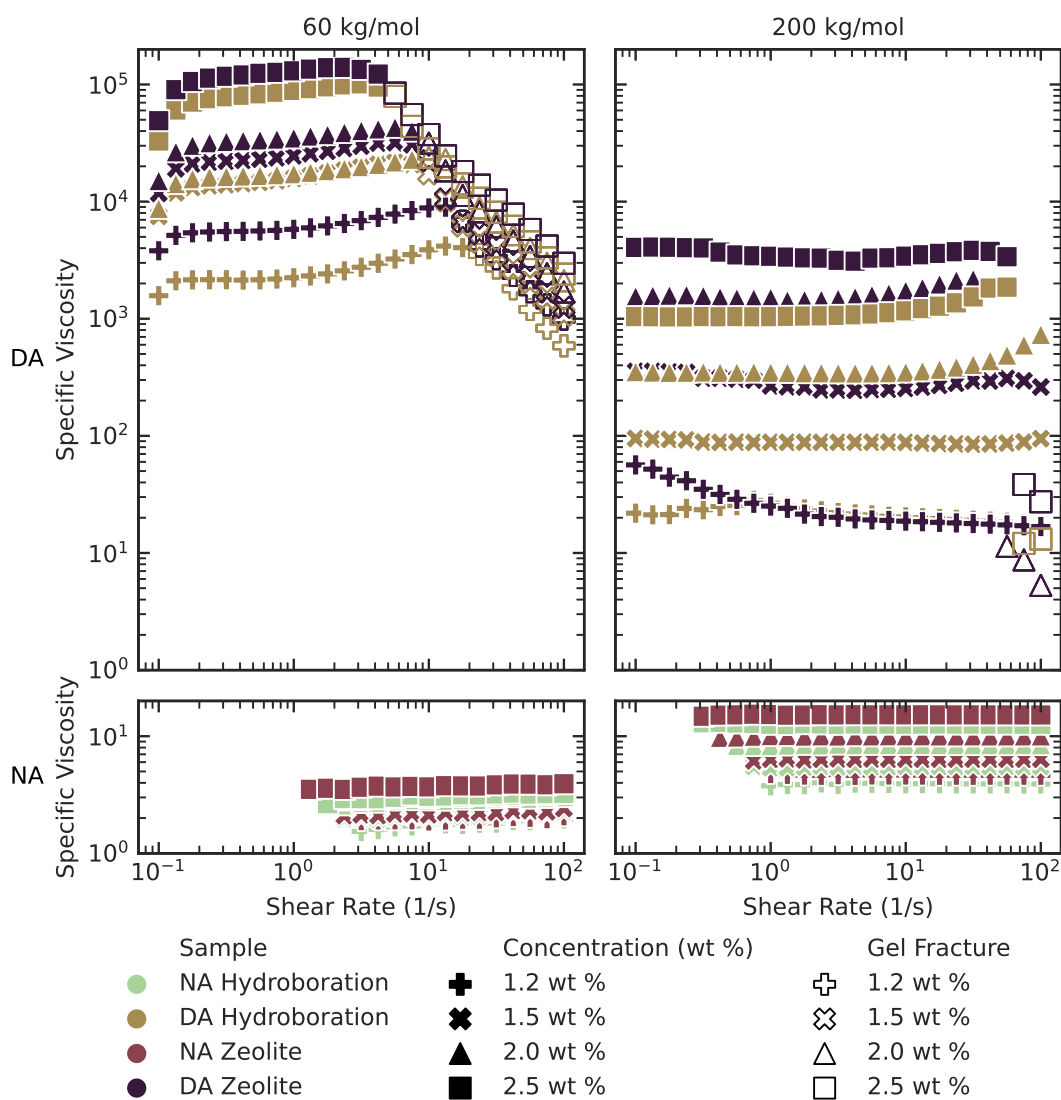
Figure 5.2: Specific viscosities as a function of shear rate of solutions of (bottom) non-associative (NA) and (top) self-associative (DA) polymers made from hydroboration-treated COD (hb) and zeolite-treated COD (z) at concentrations of 1.2 wt%, 1.5 wt%, 2.0 wt%, and 2.5 wt% in decalin with molecular weights of approximately (left) 60 kg/mol and (right) 200 kg/mol. Hollow symbols indicate gel fracture. Figures 5.3, 5.5, and 5.2 (left) depict the same data. Figures 5.4, 5.6, and 5.2 (right) depict the same data.
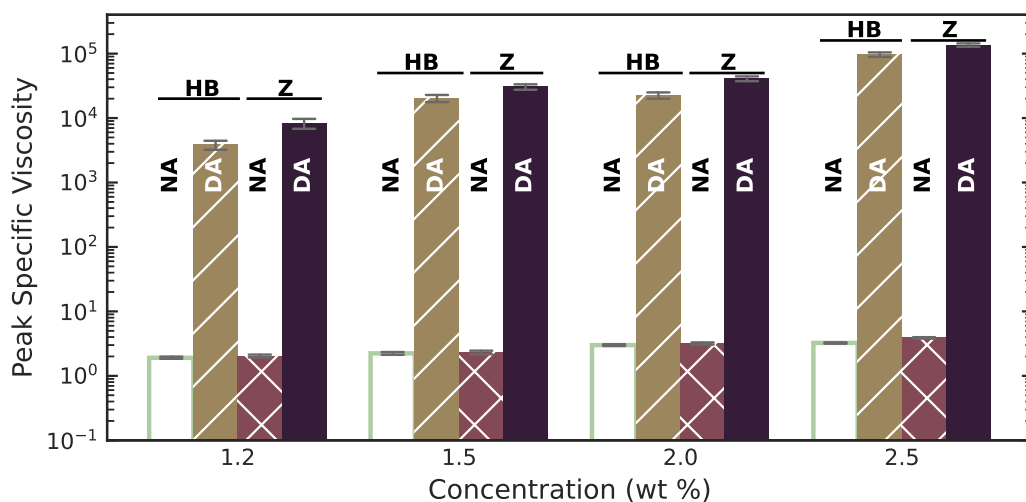
Figure 5.3: Peak specific viscosities of solutions of non-associative (NA) and self-associative (DA) polymers made from hydroboration-treated COD (hb) and zeolite-treated COD (z) at concentrations of 1.2 wt%, 1.5 wt%, 2.0 wt%, and 2.5 wt% in decalin with molecular weights of approximately 60 kg/mol. Error bars represent a 95% confidence interval. Figures 5.3, 5.5, and 5.2 (left) depict the same data.
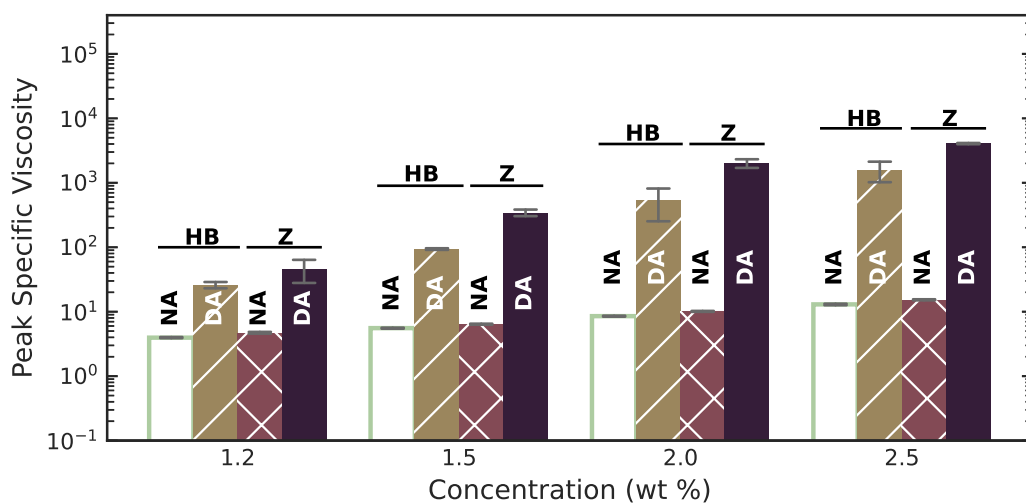
Figure 5.4: Peak specific viscosities of solutions of non-associative (NA) and self-associative (DA) polymers made from hydroboration-treated COD (hb) and zeolite-treated COD (z) at concentrations of 1.2 wt%, 1.5 wt%, 2.0 wt%, and 2.5 wt% in decalin with molecular weights of approximately 200 kg/mol. Error bars represent a 95% confidence interval. Figures 5.4, 5.6, and 5.2 (right) depict the same data.
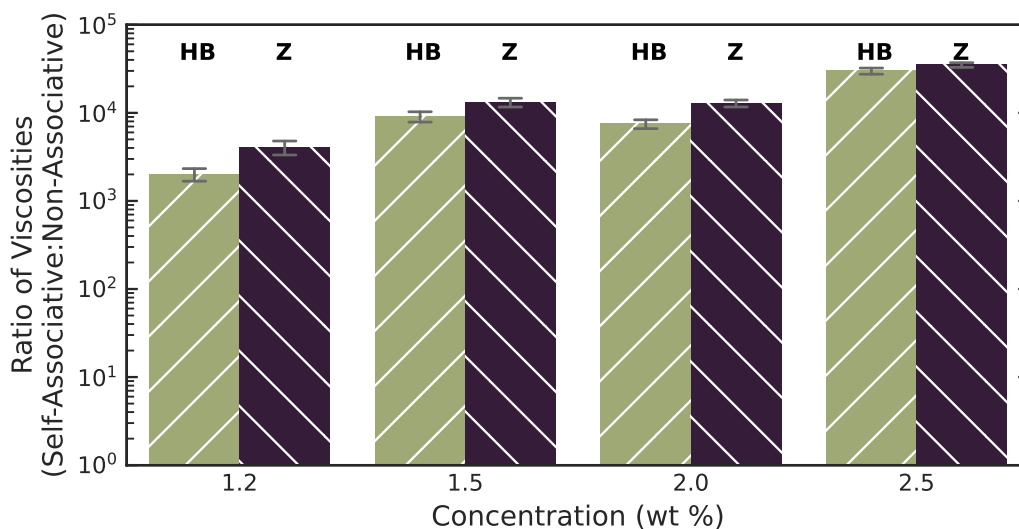
Figure 5.5: Ratio of peak viscosities of solutions of self-associative (DA) polymers to non-associative (NA) polymers made from hydroboration-treated COD (hb) and zeolite-treated COD (z) at concentrations of 1.2 wt%, 1.5 wt%, 2.0 wt%, and 2.5 wt% in decalin with molecular weights of approximately 60 kg/mol. Error bars represent a 95% confidence interval. Figures 5.3, 5.5, and 5.2 (left) depict the same data.
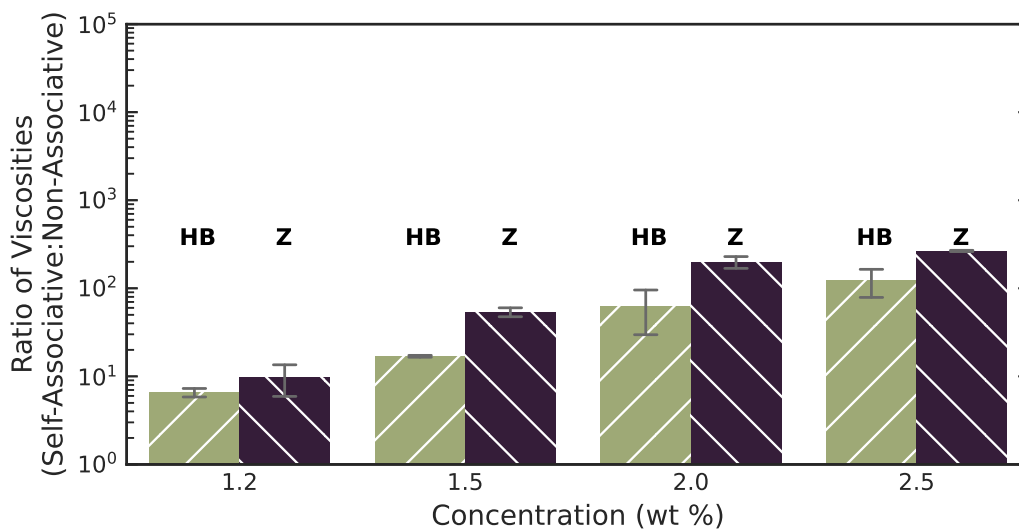
Figure 5.6: Ratio of peak viscosities of solutions of self-associative (DA) polymers to non-associative (NA) polymers made from hydroboration-treated COD (hb) and zeolite-treated COD (z) at concentrations of 1.2 wt%, 1.5 wt%, 2.0 wt%, and 2.5 wt% in decalin with molecular weights of approximately 200 kg/mol. Error bars represent a 95% confidence interval. Figures 5.4, 5.6, and 5.2 (right) depict the same data.
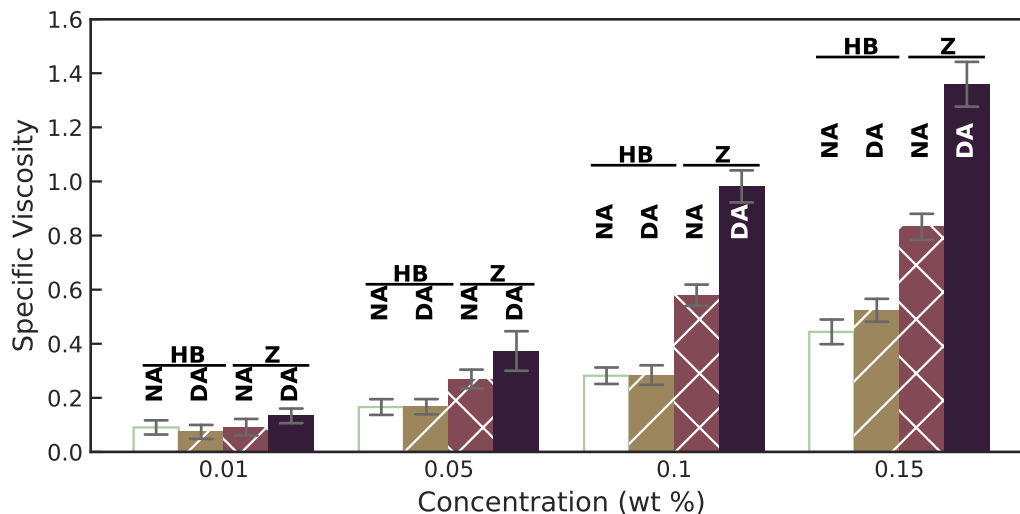
Figure 5.7: Specific viscosities of solutions of the highest readily accessible molecular weights of non-associative (NA) and self-associative (DA) polymers made from hydroboration-treated COD (hb) at approximately 200 kg/mol and zeolite-treated COD (z) at approximately 1 Mg/mol at concentrations of 0.01 wt%, 0.05 wt%, 0.1 wt%, and 0.15 wt% in decalin. Error bars represent a 95% confidence interval. Figures 5.7 and 5.8 depict the same data.
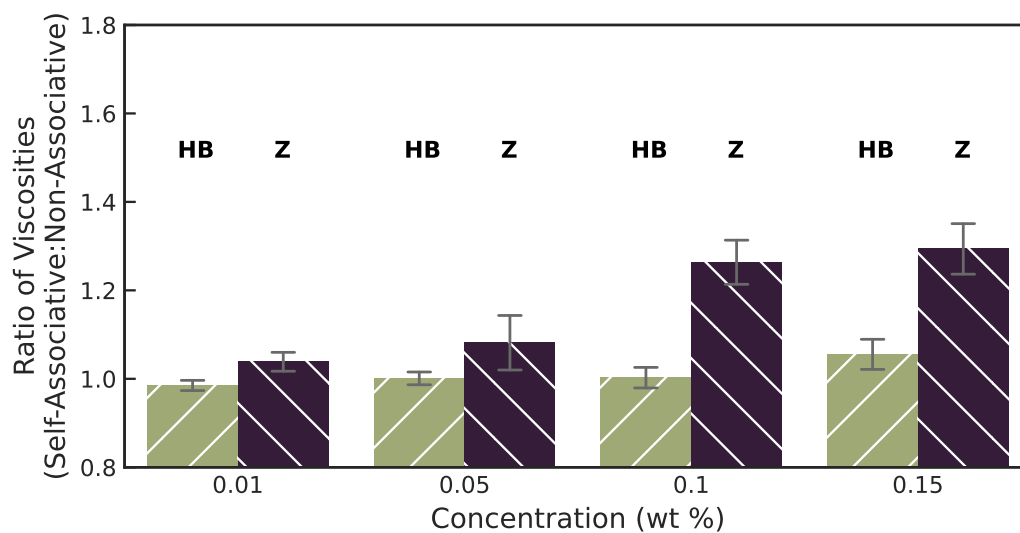
Figure 5.8: Ratio of viscosities of solutions of self-associative (DA) polymers to non-associative (NA) polymers at the highest readily accessible molecular weights of non-associative (NA) and self-associative (DA) polymers made from hydroboration-treated COD (hb) at approximately 200 kg/mol and zeolite-treated COD (z) at approximately 1 Mg/mol at concentrations of 0.01 wt%, 0.05 wt%, 0.1 wt%, and 0.15 wt% in decalin. Error bars represent a 95% confidence interval. Figures 5.7 and 5.8 depict the same data.

5.4 Discussion

Comparing the peak specific viscosities of polymer solutions made from zeolite-treated and hydroboration-treated COD at high concentrations, the effect of molecular weight on end-group fidelity is observed. The self-associative polymers made from zeolite-treated COD significantly increase the viscosity at both 60 and 200 kg/mol at multiple concentrations compared to the self-associative polymers made from hydroboration-treated COD, but the relative effect at the higher molecular weight is larger, indicating that end-group control is diminished as molecular weight increases. As molecular weight increases, the proportion of intentional di-acid-functionalized CTA to potential contaminant CTAs present in the treated COD will decrease. A reduction in rheological potency of association for polymers from hydroboration-treated COD compared to those from zeolite-treated COD is evidence for unintentional chain transfer and unwanted non-associative end-group installation.

At low concentrations (< 0.1 wt%), comparing the nominally "self-associative" and non-associative polymers from hydroboration-treated COD at a COD/CTA ratio of 14,000 showed indistinguishable specific viscosities. This evidence suggests the majority of chain ends in the nominally "self-associative" polymer from hydroboration-treated PCOD have unknown end-group structure from impurities rather than CTA, qualitatively agreeing with population balance models of mixtures of non-functional and functional chain ends.[4] In contrast, polymers from zeolite-treated COD showed substantially greater viscosity compared to their non-associative counterparts at these same concentrations. The difference in viscosity versus concentration suggests a twofold reduction in apparent overlap concentration due to end-to-end association. Maintaining control of associative end-groups to a high degree of polymerization is essential for formation of a distribution of supramolecules that includes ultralong

species responsible for mist control and drag reduction.[3,4]

5.5   Conclusion

Highly-potent long end-associative polymers ($> 40,000$ backbone atoms, bba) resist shear degradation and retain efficacy compared to traditional polymers with $\geq 10^6$ bba,[3] even at low concentrations (< 0.1 wt%). This efficacy depends on end-group fidelity–the presence of mono-telechelic polymers causes "termination" of what would otherwise be the most effective long linear chains.[4] Although it is difficult to use NMR to quantify the fidelity of end-functionalization as molecular weight increases,[14] the rheological properties of solutions of the resulting polymers provide a sensitive indicator of the loss of end-group control.

Using shear rheology as our detection tool, we were able to reveal differences in monomer purity not visible in NMR through the diminished self-association present in the polymers synthesized from hydroboration-treated COD. By distinguishing between polymer candidates obtained through different routes that look similar under other detection tools such as gel permeation chromatography and NMR, we can select more effective mist control and drag reduction agents for such safety and sustainability applications as suppressing fire in lubricant leaks and decreasing pump power requirements.

References

[1] D. Vinciguerra, J. Tran, and J. Nicolas. "Telechelic Polymers from Reversible-Deactivation Radical Polymerization for Biomedical Applications". In: *Chemical Communications* 54.3 (2018), pp. 228–240. ISSN: 1359-7345, 1364-548X. DOI: 10.1039/C7CC08544C. URL: http://xlink.rsc.org/?DOI=C7CC08544C (visited on 03/05/2019).

[2] L. A. Schwegler et al. "Preparation of Telechelic Polysilylenes: A General Methodology for the Synthesis of Polysilylene-Based Triblock Copolymers". In: *Macromolecules* 32.18 (Sept. 1999), pp. 5901–5904. ISSN: 0024-9297, 1520-5835. DOI: 10.1021/ma981446r. URL: https://pubs.acs.org/doi/10.1021/ma981446r (visited on 03/05/2019).

[3] M.-H. Wei et al. "Megasupramolecules for Safer, Cleaner Fuel by End Association of Long Telechelic Polymers". In: *Science* 350.6256 (Oct. 2, 2015), pp. 72–75. ISSN: 0036-8075, 1095-9203. DOI: 10.1126/science.aab0642. URL: http://www.sciencemag.org/cgi/doi/10.1126/science.aab0642 (visited on 03/17/2016).

[4] R. L. A. David. "Associative Polymers as Antimisting Agents and Other Functional Materials via Thiol-Ene Coupling". Pasadena, California: California Institute of Technology, Mar. 7, 2008. 189 pp. URL: http://thesis.library.caltech.edu/2173/.

[5] S. Ji, T. R. Hoye, and C. W. Macosko. "Controlled Synthesis of High Molecular Weight Telechelic Polybutadienes by Ring-Opening Metathesis Polymerization". In: *Macromolecules* 37.15 (July 2004), pp. 5485–5489. ISSN: 0024-9297, 1520-5835. DOI: 10.1021/ma0493067. URL: http://pubs.acs.org/doi/abs/10.1021/ma0493067 (visited on 03/23/2016).

[6] R. Walker, R. M. Conrad, and R. H. Grubbs. "The Living ROMP of *Trans*-Cyclooctene". In: *Macromolecules* 42.3 (Feb. 10, 2009), pp. 599–605. ISSN: 0024-9297, 1520-5835. DOI: 10.1021/ma801693q. URL: https://pubs.acs.org/doi/10.1021/ma801693q (visited on 06/15/2020).

[7] T. C. Chung and M. Chasmawala. "Synthesis of Telechelic 1, 4-Polybutadiene by Metathesis Reactions and Borane Monomers". In: *Macromolecules* 25.20 (1992), pp. 5137–5144. URL: http://pubs.acs.org/doi/pdf/10.1021/ma00046a004 (visited on 06/27/2017).

[8] M. A. Hillmyer and R. H. Grubbs. "Preparation of Hydroxytelechelic Poly(Butadiene) via Ring-Opening Metathesis Polymerization Employing a Well-Defined Metathesis Catalyst". In: *Macromolecules* 26.4 (July 1993), pp. 872–874. ISSN: 0024-9297, 1520-5835. DOI: 10.1021/ma00056a051. URL: http://pubs.acs.org/doi/abs/10.1021/ma00056a051 (visited on 07/08/2019).

[9]   D. Reyx, M. Hamza, and I. Campistron. "Use of the metathesis reaction in the synthesis of alpha,omega-bifunctional polymers: Part 3: Optimizing conditions for obtaining dienic and trienic compounds by cometathesis of cyclopentene with 4-octene and dimethyl-3-hexene-dioate". In: *Journal of Molecular Catalysis* 42.3 (1987), pp. 289–299.

[10]   H. Martinez et al. "Ring-Opening Metathesis Polymerization of 8-Membered Cyclic Olefins". In: *Polymer Chemistry* 5.11 (2014), p. 3507. ISSN: 1759-9954, 1759-9962. DOI: `10.1039/c3py01787g`. URL: `http://xlink.rsc.org/?DOI=c3py01787g` (visited on 03/25/2019).

[11]   C. W. Bielawski, D. Benitez, and R. H. Grubbs. "Synthesis of Cyclic Polybutadiene via Ring-Opening Metathesis Polymerization: The Importance of Removing Trace Linear Contaminants". In: *Journal of the American Chemical Society* 125.28 (July 2003), pp. 8424–8425. ISSN: 0002-7863, 1520-5126. DOI: `10.1021/ja034524l`. URL: `http://pubs.acs.org/doi/abs/10.1021/ja034524l` (visited on 07/05/2017).

[12]   G. Oenbrink and T. Schiffer. "Cyclododecatriene, Cyclooctadiene, and 4-Vinylcyclohexene". In: *Ullmann's Encyclopedia of Industrial Chemistry*. Ed. by Wiley-VCH Verlag GmbH & Co. KGaA. Weinheim, Germany: Wiley-VCH Verlag GmbH & Co. KGaA, Oct. 15, 2009. ISBN: 978-3-527-30673-2. DOI: `10.1002/14356007.a08_205.pub2`. URL: `http://doi.wiley.com/10.1002/14356007.a08_205.pub2` (visited on 01/22/2019).

[13]   L. G. D. Hawke et al. "Viscoelastic Properties of Linear Associating Poly(n-Butyl Acrylate) Chains". In: *Journal of Rheology* 60.2 (Mar. 2016), pp. 297–310. ISSN: 0148-6055, 1520-8516. DOI: `10.1122/1.4942231`. URL: `http://scitation.aip.org/content/sor/journal/jor2/60/2/10.1122/1.4942231` (visited on 03/28/2016).

[14]   Y. Xia et al. "Ring-Expansion Metathesis Polymerization: Catalyst-Dependent Polymerization Profiles". In: *Journal of the American Chemical Society* 131.7 (Feb. 25, 2009), pp. 2670–2677. ISSN: 0002-7863, 1520-5126. DOI: `10.1021/ja808296a`. URL: `http://pubs.acs.org/doi/abs/10.1021/ja808296a` (visited on 04/09/2015).

[15]   J. A. Kornfield et al. "US Patent 10112878, Molecular Sieves Mediated Unsaturated Hydrocarbon Separation and Related Compositions, Materials, Methods and Systems". Pat. 10112878. CALIFORNIA INSTITUTE OF TECHNOLOGY. Oct. 30, 2018. URL: `http://patft.uspto.gov/netacgi/nph-Parser?Sect1=PTO1&Sect2=HITOFF&d=PALL&p=1&u=%2Fnetahtml%2FPTO%2Fsrchnum.htm&r=1&f=G&l=50&s1=10,112,878.PN.&OS=PN/10,112,878&RS=PN/10,112,878` (visited on 12/21/2018).

[16] J. A. Kornfield et al. "US Patent 10427995, Molecular Sieves Mediated Unsaturated Hydrocarbon Separation and Related Compositions, Materials, Methods and Systems". U.S. pat. 10427995B2. California Institute of Technology CalTech. Oct. 1, 2019. URL: https://patents.google.com/patent/US10427995B2/en?oq=10427995 (visited on 05/13/2021).

[17] J. A. Kornfield et al. "US Patent 10781150, Molecular Sieves Mediated Unsaturated Hydrcarbon Separation and Related Compositions, Materials, Methods and Systems". U.S. pat. 10781150B2. California Institute of Technology CalTech. Sept. 22, 2020. URL: https://patents.google.com/patent/US10781150B2/en?oq=10781150 (visited on 05/13/2021).

[18] *Avogadro: An Open-Source Molecular Builder and Visualization Tool. Version 1.2.0. http://avogadro.cc/.* Version 1.2.0. 2012. URL: http://avogadro.cc/.

[19] M. D. Hanwell et al. "Avogadro: An Advanced Semantic Chemical Editor, Visualization, and Analysis Platform". In: *Journal of Cheminformatics* 4.1 (Dec. 2012). ISSN: 1758-2946. DOI: 10.1186/1758-2946-4-17. URL: https://jcheminf.biomedcentral.com/articles/10.1186/1758-2946-4-17 (visited on 07/16/2019).

[20] D. H. Olson et al. "Crystal Structure and Structure-Related Properties of ZSM-5". In: *The Journal of Physical Chemistry* 85.15 (July 1981), pp. 2238–2243. ISSN: 0022-3654, 1541-5740. DOI: 10.1021/j150615a020. URL: http://pubs.acs.org/doi/abs/10.1021/j150615a020 (visited on 01/16/2019).

[21] K. Momma and F. Izumi. "*VESTA 3* for Three-Dimensional Visualization of Crystal, Volumetric and Morphology Data". In: *Journal of Applied Crystallography* 44.6 (Dec. 1, 2011), pp. 1272–1276. ISSN: 0021-8898. DOI: 10.1107/S0021889811038970. URL: http://scripts.iucr.org/cgi-bin/paper?S0021889811038970 (visited on 07/21/2020).

[22] B. Li. "Ring/Chain versus Network: Architecture Induced by Self- versus Pairwise- Association of Telechelic Polymers". Pasadena, California: California Institute of Technology, 2016. 244 pp.

Chapter 6

INCORPORATING EVIDENCE-BASED TEACHING TECHNIQUES INTO CALTECH CLASSROOMS

6.1 Introduction

As we do research to understand new and old discoveries, through experiments, theory, and simulation, we learn both about the underlying explanations for these phenomena and how to improve our methodology. New techniques in science and engineering allow us to uncover physics on the subatomic scale and on the galactic. By iterating, trying new processes, and sometimes succeeding, sometimes not, we grow as a scientific community with new knowledge and expertise.

Much as we experiment in our laboratories, we can also experiment in our classrooms. As more instructors engage in trying new teaching techniques and documenting the results, the field of pedagogy develops guidance on best practices and how we can use evidence-based teaching techniques to improve our classrooms. Research on teaching demonstrates that implementing inclusive and structured improvements into the classroom benefits all students, particularly those that are often underserved in college classrooms (first-generation students, racially and ethnically minoritized students, women and gender minorities, students with disabilities).[1–7]

In this chapter, I will introduce evidence-based teaching techniques motivated by pedagogical research literature and use examples from my teaching experiences to demonstrate these techniques and their impact, while reflecting on how to iterate to improve the implementation of the technique.

6.2 Backwards Design

Technique and Motivation

Traditionally, many courses were designed around teaching to cover a specific set of content over a term, to use a particular textbook, and to consist of a specific number of lectures per week. As syllabi and other formal requirements for courses were introduced as a part of cross-course curricula, intended learning outcomes were retroactively ascribed to fit those prior choices.[8]

In "backwards design," learning outcomes—goals for knowledge and skills students should have acquired by the end of course—are constructed first, keeping in mind that learning outcomes should be clear and measurable. Assessment is then structured to measure to what extent these outcomes have been achieved. Content, teaching methods, and supporting materials are then designed and chosen to directly address one or more of those learning outcomes.[8,9]

Backwards design leads to intentional course structuring, which benefits both instructors and learners, and assists students in acquiring the knowledge and skills they need to retain from the course to proceed into future education and careers.[9]

Implementation

In my second time as a teaching assistant for heat transfer, I sought to use backwards design and learning outcomes to better structure assessment in the course. At the start of the term, we laid out the learning outcomes that would be expected for students entering the next course in the series (fluid mechanics) and for chemical engineers in the workplace (Figure 6.1). I then went through all of the existing homework assignments for the course and looked for how these learning outcomes intersected with the problems that were posed (Figure 6.2).

Learning Outcomes

Problem-Solving Skills
- <u>Approximation</u>: Apply appropriate approximations to make quick estimates
- <u>Assumptions</u>: Specify assumptions that make problems solvable, while still applicable
- <u>Reasoning</u>: Explain problem solutions using physical and mathematical reasoning
- <u>Reality Check</u>: Assess reasonableness and accuracy of answers

Problem-Solving Toolkit
- <u>Dimensional Analysis</u>: Assess the relative importance of different phenomena based on different values of a dimensionless group
- <u>Differential Equations</u>: Solve ordinary and partial differential equations for scalar dependent variables, using techniques like separation of variables and Fourier analysis to address partial differential equations
- <u>Boundary Conditions</u>: Identify and justify appropriate boundary conditions for physical situations
- <u>Methods of Solution</u>: Implement analytical, numerical, and computational methods to solve governing equations

Transport Phenomena
- <u>Conservation Principles</u>: Use conservation principles to derive governing rate equations, using techniques such as shell and macroscopic balances
- <u>Macroscopic Applications</u>: Apply conservation principles to broad-scale situations, like the Earth's atmosphere, where microscopic details are either unknown or more complex than the desired model requires
- <u>Microscopic Applications</u>: Apply conservation principles to small-scale situations, where microscopic details about the system are desired, including positional information
- <u>Constitutive Equations</u>: Relate fluxes to driving forces for transport through constitutive equations

Heat Transfer
- <u>Conduction</u>: Apply Fourier's "Law" and solve 1D and 2D conduction problems in solid and fluid materials with a variety of sources and sinks of energy
- <u>Convection</u>: Apply Newton's "Law" of Cooling with appropriate heat transfer coefficient correlations to convection problems
- <u>Radiation</u>: Identify roles of absorptivity, emissivity, reflectivity, and view factors in radiative heat transfer problems
- <u>Multimode</u>: Solve problems in which conduction, convection, and/or radiation coexist and "compete" and assess the relative importance of different routes of heat transfer

Figure 6.1: Example of syllabus learning outcomes for a heat transfer course.

1. **Atomic Bomb Energy** *(15 points)*
Learning Outcomes:
- Apply dimensional analysis to find dimensionless groups
- Estimate values of dimensionless groups from data

Scientists took high-speed photographs of an atomic bomb blast during a test in 1945 at Alamagordo, NM. After the war, these high-quality photographs appeared in a 1947 issue of *Life Magazine*. The U.S. military worked hard to protect the secrets of the bomb program for many years, and they unknowingly gave away vital information. British and Soviet scientists estimated the energy of the test bomb using only these *Life Magazine* pictures and some knowledge of the physics of explosions and shockwaves.

You'll use dimensional analysis to uncover this secret, too. And you'll only need **_one_** of the published pictures. Assume a total amount of energy, E, dumps into an infinitesimal volume very rapidly. Furthermore, assume the resulting spherical shockwave with radius, $r(t)$, expands into the surrounding undisturbed air with density, ρ.

  (a) Since there are four variables and three different units of measurement, a single dimensionless number adequately represents the physics. Since there is only one dimensionless number, it remains constant during the expansion of the shockwave. Identify this dimensionless number—not by name, but by the ratio of constants and variables. Show how you arrived at your result and check whether the final result is dimensionless. *(8 points)*
  (b) Even though you'll assume that the constant is unity for part (c), describe at least one simple model experiment to estimate the actual value of this constant. *(2 points)*
  (c) Use the figure to estimate the value of energy. Assume the value of the dimensionless group from (a) is 1. (Express your answer in T with one significant digit, where T is tons of TNT and $1\ T \approx 4.2 \times 10^9$ Joules.) *(5 points)*
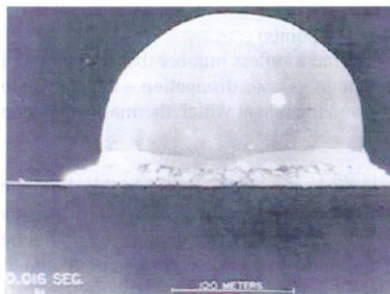
Figure 1.1: Shockwave from the Trinity atomic bomb test. The image shows a hemispherical shockwave. The time stamp on the photo is 0.016 sec. A scale bar indicates a distance of 100 meters. The shockwave is approximately 2.1 times the scale bar in width and 1.3 times the scale bar in height. Source: Taylor, G. The formation of a blast wave by a very intense explosion. II. The atomic explosion of 1945. *Proc. R. Soc. Lond. Ser. Math. Phys. Sci.* 175–186 (1950).

Figure 6.2: Example of highlighting the learning outcomes in an existing assignment.

The result had a two-fold benefit—we eliminated or adjusted homework problems that did not contribute to students achieving learning outcomes, and students were able to connect the practice they did on the homework to the overall goals of the course. Fundamentally, however, this restructuring was not true backwards design—much of the course stayed the same and did not incorporate the learning outcomes as the driving principle.

In designing and teaching a survey course on viscoelasticity for undergraduate students, I was able to incorporate backwards design from the beginning of the course (Figure 6.3). Each learning outcome met three criteria: 1) it was accomplishable with only three hours of total class content a week, 2) it was specific enough to allow for assessment, and 3) it would not require that the students have prior knowledge of topics in fluid mechanics or materials science (because the course had no prequisites and participation crossed many majors).

The learning outcomes in the syllabus then translated into learning outcomes for individual assignments (Figure 6.4). These assignments acted as both the practice and the assessment of working toward learning outcome (formative assessment).

During the term, assignments and class activities structured around the learning outcomes were generally successful: assessment of student learning outcomes demonstrated that students were practicing the desired skills. In contrast, class sessions in which I did not follow backward design were not as successful. For example, my lecture on normal stresses in viscoelastic flows, an important concept in understanding behaviors such as rod-climbing in bread dough, stood out to me as a failure to design towards learning outcomes. As the instructor, I had instead imposed my preconception that the mathematics of normal stresses was essential. I failed to paln for students unfamiliar

Reading Abstracts (Discussion Forum Post)
Due: Sunday, April 8th, 11:59 pm

Learning Outcome:
Students will be able to discuss and assess literature in the field of viscoelasticity.

Task:
Read the abstract provided. Following the guidelines from class (repeated below as a Reminder) on how to break down abstracts, make a post in the Week 1 Forum answering the following (label which part is which!):

1. What is/are the main conclusion(s) you saw in the abstract?
2. What key terms might you need to look up to read this paper? (List the terms, you don't have to look them up for this post.)
3. Why would someone in the field of viscoelasticity care about the results presented in this paper?

Reminder
Suggested steps for breaking down abstracts:
1. Look for keywords in the title.
2. Search for main ideas of abstract.
   a. Motivation: Why would someone care about the results presented in this paper?
   b. Main conclusion(s): What are the 1–2 most important things concluded in this abstract?
3. Make a list of key terms you might need to look up before you could read the paper.
4. Questions to ask yourself (not required for this post):
   a. What evidence would I need to see to believe the conclusion(s)?
      i. If you have prior knowledge, sketch what you might expect a figure with that evidence to look like.
   b. What could I do with the conclusions?

Figure 6.3: Example of syllabus learning outcomes for a course on viscoelasticity.

with tensor math, including most of my target audience—first- and second-year non-engineering students. As soon as I gave the lecture, I observed that students left class confused, without developing a deeper understanding of viscoelastic materials. Class sessions that included group discussion of abstract concepts and hands-on labs designed to address specific learning outcomes had greater positive impact on student learning.

Reading Abstracts (Discussion Forum Post)
Due: Sunday, April 8th, 11:59 pm

Learning Outcome:
Students will be able to discuss and assess literature in the field of viscoelasticity.

Task:
Read the abstract provided. Following the guidelines from class (repeated below as a Reminder) on how to break down abstracts, make a post in the Week 1 Forum answering the following (label which part is which!):

1. What is/are the main conclusion(s) you saw in the abstract?
2. What key terms might you need to look up to read this paper? (List the terms, you don't have to look them up for this post)
3. Why would someone in the field of viscoelasticity care about the results presented in this paper?

Reminder
Suggested steps for breaking down abstracts:
1. Look for keywords in the title
2. Search for main ideas of abstract
   a. Motivation: Why would someone care about the results presented in this paper?
   b. Main conclusion(s): What are the 1-2 most important things concluded in this abstract?
3. Make a list of key terms you might need to look up before you could read the paper
4. Questions to ask yourself (not required for this post)
   a. What evidence would I need to see to believe the conclusion(s)?
      i. If you have prior knowledge, sketch what you might expect a figure with that evidence to look like
   b. What could I do with the conclusions?

Figure 6.4: Example of structuring an assignment to address a single learning outcome for a course using backwards design.

Next Steps

Taking the lessons from both restructuring the heat transfer course assignments and building the viscoelasticity course from the ground up, my next steps in teaching a course would be to apply backwards design not just to assignments and activities, but to each individual class period. Evaluating content through the lens of backward design assists in allocating instruction time to the most valuable activities—those that will give students the most insight.

As discussed below in Scaffolding and Transparent Teaching, clear discussion of desired outcomes from course elements also helps students structure their learning time and meet expectations, resulting in a course where diverse students can more readily thrive.

6.3 Scaffolding

Technique and Motivation

Scaffolding is explicit structure in coursework that walks students through the steps needed to complete the tasks requested.[10] In a project setting, it can look like outlining each deliverable and what incremental stages those deliverables need to go through to become final products. In a homework assignment setting, it could include explicitly asking students to setup the problem before solving it, to uncorporate specific details in their solutions, and to analyze if a result seems reasonable.

Scaffolding helps students build metacognition and self-regulation skills—i.e., learning how to learn and how to manage their time while learning.[10] By structuring course assignments with each step intentionally laid out, students can look at the whole assignment and start to make better predictions of how long it will take them, where they can anticipate that they will need to ask questions, and how to schedule out their work time to complete the assignment. In assignments or projects that take place over a longer period, scaffolding gives structured check-in points via intermediate work due prior to the final deadline. These check-ins are additional opportunities for feedback, where students who are confused or lost can get help sooner, and where instructors can intervene if a student is overwhelmed or missing deadlines, instead of at the end of a term where intervention may be too late.

Implementation

In the viscoelasticity survey course, I used writing a paragraph for a *Wikipedia* article relevant to the course material as a term-long project (Figure 6.5). The project began with a brainstorming step, and progressed through outlining, drafting, peer feedback, and revising before the students turned in the final results. The intention of scaffolding the project and deliminating so many incremental stages was to prevent student procrastination from interfering with their ability to give worthwhile feedback before the final due date and to make the project feel meaningful over the course of the term, rather than a rushed project at the end.

Final Project
Due dates throughout the quarter

For the final project for this course, you will write or extend a short *Wikipedia* article on a topic not already well-covered on *Wikipedia*. For this project, expect to find at least 1–2 relevant literature papers as sources and/or accompanying material.

Learning Outcomes:
Students will be able to:
- Differentiate between solid, liquid, and viscoelastic material properties.
- Discuss literature in the field of viscoelasticity.
- Explain the physical behavior corresponding to models of viscoelasticity.
- Hypothesize qualitative behavior of viscoelastic materials.

General Timeline:
- Week 3: Submit list of 2–3 possible topics
- Week 5: Choose topic
- Week 6: *Wikipedia* Course
- Week 6–7: Outline
- Week 8: Draft for peer feedback
- Finals: Final version due

Task:
Through this project, you will contribute approximately 1–2 paragraphs of material towards *Wikipedia* article(s). The goal is to have well-cited text that is accurate in a technical sense, while still accessible to people outside the field of viscoelasticity.

You can either choose a single topic and contribute 1–2 paragraphs of material or add citations and clarify material across multiple articles totaling 1–2 paragraphs.

Grading:
The final project is worth 40% of your grade in total, and is graded out of 100 points total. See the Week-by-Week breakdown for value of individual parts.

Submission:
All portions of this project will be submitted through Moodle. If you would like to, you may make a *Wikipedia* account of your own and submit your modifications to the article(s) you have worked on throughout this project. Editing *Wikipedia* with your final version of the articles is encouraged but not required as a part of this course.

(a) Overall structure of the final project.

Week-by-Week Breakdown

<u>Week 3</u>
Task: Look at *Wikipedia* and come up with at least 2–3 topics that you think would be suitable to write a short article for or add material and sources to
Expected Outputs:
Submit a document containing the following to Moodle:
- List of at least 2–3 topics (and any corresponding *Wikipedia* links)
Due Date: Wednesday, April 25th, 2:00 pm
Grading: Completion—worth 10 points (4% of final grade)

Suggestions for finding suitable topics:
- Start from the articles on viscoelasticity, rheology, or the names of any topics on the syllabus. Look for short or unclear articles, articles with warnings that they need better citations or clarifications, or non-existent articles (usually in red on a page, or not found through a search).
- Look up viscoelastic materials discussed in class or elsewhere and see if they have a section on their viscoelasticity. If the section is nonexistent, confusing, and/or inaccurate, it will likely be a suitable topic.
- If your research field/other interests include topics related to viscoelasticity, try looking up those topics and see if articles exist and contain relevant information on viscoelasticity.
- Talk to Red for suggestions of topics if you aren't finding topics that you think would work.

<u>Week 5</u>
Task: Look at feedback on topics and choose which topic(s) you want to pursue.
Expected Output:
Submit the following to Moodle:
- Topic(s) chosen
- Original versions of article(s) for each topic chosen (pdfs or copy-pasted text)
Due Date: Wednesday, May 9th, 2:00 pm
Grading: Completion—worth 10 points (4% of final grade)

<u>Week 6</u>
Task: Complete course on how to write for *Wikipedia* for students (~1 hour). https://en.wikipedia.org/wiki/Wikipedia:Training/For_students
Expected Output:
- Submit a screenshot of confirmation of completion on Moodle (note: you are not required to make a *Wikipedia* account—you can instead screencap the last page of the training)
Due Date: Wednesday, May 16th, 2:00 pm
Grading: Completion—worth 10 points (4% of final grade)

(b) Week-by-week breakdown (part 1).

<u>Week 6–7</u>
Task: Outline your writing on your topic(s). Look up literature articles you want to use (note: *Wikipedia* prefers secondary sources, like review articles, instead of primary sources) and prepare citations.
Expected Output:
Submit the following to Moodle:
- Outline of what information you plan on incorporating into the article(s) (does not have to have finalized language).
- Citations/Source documents for information.
- Any questions you have about what you are writing about, how to write the sections, or what sources to use.
Due Date: Wednesday, May 23rd, 2:00 pm
Grading: Rubric provided during Week 6, worth 10 points (4% of final grade)
*Points lost in this phase can be earned back in the Draft phase

<u>Week 8</u>
Task: Draft your contributions to the *Wikipedia* article(s) you chose with citations. Include any surrounding text necessary for clarity and indicate what text is yours. Print out at least 4 copies for peer feedback in class (or email Red your draft by midnight on Tuesday to have Red print them out).
Expected Output:
Bring to class:
- Draft of contributions with citations, along with surrounding text (if applicable).
- Something with which to take notes on peer feedback.
Due Date: Wednesday, May 30th, 11:00 am ****Note that the draft needs to be ready for class and you will need to print copies/email Red your draft beforehand.
Grading: Rubric provided during Week 7, worth 20 points (8% of final grade)
*Points lost in this phase can be earned back in the Final Version phase

<u>Week 9-Finals</u>
Task: Using your draft and any peer/instructor feedback, revise your contributions to the *Wikipedia* article and submit a final version. If you have a revised draft you would like feedback on before submitting, email Red at least 48 hours prior to the final deadline.
Expected Outputs:
Submit the following on Moodle:
- New version of article(s)/article section(s) with and without your changes indicated on the document.
- 1–2 sentences on how you incorporated feedback.
Due Date: Wednesday, June 13th, 11:59 pm
Grading: Rubric provided during Week 7, worth 40 points (16% of final grade)

(c) Week-by-week breakdown (part 2).

Figure 6.5: Example of scaffolding a final project over the course of a term.

Throughout the project, students were able to respond to feedback at each stage and adjust their work accordingly. Students who wanted to go above and beyond had the opportunity to invest more time (one student prepared an entire article, rather than one paragraph); students new to the field and less experienced in writing got support at multiple stages in finding good resources and writing well. As an instructor, I practiced laying out the tasks clearly and setting up reasonable expectations that the students could meet during the allotted class hours, but still facilitated them progressing towards learning outcomes.

Even in more advanced courses, students may not structure their time well or feel comfortable asking for feedback early. I attempted to support students who did not fully understand the expectations for a final presentation in a graduate-level polymer physics course, by adding an additional step that enabled me, as a teaching assistant, to identify and help students who were unsure how to craft a presentation. The additional step of creating a single summary slide that outlined their presentation (Figure 6.6) was particularly relevant to the undergraduate and first-year graduate students in the polymer physics course, who did not have much practice in giving technical talks to a professorial audience.

Next Steps

Based on my experiences with scaffolding final projects for students, I plan to implement scaffolding as early as the first homework assignments, particularly in introductory courses with many first-year undergraduate students who need the most structure as they learn how to learn in a college setting. In courses where presentations are the final product, I would use in-class practice mini-presentations at multiple points over a term to identify where students need the

Summary Slide Guidelines
The talk will primarily be composed of 4 sections:
- Background/Motivation
- Problem Framing
- Approach
- Expected Results

The summary slide (due May 28th) should contain the biggest feature of each part (4 quadrants each with an image and/or minimal text is one way to make the slide).

The objectives of this assignment are:
- Solidify your idea(s) of what will go in each section
- Make a summary slide that can be used at the beginning and/or end of your talk
- Provide an opportunity for the TA to give feedback on all major sections of your presentation prior to the final presentation

Make sure you include your references!

Figure 6.6: Example of scaffolding a presentation.

most support in their presentation skills. In future writing projects, I would coordinate with campus resources like the writing center to connect students with expertise outside my domain and to build in additional feedback as a part of the intermediate stages.

6.4 Transparent Teaching

Technique and Motivation

In many STEM classrooms, assignments and exams are structured as a series problem statements in which students are asked to find some unknown quantity given some known information about a situation. The value of finding each solution is often assumed to be obvious—the students will practice a concept directly related to the problem, whether it be a problem-solving approach or incorporating information they have learned through the class. For a student new to a field and not aware of how to organize the information they are receiving or how to prioritize their time spent learning, the implicit aspects of these

questions can inhibit their ability to effectively use the problem presented as a learning tool. The concept of transparent teaching seeks to make the implicit expectations and purpose of assignments clear and available to students through explicit discussion of both the motivation of the questions being asked and the grading criteria that will be used to evaluate their work.[3,11]

Making an assignment "transparent" consists of including three components: a specific purpose (tied to the learning outcomes of the course and how it is useful for students in the long-term), a clear outline of tasks (to make explicit what is expected of students), and criteria for evaluation (including examples of critiqued work demonstrating what would be considered excellent). As discussed in Backwards Design, focusing work expected of students on learning outcomes helps instructors ensure that each question contributes to the goals of the course and assists students in seeing the importance of the work in the context of the course, the larger trajectory through the curiculum, and their future life and career. The outline of the tasks expected can be tailored to the level of scaffolding that fits the students and the course, while still stating what is to be done and how to go about it (including what can seem like simple instructions such as "solve this equation by hand" or "include units at all intermediate steps," but might not be assumed by students). Criteria with examples allow students to develop self-assessment skills where they can start to predict how they are doing on a particular problem before they turn it in. Students can then ask for help sooner to address gaps in knowledge or approach. Outlining criteria prior to handing out an assignment also challenges instructors to clearly articulate what they are looking for, which is one way to combat unconscious bias in evaluation.[12]

Transparent teaching improves the experiences of all students, with additional gains for students from minoritized groups.[13] In a large-scale study of 1,800

students across seven institutions, students in courses with two transparently-designed replacement assignments demonstrated gains in belonging, confidence, and job-relevant skills compared to students who experienced traditional homework assignments. In particular, underserved students (under-represented racial and ethnic identity, low-income, and/or first-generation) showed even larger benefits than their majority peers. Students responded positively to knowing the assignment's purpose and relationship to the course as a whole, and understood what they should do and how they would be evaluated.[3,11,13]

Implementation

As a teaching assistant for the heat transfer course, I included both the learning outcomes and a set of expectations for elements of a problem solution on every homework set (Figure 6.7). By doing so, students knew before they turned in the first assignment what graders would be looking for as a baseline, instead of finding out when the graded assignments were returned to them (usually upon turning in set 2) what our expectations were. In addition, the learning outcomes could direct them to useful reading if they found gaps in their understanding during the assignment.

On the graders' side, I developed rubrics for point-by-point breakdown of many of the problems assigned; however, these granular criteria were not shared with students until after grading was completed, failing to be as transparent as would be desired.

In structuring the final project for the viscoelasticity course, I incorporated transparent teaching practices at each stage of the writing process (Figure 6.8). Each section of the project sets out the task to be accomplished, what I expected the student to take action on, and the rubric (grading criteria)

ChE103a: Heat Transfer
Problem Set # 1: Dimensional Analysis; Fourier's "Law" of Conduction
Due: **Monday, 02 Oct 2017 in class**

Completing this set is practice for:

I.   Dimensionless Groups
     Suggested Reading: See Folder on Moodle—Short Version of
     Dimensional Analysis Tutorial [DAT] highly recommended, others
     optional
     a. Applying dimensional analysis to find dimensionless groups
     b. Estimating values of dimensionless groups from data
     c. Scaling a given equation to find an appropriate dimensionless group
     d. Judging the relative importance of different phenomena in a situation
        based on different values of a dimensionless group

II. Conduction
     Suggested Reading: BSL 9.1
     a. Defining thermal conductivity (in symbols and words)
     b. Estimating thermal conductivity from data
     c. Evaluating qualitatively the relative flux and temperature drops in
        different materials based on thermal properties
     d. Finding temperature profiles using Fourier's "Law" of Conduction

Expectations for each problem:

- Restate the problem
  - o Write down any given information
  - o Sketch a picture or diagram
  - o Label/define all variables/symbols used
- State your assumptions
- Clearly write out your solution
  - o Include helpful notes about your steps, especially if you tried multiple
       tactics to a problem or if you made new assumptions during a problem
  - o Usually more than just equations is needed—show the flow between
       different steps and explain why
- Evaluate whether your answer is reasonable
  - o If numerical, is the order of magnitude in the right range?
  - o If numerical, how many significant digits? (How precise is your answer?)
  - o If symbolic, does the dependence on the different variables make sense?
  - o If numerical or symbolic, what are the units/dimensions? (Is it a length
       with units of meter/second? If so, something has gone wrong.)
- Cite your sources (if sources outside of the problem set are used)
- Unless otherwise stated, software packages such as Mathematica should only
  be used to CHECK your work, and should not replace your own solution to a
  problem

Figure 6.7: Example of outlining expectations.

for that section, and the project as a whole was motivated using the course learning outcomes (Figure 6.5).

Final Project Draft

Due Wednesday, May 30th, 2018, 11:00 am

Task: Draft your contributions to the Wikipedia article(s) you chose with citations. Include any surrounding text necessary for clarity and indicate what text is yours. Print out at least 4 copies for peer feedback in class (or email Red your draft by midnight on Tuesday to have Red print out).

Expected Output:

Bring to class:
- Draft of contributions with citations, along with surrounding text (if applicable)
- Something with which to take notes on peer feedback

Due Date: Wednesday, May 30th, 11:00 am ****Note that the draft needs to be ready for class and you will need to print copies/email Red your draft beforehand.

Grading: Worth 20 points (8% of final grade)

*Points lost in this phase can be earned back in the Final Version phase

Content:

You are expected to compose your full contributions to the Wikipedia article(s). It needs to be written clearly enough that I can understand it and be accurate according to your sources.

Language:

Your contributions should be written in such a way that they could be submitted to their Wikipedia article. My expectations are:
- Tone is formal (think an encyclopedia, not a journal article, or look at good Wikipedia articles)
- Minimize jargon and overly technical language
- Is your contribution understandable to a layperson in the context of the whole article?

See https://en.wikipedia.org/wiki/Wikipedia:Writing_better_articles if you need more guidelines

Sources/Citations:

Sources should be appropriate for Wikipedia—secondary sources like review articles or textbooks and properly cited (see https://en.wikipedia.org/wiki/Wikipedia:Tutorial/Citing_sources for how to format the citations). These sources may be the same sources from the outline stage if they were accepted at that stage.

Address Feedback:

Address all feedback from the outline stage by either implementing suggestions or by providing (sufficient) justification for why your contribution will be better/more accurate/clearer/etc. by not implementing the feedback (please do challenge my suggestions if they don't work for you). This part is where you earn back points from the Outline stage. Please indicate what changes you made in response to feedback.

(a) Transparent teaching structured assignment

Rubric: Intermediate points can be earned for intermediate work and points lost can be earned back by addressing issues when submitting Final Version

	Excellent (full points)	Acceptable (half points)	Missing (no points)
Content (Max 5 points)	Enough content is present to fill 1-2 paragraphs of material). Information is accurate and clear	Enough content is present to fill 1-2 paragraphs, but information is inaccurate and/or unclear OR information present is not enough to compose final article	No content present
Language (Max 6 points)	Article content is primarily written in Wikipedia-appropriate style/language	Article content is partially written in Wikipedia-appropriate style/language	Draft is exclusively in jargon
Sources (Max 2 points)	Appropriate source(s) present (1-2 at least, from secondary source) and cited using Wikipedia's citation tools	Appropriate source present but not cited, or citation present for an inappropriate source	No sources present
Address Issues (Max 5 points plus additional points lost at Outline)	Addresses all feedback from outline stage, either by modifying the work or providing sufficient justification	Addresses some feedback from outline stage	Did not address feedback from outline
Peer Feedback (Max 2 points, earned in class)	Participated in giving peer feedback	Was present, but not engaged in giving feedback to peers	Did not give feedback to peers

(b) Example of a grading rubric available to students

Figure 6.8: Example of transparent assignment

As an instructor, I noticed that grading using a rubric improved my consistency between students and removed moments of doubt as to whether I was giving the student the grade they deserved. Additionally, students met my expectations more consistently, particularly when revising for later versions, as they knew what I would be looking for.

Transparent teaching is beneficial to instructors as well as to students. As a part of preparing class materials for hand off to the next teaching assistant for a polymer physics course, I wrote up a set of suggestions for giving feedback to students, as I also struggled with knowing how to guide them in the project. Having explicit criteria to check for can prompt efficient time spent giving feedback and prevents loss of institutional memory during gaps in the teaching of the course.

Next Steps

In transparent teaching, an important component in addition to clear grading criteria is examples of critiqued student work. As a new instructor, I did not have examples of past student work to use in my viscoelasticity course. Going forward, a goal each time teaching a course would be to collect useful student example work that exemplifies the overall expectations, but still has room to be critiqued using the rubric. In science courses with problem sets, this process can be difficult because of reuse of problems from year to year in order for assignment quality to benefit from iterating. Responses to practice or past year exam problems may be a route to collecting good examples while not compromising students' abilities to use problems as a way to evaluate their own learning. In projects or presentations where the topics are chosen by the students, a prior year's work can be used for demonstrations without interfering with assessing student responses to new problems.

Summary Slide Feedback Guidelines
The summary slide is the last chance for formal feedback before the final presentation. Students who did not have much at this stage did not do as well in their presentations.
For each section, look for the following:
- Background/Motivation:
  - Cartoons/figures that relay the main concepts
  - Setup for why the topic is of current interest
  - Polymer focus (versus biological, colloid, etc.)
- Problem framing:
  - Clear and specific question(s) to address
  - Convincing reason why the problem is important and relevant
  - An answer for what is missing/insufficient in the literature
- Approach:
  - A feasible and clear plan of approaching the problem
  - Something substantially new/original
    - Avoid "just simulate it" (If they are proposing a simulation, what new elements compared to the literature would they be introducing?)
    - Going at least one step beyond their sources or taking a very different tactic to the literature
  - Theoretical tactic (not only experimental, but experiments can be a supplement)
  - Reasonable set of parameters and explanations for why they are included (and not others)
- Expected Results
  - Qualitative behavior changes (regimes of behavior based on parameters in the problem for example)
    - Sketching comparison curves is one good way to look at it
    - If they have taken issue with a quantitative flaw in the literature, their expected results will need to be more quantitative in nature
  - Specificity in expectations (vague descriptions are easy to tear apart/question, more specific predictions help give the approach weight and help students avoid pitfalls around over-claiming)
  - Avoiding "too expected" of expected results (i.e., "this will behave just like another system"—why do we want to do the approach if the results are exactly the same as the other one?)
  - Comparison to literature results (experimental and theoretical ideally)

Students are not likely to be able to fit all of these parts on the summary slide, but you'll want to prompt the other parts in your feedback.

Emphasize to students that they don't actually have to solve the problem (by simulation or fully solving the theory).

Figure 6.9: Example of transparency for a teaching assistant for giving feedback to students.

6.5 Peer Interaction

Technique and Motivation

In a traditional classroom experience, an instructor primarily lectures, with occasional pauses for students to ask questions and calling on students to respond to instructor questions. The interaction is primarily between a single student and the instructor, although student questions and responses benefit the whole classroom. In alternate models of classroom engagement, students can be asked to interact directly with each other as well as with the instructor. Three possible implementations of interactive teaching are discussed below: think-pair-share, teamwork, and peer review.

Implementation

Think-Pair-Share (TPS) is a documented and researched model of peer-based interactive teaching, in which students are given a question to think about their response to (Think), then asked to discuss their thoughts with a neighbor or small group (Pair), and students have an opportunity to convey their group responses (Share). TPS has been shown to increase engagement and confidence of students who may not otherwise feel comfortable with speaking in class due to a variety of reasons, such as personality, perceived ability, or previously experienced microaggressions, although the share step must still be carefully tailored to the classroom environment.[14–16]

In recitation sections as a teaching assistant for heat transfer, I used TPS as a tool for assessing where students were confused about the material. During lectures, students often did not speak up about where they did not understand the approach to solving the problems. In recitation, posing smaller problems and floating between groups to listen to the discussion often told me much more about what had been missed during class time. The peer teaching that

occurred between students also helped address gaps in learning that would be difficult to identify until after an assignment was turned in.

Teamwork between students can also act as a way to facilitate peer teaching. For low-stakes, in-class activities, students working together to brainstorm and solve problems can act as an extended TPS. In the viscoelasticity course, students worked in pairs on in-class labs, designing their own procedures to assess materials (Figure 6.10). In addition to completing the required analysis, students brought up their own experiences and independent research, which enhanced the discussion with their peer and supplemented the required pre-lab reading.

As a part of the on-going final project for the viscoelasticity course, I also set up a structured peer review session in which students read each other's work and gave constructive feedback (Figure 6.11). By directing students to consider different aspects of their peers' work, we collectively worked to avoid some pitfalls common to mentoring and feedback.[17] Students were able to hear a mixture of positive, critical, and neutral thoughts from their peers, and then make choices about what they wanted to implement, and justify their choice if they decided to not implement a piece of feedback.

Next Steps

As learned throughout teaching the viscoelasticity course, I seek to teach in a mode dominated peer work, either through TPS, in-class activities, or models like flipped classroom (where lectures are pre-recorded and students work on homework problems in class). Brief periods of in-class lecture can be used to recap topics, frame discussions, address common misconceptions, and wrap-up key points to remember, which keeps them short enough for students to pay attention to and primarily utilizes class time to be interactive.

Ice-Cold Silly Putty (Lab 2)
Due Dates: Hypothesis due May 9th, 2018, 11:00 am
Write-up due May 16th, 2018, 2:00 pm

Learning Outcome:
Students will be able to hypothesize qualitative behavior of viscoelastic materials, then perform experiments to test those hypotheses.

Task:
In this lab, you will manipulate the temperature of silly putty to demonstrate how viscoelastic properties change with temperature.

Expected Outputs:
You should prepare a document (or documents) with the following and submit it to the assignment on Moodle by the due dates and time.
   • Hypothesis [Due before the lab, see Moodle] (10%)
   • Observations [Scan/readable photo of handwritten copy or typed] (50%)
   • Answers to Questions (10% each)
In addition, participation in the lab will be part of your participation grade.

Introduction:
Time-temperature superposition is the concept that the time scale of perturbation and the temperature of a sample of viscoelastic material contribute to the measured properties in a coupled way. Raising the temperature of a sample decreases the relaxation time, while decreasing the temperature increases the relaxation time, allowing experiments to be conducted over a range of effective time scales for the sample, even if your equipment is limited in the range of time scales it can perform experiments over.

Collaboration and Participation:
Please formulate your hypotheses on your own—they are graded on completion, not accuracy. (See the Moodle)
You will be expected to work together in teams for this lab for collecting observations. You are encouraged to work together on recording observations and evaluating your hypotheses. Please submit your own answers to the questions, though you may discuss the answers with each other.
Participation in the lab itself will be part of your participation grade. Please let Red know ASAP if you will be absent so that they can organize a make-up session.

Figure 6.10: Example of collaboration and participation instructions.

Peer Feedback Prompts

You will have 4 mini-meetings over the course of the class, 1 for each prompt. With each new person, read the prompt and spend a few minutes reading their contribution(s). Then, each take a turn talking about the prompt for the other's contribution, while the author records notes about their contribution under the prompt on their sheet.

1. Look at the content of the contribution(s). Does the content make sense? Are there any spots you are confused or unsure? What parts seem ambiguous, if any?

2. Look at the language in the contribution(s). Evaluate how accessible the article is you and how accessible the article is to a layperson. Look for: jargon, highly technical sentences, or required field-specific knowledge.

3. Look at the context of the contribution(s). Does it make sense in context, either as part of an article or as a new article?

4. Look at the contribution(s). What is the strongest part? What is the weakest part? Ask the author what sections they are worried about.

Figure 6.11: Example of peer review instructions.

6.6   Striving Toward Inclusive Classrooms

My driving motivation in implementing each of these techniques is to be a better teacher and include all of my students in my instruction. I try to accomplish these core goals by iterating and learning. No two groups of students are identical—as the world around us changes, so too do our students and so can our teaching. Adopting evidence-based teaching practices into our classrooms can help us better serve students with diverse backgrounds and identities, while overall raising the bar for instruction and learning.

References

[1] N. Kober et al. *Reaching Students: What Research Says About Effective Instruction in Undergraduate Science and Engineering*. Washington, D.C.: National Academies Press, Jan. 15, 2015, p. 18687. ISBN: 978-0-309-30043-8. DOI: 10.17226/18687. URL: http://www.nap.edu/catalog/18687 (visited on 05/05/2021).

[2] Committee on Barriers and Opportunities in Completing 2-Year and 4-Year STEM Degrees et al. *Barriers and Opportunities for 2-Year and 4-Year STEM Degrees: Systemic Change to Support Students' Diverse Pathways*. Ed. by S. Malcom and M. Feder. Washington, D.C.: National Academies Press, 2016, p. 21739. ISBN: 978-0-309-37357-9. DOI: 10.17226/21739. URL: http://www.nap.edu/catalog/21739 (visited on 05/05/2021).

[3] M.-A. Winkelmas et al. "A Teaching Intervention That Increases Underserved College Students' Success". In: *Peer Review* 18 (No. 1/2 Winter/Spring 2016), pp. 31–36. URL: https://cte.ku.edu/sites/cte.ku.edu/files/docs/Branding/Winkelmes%20et%20al%202016%20Transparency%20and%20Underserved%20Students.pdf (visited on 08/18/2021).

[4] T. B. McNair. "Designing Purposeful Pathways for Student Achievement through Transparency and Problem-Centered Learning". In: *Peer Review* 18.1/2 (July 2, 2016). URL: https://www.aacu.org/peerreview/2016/winter-spring/guesteditor (visited on 08/18/2021).

[5] S. Powell and S. Arora-Jonsson. "The Conundrums of Formal and Informal Meritocracy: Dealing with Gender Segregation in the Academy". In: *Higher Education* (May 28, 2021). ISSN: 0018-1560, 1573-174X. DOI: 10.1007/s10734-021-00719-2. URL: https://link.springer.com/10.1007/s10734-021-00719-2 (visited on 08/16/2021).

[6] V. Sovero, M. Buchinsky, and M. D. Baird. "Playing Catch up: A Term-Level Investigation of the Racial Gap in STEM Retention". In: *Economics of Education Review* 83 (Aug. 2021), p. 102146. ISSN: 02727757. DOI: 10.1016/j.econedurev.2021.102146. URL: https://linkinghub.elsevier.com/retrieve/pii/S0272775721000650 (visited on 02/10/2022).

[7] N. C. for Science and Engineering Statistics. *Women, Minorities, and Persons with Disabilities in Science and Engineering: 2021*. Special Report NSF 21-321. Alexandria, VA: National Science Foundation, 2021. URL: https://ncses.nsf.gov/wmpd (visited on 02/08/2022).

[8] G. Wiggins and J. McTighe. "What Is Backward Design?" In: *Association for Supervision and Curriculum Development* (1998), p. 11.

[9]   R. Bowen. *Understanding by Design.* Vanderbilt University Center for Teaching. 2017. URL: `https://cft.vanderbilt.edu/guides-sub-pages/understanding-by-design/` (visited on 04/30/2022).

[10] T.-C. Lin et al. "A Review of Empirical Evidence on Scaffolding for Science Education". In: *International Journal of Science and Mathematics Education* 10.2 (Apr. 2012), pp. 437–455. ISSN: 1571-0068, 1573-1774. DOI: `10.1007/s10763-011-9322-z`. URL: `http://link.springer.com/10.1007/s10763-011-9322-z` (visited on 08/16/2021).

[11] M.-A. Winkelmas. "Transparency in Teaching: Faculty Share Data and Improve Students' Learning". In: *Liberal Education* 99.2 (Apr. 22, 2013). URL: `https://www.aacu.org/publications-research/periodicals/transparency-teaching-faculty-share-data-and-improve-students` (visited on 08/19/2021).

[12] N. D. Young, E. Jean, and T. A. Citro. *Acceptance, Understanding, and the Moral Imperative of Promoting Social Justice Education in the Schoolhouse.* Vernon Press, Sept. 3, 2019. 144 pp. ISBN: 978-1-62273-644-7. Google Books: `qoKSDwAAQBAJ`.

[13] K. Fisher et al. "Building a Culture of Transparency". In: *Peer Review* 18.1/2 (July 2, 2016). URL: `https://www.aacu.org/peerreview/2016/winter-spring/Fisher` (visited on 08/18/2021).

[14] A. A. A. Raba. "The Influence of Think-Pair-Share (TPS) on Improving Students' Oral Communication Skills in EFL Classrooms". In: *Creative Education* 8.1 (1 Jan. 6, 2017), pp. 12–23. DOI: `10.4236/ce.2017.81002`. URL: `http://www.scirp.org/Journal/Paperabs.aspx?paperid=73454` (visited on 04/30/2022).

[15] K. M. Cooper, J. N. Schinske, and K. D. Tanner. "Reconsidering the Share of a Think–Pair–Share: Emerging Limitations, Alternatives, and Opportunities for Research". In: *CBE—Life Sciences Education* 20.1 (Mar. 2021), fe1. ISSN: 1931-7913. DOI: `10.1187/cbe.20-08-0200`. URL: `https://www.lifescied.org/doi/10.1187/cbe.20-08-0200` (visited on 04/30/2022).

[16] L. Mundelsee and S. Jurkowski. "Think and Pair before Share: Effects of Collaboration on Students' in-Class Participation". In: *Learning and Individual Differences* 88 (May 2021), p. 102015. ISSN: 10416080. DOI: `10.1016/j.lindif.2021.102015`. URL: `https://linkinghub.elsevier.com/retrieve/pii/S1041608021000522` (visited on 04/30/2022).

[17] G. L. Cohen, C. M. Steele, and L. D. Ross. "The Mentor's Dilemma: Providing Critical Feedback Across the Racial Divide". In: *Personality and Social Psychology Bulletin* 25.10 (Oct. 1999), pp. 1302–1318. ISSN: 0146-1672, 1552-7433. DOI: `10.1177/0146167299258011`. URL: `http:`

`//journals.sagepub.com/doi/10.1177/0146167299258011` (visited on 02/09/2022).

A p p e n d i x   A

AUTOMATING ANALYSIS OF DRIPPING-ONTO-SUBSTRATE EXTENSIONAL RHEOMETRY

The automation techniques dicussed in this chapter were pioneered by Robert Learsch, and then formalized in the python package *dosertools*, which was co-developed by Robert Learsch and Red Lhota. The *dosertools* package is hosted at https://github.com/rlearsch/dosertools, along with documentation, and is installable via *pip install dosertools* for use with Python 3.8+.

A.1   Premise

Dripping-onto-substrate extensional rheometry (DoSER), as introduced in Chapter 1 is a form of capilliary break-up rheometry where a fluid is dripped from a nozzle onto a substrate and the resulting liquid bridge is observed via a high-speed camera. The diameter of the liquid bridge as a function of time is extracted from these videos and analyzed to determine key quantitative information about the fluid. Prior literature completed several steps in this analysis via user inspection; through the *dosertools* package, we sought to automate each step of the processing to reduce user-to-user variation and improve our reproducibility.

A.2   Background Subtraction and Binarization

Because light sources and cameras are not always uniform in their ability to produce and observe (respectively) light, we use background subtraction to reduce the impact of noise and other features of a non-uniform background (such as particulates on a lens or a dead pixel) on our processed images and thus

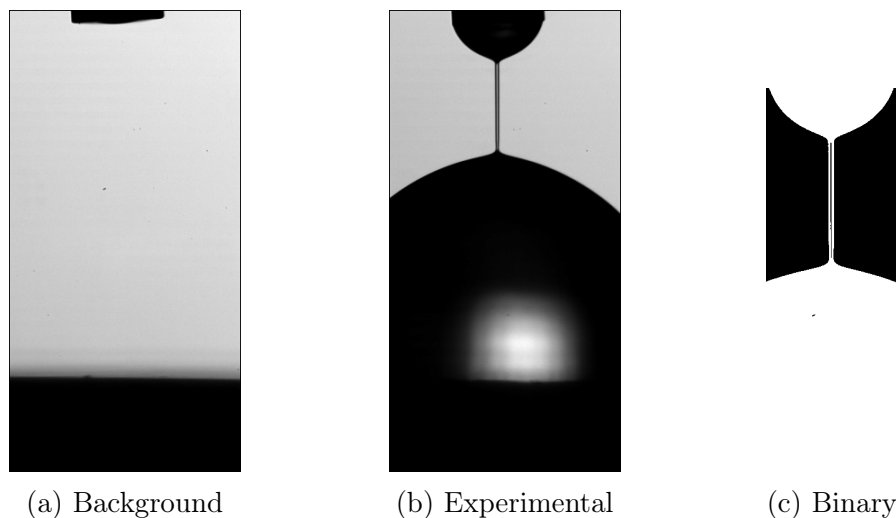(a) Background   (b) Experimental   (c) Binary

Figure A.1: Example (a) background, (b) experimental, and (c) binarized images for a 6M PEO, 0.0066 wt% in diionized water solution.

our diameter data. Our recommended best practice is to capture a 100 frame background video of the nozzle in its experimental position above a substrate with both a clean nozzle and substrate (Figure A.1(a)). In our experiments, it was sufficient to capture a single background video for a group of 5 experimental runs; however, if the light source and/or camera varies on shorter time scales, we recommend a background paired with each experimental video (Figure A.1(b)).

To perform the background subtraction, the *dosertools* package uses the median of the background frames, crops both the image and the background, subtracts the background median from the image, then rescales the background subtracted image based on the maximum pixel value.

After background subtraction, the images are binarized using the Otsu threshold method. Compared to the literature method, where an arbitrary cutoff value for binarization is chosen by the user,[1–5] the Otsu threshold does not require a user determined cutoff as it uses an algorithm to decide the cutoff that creates the two most distinct "bins" for the image.

After binarization, pixels where either the fluid, the nozzle, or the substrate are visible will be white, while the surrounding background will be black (Figure A.1(c)).

A.3 Liquid Bridge Diameter

To process the binary images into normalized diameter data, the *dosertools* package determines the diameter of the liquid bridge at all heights, then extracts the minimum diameter. In addition, the nozzle diameter is determined from either the background or experimental video, depending on which video has an image of a clean nozzle.

First, *dosertools* determines if the liquid bridge has already pinched off by looking for rows where no white pixels are present. If the liquid bridge is still intact, the minimum diameter is then computed as the average diameter of all diameters within 2 pixels of the absolute minimum. This averaging alleviates observed problems with stair stepping in the diameter with time due to the finite size of a pixel. By taking the average with similar rows, we obtain a better estimate of the minimum diameter. This minimum diameter (D) is divided by the nozzle diameter (D_0) determined earlier to obtain the normalized diameter (D/D_0) (Figure 1.8).

The frames-per-second reported for the video is used in conjunction with the frame number to determine the time (t) for each frame.

A.4 Determining the Critical Time

Core to the principle of DoSER is quantifying the slope of the elastocapillary (EC) regime to find the extensional relaxation time. To do so, and to fairly compare videos which may have different relative start and end times depending on user choices of when to cut videos, the critical time of transi-
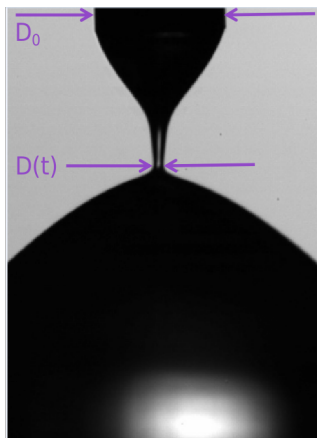
Figure 1.8: Example DoSER image showing the needle diameter D_0 and the minimum diameter of the liquid bridge $D(t)$. (repeated from page 16)

tion from either the inertio-capillary or the visco-capillary regime to the EC regime is used to align the normalized diameter data. Prior literature determined the critical time by inspection.[1-5] Robert Learsch developed a method for detecting the critical time through finding the moment of maximum strain rate within the window of normalized diameter in which transition occurs, which was implemented in the *dosertools* package. By finding the critical time systematically rather than by inspection, we significantly reduced user-to-user variation in analysis.

The *dosertools* determines the instantaneous measured strain rate via Equation A.1. An example strain rate curve is shown in Figure A.2. Given a window of normalized diameter values, it then finds the maximum strain rate in that window and specifies the time at the maximum strain rate as the critical time (t_c). Limiting the lower bound for the window of possible critical time addresses issues of noise in the data as the liquid bridge shrinks in diameter and becomes more difficult to accurately measure.

$$\dot{\epsilon} = \frac{-2(\frac{D/D_0}{dt})}{D/D_0} \tag{A.1}$$
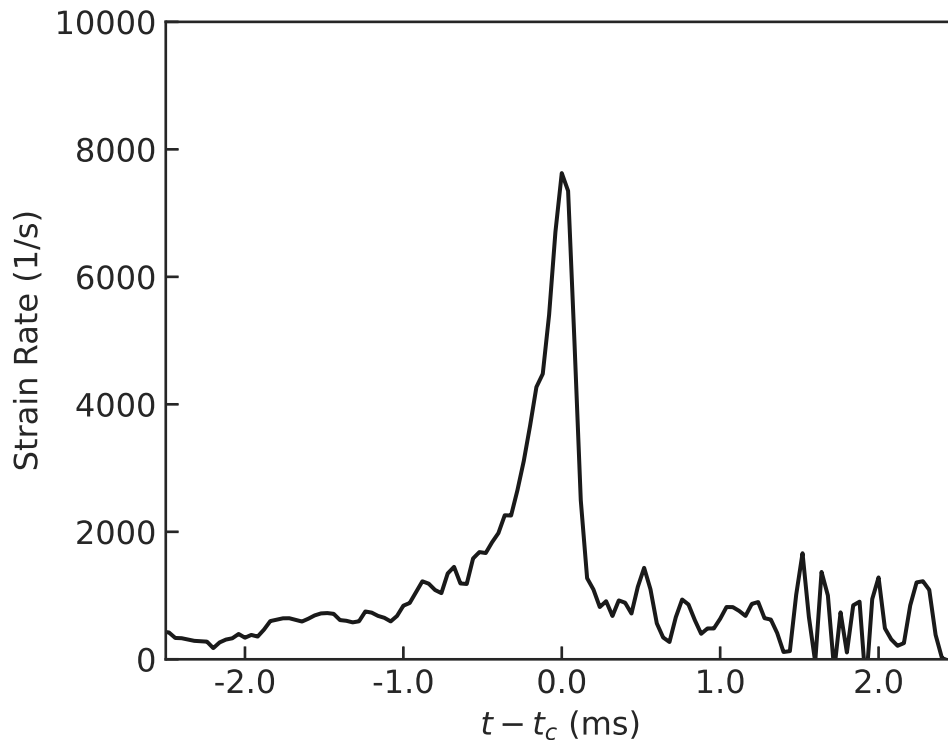
Figure A.2: Example of strain rate curve from a DoSER run.

A.5 Extensional Properties

Once the critical time has been determined, the EC regime (Equation 1.6) will consist of the data after the critical time and before the finite-extensibility regime (Figure 1.6). To determine the extensional relaxation time (λ_E), a linear regression is performed on data recast as $ln(D/D_0)$ versus $t - t_c$ (Equation A.2). The slope (m) obtained is thus used to calculate λ_E ($\lambda_E = -1/(3m)$).

$$\ln\left(\frac{D(t)}{D_0}\right) = A - \frac{1}{3\lambda_E}(t - t_c) \tag{A.2}$$

The process of determining the extensional viscosity of a solution from the liquid bridge diameter as a function of time will be discussed as part of Robert Learsch's thesis.
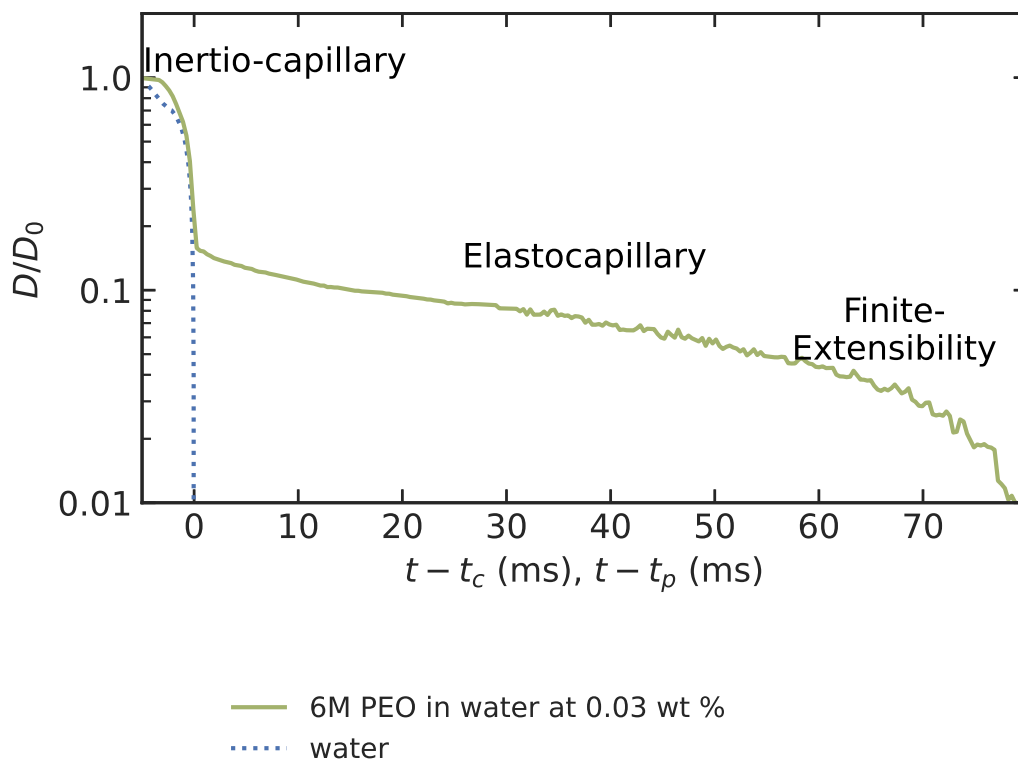
Figure 1.6: Example of measured capillary thinning for a polymer solution compared to water, demonstrating transitions for the polymer solution from the inertio-capillary regime (corresponding to water alone) to the elastocapillary regime, followed by finite-extensibility. (repeated from page 13)

A.6 Next Steps

The *dosertools* package uses arbitrary cutoffs for the fitting of the elastocapillary (EC) regime–work is ongoing to detect the beginning of the EC regime and the beginning of the finite-extensibility regime; however, finite resolution of the camera may mean that the finite-extensibility may not occur within the observable time of the thread, and the initial transition to EC does not immediately reach a exponential decay, inhibiting automation of this step. Additionally, the majority of data tested with *dosertools* has been from a single instrument–testing under other conditions and with other equipment will determine how robust the automation process is to alternate conditions.

References

[1] J. Dinic et al. "Extensional Relaxation Times of Dilute, Aqueous Polymer Solutions". In: *ACS Macro Letters* 4.7 (July 21, 2015), pp. 804–808. ISSN: 2161-1653, 2161-1653. DOI: `10.1021/acsmacrolett.5b00393`. URL: `http://pubs.acs.org/doi/abs/10.1021/acsmacrolett.5b00393` (visited on 03/17/2016).

[2] J. Dinic, L. N. Jimenez, and V. Sharma. "Pinch-off Dynamics and Dripping-onto-Substrate (DoS) Rheometry of Complex Fluids". In: *Lab on a Chip* 17.3 (2017), pp. 460–473. ISSN: 1473-0197, 1473-0189. DOI: `10.1039/C6LC01155A`. URL: `http://xlink.rsc.org/?DOI=C6LC01155A` (visited on 02/10/2020).

[3] J. Dinic, M. Biagioli, and V. Sharma. "Pinch-off Dynamics and Extensional Relaxation Times of Intrinsically Semi-Dilute Polymer Solutions Characterized by Dripping-onto-Substrate Rheometry". In: *Journal of Polymer Science Part B: Polymer Physics* 55.22 (Nov. 15, 2017), pp. 1692–1704. ISSN: 08876266. DOI: `10.1002/polb.24388`. URL: `http://doi.wiley.com/10.1002/polb.24388` (visited on 03/05/2020).

[4] J. Dinic and V. Sharma. "Macromolecular Relaxation, Strain, and Extensibility Determine Elastocapillary Thinning and Extensional Viscosity of Polymer Solutions". In: *Proceedings of the National Academy of Sciences* 116.18 (Apr. 30, 2019), pp. 8766–8774. ISSN: 0027-8424, 1091-6490. DOI: `10.1073/pnas.1820277116`. URL: `http://www.pnas.org/lookup/doi/10.1073/pnas.1820277116` (visited on 05/05/2021).

[5] J. Dinic and V. Sharma. "Flexibility, Extensibility, and Ratio of Kuhn Length to Packing Length Govern the Pinching Dynamics, Coil-Stretch Transition, and Rheology of Polymer Solutions". In: *Macromolecules* 53.12 (June 23, 2020), pp. 4821–4835. ISSN: 0024-9297, 1520-5835. DOI: `10.1021/acs.macromol.0c00076`. URL: `https://pubs.acs.org/doi/10.1021/acs.macromol.0c00076` (visited on 05/05/2021).

A p p e n d i x   B

POLYMER SYNTHESIS OF END-FUNCTIONAL POLYCYCLOOCTADIENE

All methods contained within written and performed by Hojin Kim.

B.1   Experimental Methods

Materials

All chemical reagents were obtained at 98-99% purity from Sigma-Aldrich or Alfa Aesar, unless specified otherwise. Magnesol®XL was purchased from The Dallas Group of America, Inc. ZSM-5 used was NH_4-ZSM-5, SiO_2:Al_2O_3 = 50:1 (Alfa Aesar). ^{1}H-NMR spectra were recorded in $CDCl_3$ or DMSO-d6 (Cambridge Isotope Laboratories) using a Varian Inova 500 spectrometer (500 MHz) with 128 scans. The molecular weights and dispersity index of the polymers were determined on a GPC system with a Wyatt DAWN EOS multi-angle laser light scattering detector (λ=690nm), a Waters 410 differential refractometer (RI) (λ=930nm), and four Agilent PLgel columns (pore size 103, 104, 105, and 106 Å) connected in series. THF was used as the eluent at the flow rate of 0.9mL/min with a temperature of 35°C. The data were analyzed using Wyatt Astra Software (version 5.3.4) using the Zimm fitting formula with $dn/dc = 0.125$ mL/g for PCOD in THF to obtain weight-average molecular weight (M_w) for each polymer reported.

Purification of Cyclooctadiene Monomer by Hydroboration with $BH_3 \cdot THF$

Representative procedure adapted from Ji and coworkers,[1] with the Magnesol®XL treatment of Wei and coworkers' procedure.[2] Instead of drying

Magnesol®XL with CaH_2 as in Wei and coworkers' procedure, Magnesol®XL was heated and vacuum-dried to remove moisture in this work.

Redistilled-grade cis-1,4-COD (66.7 g, 0.62 mol) was syringe transferred to a Schlenk flask in an ice bath under argon. 1M $BH_3 \cdot THF$ complex (108 ml, 0.11 mol) was slowly added into the flask. The flask was left to stir under argon at room temperature overnight. THF was evaporated under reduced pressure at room temperature until the concentration of residual THF in the mixture was below 300 ppm (verified by ^{1}H-NMR analysis). The COD was vacuum distilled from the mixture at 40°C. In a separate Schlenk flask, 9 g of Magnesol®XL (pre-dried under vacuum at 100°C) was added with a stir bar, and the air in the flask was removed via vacuum and the flask filled with argon. The distilled COD was syringe transferred into the Magnesol®XL and stirred under argon at room temperature overnight. After stirring with Magnesol®XL, the COD was vacuum distilled again from the Magnesol®XL mixture to a Schlenk flask in a dry-ice tub. After distillation, the flask was sealed with a Suba-Seal rubber septum under continuous argon flow, and stored in a freezer at -30°C. The purified COD was weighed to determine yield (35.3 g, 0.33 mol, 53.4% yield) and vacuum distilled again prior to use.

Purification of COD Monomer by ZSM-5

In a Schlenk flask, 2.5 g of Magnesol®XL, and 3.6 g of ZSM-5 were added without a stir bar. To remove water, the mixture of particles was dried overnight under vacuum at 100°C. After cooling the flask to room temperature, a stir bar was added and the flask was sealed with a Suba-Seal rubber septum, evacuated, and filled with argon. To the sealed flask, as-received redistilled-grade COD (26.5 g, 0.24 mol) was syringe transferred, and stirred at room temperature overnight. The COD was then vacuum distilled from the mixture to a
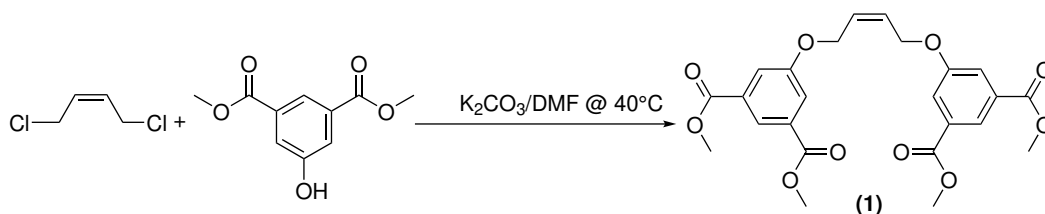
Scheme B.1: Reaction of dimethyl 5-hydroxyisophthalate and *cis*-1,4-dichloro-2-butene to form a tetra methyl ester intermediate, product **(1)**.

Schlenk flask in a dry-ice tub. After distillation, the flask was sealed with a Suba-Seal rubber septum under continuous argon flow, and stored in a freezer at -30°C. The purified COD was weighed to determine yield (25.2 g, 0.23 mol, 96.0% yield) and vacuum distilled again prior to use.

Synthesis of Tetra Methyl Ester Intermediate (1)

Dimethyl 5-hydroxyisophthalate (7.28 g, 34 mmol) and dry K_2CO_3 (7.06 g, 51 mmol) were weighed and loaded into a round-bottom flask (RBF). DMF (60 ml) was added into the flask, followed by *cis*-1,4-dichloro-2-butene (2.00 g, 15.3 mmol). The RBF was placed in an oil bath at 40°C and stirred overnight (Scheme B.1). The reaction mixture was poured into a separatory funnel, diluted with DCM (120 ml), washed with water (120 ml), and then 4 times with 1M HCl(aq) (120 ml each wash). The resultant organic phase was dried over $MgSO_4$ and filtered, and the solvent was removed under vacuum at room temperature. The crude product was purified by recrystallization in ethanol (40 ml) in the refrigerator overnight to yield analytically pure product (6.0 g, 12.7 mmol, 83.0% yield) as white crystals after filtration and solvent removal.

Tetra Methyl Ester Intermediate **(1)**: ^{1}H-NMR (CDCl$_3$, 500 MHz) 3.94 (s, 12H), 4.78 (d, 4H), 5.99 (t, 2H), 7.76 (d, 4H), 8.30 (t, 2H).
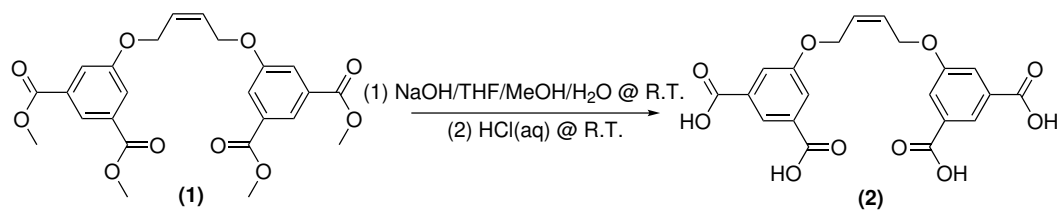
Scheme B.2: Hydrolysis of product **(1)** to produce product **(2)**, di-acid chain transfer agent (DA-CTA).

Synthesis of Di-Acid ended CTA, (DA-CTA) (2)

NaOH pellets (1.18 g, 0.030 mol) were dissolved in DI-water (6 ml) in a RBF, and methanol (12 ml) was added. The tetra methyl ester intermediate **(1)** (1 g, 2.1 mmol) was dissolved in THF (18 ml) in a separate container, and added slowly to the RBF. The mixture was stirred at room temperature overnight. Next, 1M HCl(aq) (40 ml) was added slowly into the RBF (Scheme B.2). The reaction mixture was poured into a separatory funnel, diluted with ethyl acetate (125 ml), and then washed twice with water (120 ml each wash). The resultant organic phase was dried over $MgSO_4$ and filtered, and the solvent was removed under vacuum at room temperature to yield analytically pure product (0.76 g, 1.8 mmol, 86.0% yield).

DA-CTA **(2)**: ^{1}H-NMR (DMSO-d6, 500 MHz) 4.89 (d, 4H) 5.91 (t, 2H), 7.68 (d, 4H), 8.06 (t, 2H), 13.28 (br, 2H, OH).

Synthesis of macro CTAs (mCTAs)

DA-CTA **(2)** (415.5 mg, 0.99 mmol) and 2,6-di-tert-butyl-4-methylphenol (BHT, 0.1 g, 0.45 mmol) were dissolved in THF (10 ml) in a Schlenk flask. The dissolved solution was degassed by 3 freeze-pump-thaw cycles and filled with argon. To the degassed mixture, 1 ml of degassed THF solution of second generation Grubbs Catalyst (**G2**, 8.4 mg, 9.89 μmol) was syringe transferred, immediately followed by addition of degassed, freshly vacuum distilled puri-

fied COD (5.0 g, 45.8 mmol). The mixture was stirred at 40°C overnight. The reaction was stopped by exposure to the air, and diluted with THF (40 ml). The polymers were precipitated by adding the THF solution drop-wise to a large excess of methanol. Methanol was decanted, and the polymers were collected in a vial with a silicone/PTFE septum cap, and dried under high vacuum. The vial was degassed by 3 cycles of evacuating/filling argon, and stored at -30°C. An mCTA for non-associative end groups was synthesized similarly using cis-2-hexene in place of DA-CTA, with same monomer:CTA molar ratio.

Polymerization Procedure without a CTA

A representative procedure for polymerization without a CTA is presented here. Additional polymerizations were also conducted with catalyst loadings of 0.5, 2, and 3 times the amount presented below at full conversion (and 0.5 times at partial conversion), while keeping the concentrations of all other components constant. BHT (0.1 g, 0.45 mmol) was added to a Schlenk flask, and dissolved in THF (10 ml). THF solution was degassed by 3 freeze-pump-thaw cycles and filled with argon. In a separate vial, a degassed THF solution of **G2** (1 mg/ml) was prepared, and 0.19 ml (0.224 μmol) of this solution was syringe transferred into the Schlenk flask, immediately followed by addition of degassed, freshly vacuum-distilled COD (5.0g, 45.8 mmol). For full conversion, the mixture was stirred at 40°C overnight. For partial conversion, the reaction was stopped either at 8 minutes for 400,000 COD/**G2** molar ratio or 16 minutes for 200,000 COD/**G2** by opening the Schlenk flask to expose the reaction mixture to air and diluting it in non-degassed solvent. A small aliquot was diluted with a large excess of deuterated chloroform for ^{1}H NMR analysis. The remainder (approximately 15ml) was diluted with 50ml non-degassed THF.

The polymer was recovered by pouring the THF solution into acetone (600 mL) for precipitation. The resulting polymers were stored as described previously.

Telechelic PCOD

Telechelic PCOD was synthesized following same procedure for the synthesis of mCTA, using mCTA instead of CTA. All telechelic polymers used in this study were synthesized using 5 g of COD, 0.16 ml of 1 mg/ml **G2** THF solution, 0.1 g of BHT, and 10 ml of THF, with COD/mCTA molar ratios of 390, 950, 2000, 3200, 6500, 8400, and 14000.

B.2 Characterization of Materials

Purification of Cyclooctadiene

To demonstrate removal of VCH by both hydroboration and zeolite treatment methods, NMR spectra were acquired before and after purification (Figure B.1). VCH peaks appeared in the untreated COD (Figure B.1a), while residual VCH after purification (Figure B.1b and c) was below the detection limit of 100 ppm.[1] After purification, the yield of COD was less than 55% for hydroboration and greater than 95% for the zeolite treatment.

Control and Accessible Range of Polycyclooctadiene Molecular Weight

Using hydroboration-purified COD, in polymerizations spanning a broad range of COD/catalyst and COD/CTA ratios, the highest PCOD weight average molecular weight (M_w) synthesized was 240 kg/mol (degree of polymerization, $DP \sim 2500$, number average molecular weight, M_n, of 145 kg/mol) at full conversion with no CTA. Under the same conditions, zeolite-purified COD provided M_w greater than 2 Mg/mol ($M_n > 1.3$ Mg/mol). Access to even higher molecular weight non-associative PCOD was acheived with zeolite-purified COD by stopping the reactions at low conversions, reaching M_w in
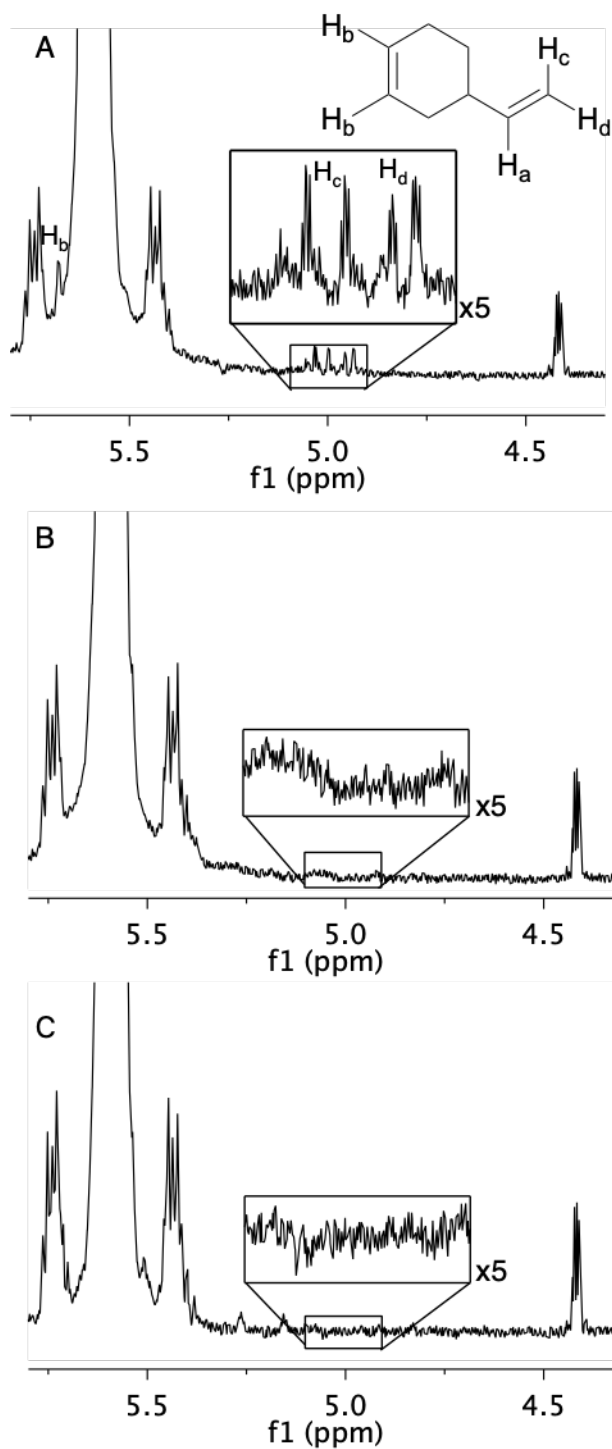
Figure B.1: (A) ^{1}H-NMR spectrum of untreated cyclooctadiene (COD) with VCH peaks at 5.67, 5.03, 5.00, 4.95, and 4.93 ppm, with labeled structure of VCH.[1] (B) ^{1}H-NMR spectrum of COD following treatment by hydroboration. (C) ^{1}H-NMR spectrum of COD following treatment by zeolite. Insets show 5x magnification of 5.1-4.9 ppm region.

Table B.1: Low Reaction Time Polymerizations

Catalyst $\left(\dfrac{molar}{ppm}\right)$	Reaction Time (min)	Conversion (%)	Trans/Cis Ratio	M_n (Mg/mol)	M_w (Mg/mol)	Đ
2.5	8	7	20/80	2.48	3.53	1.43
2.5	8	7	19/81	2.47	3.49	1.41
2.5	32	99	60/40	0.93	1.38	1.48
5	16	33	25/75	1.73	2.94	1.70
15	4	99	70/30	0.47	0.69	1.47

excess of 3 Mg/mol (M_n 2.5 Mg/mol) at the highest COD/catalyst ratio (Figure B.2).

With hydroboration-purified COD, control of molecular weight using COD/CTA ratio only extended to a COD/CTA ratio of ∼3000 (Figures B.2 and B.3). In contrast, using zeolite-purified COD, control of telechelic polymers extended to M_w over 1 Mg/mol (M_n over 740 kg/mol). The weight-average molecular weights produced from zeolite-purified COD were well fit by a logarithmic regression, with an equation $M_w[g/mol] = 390(COD/CTA)^{0.83}$ (Figure B.2), where the 95% confidence interval for the exponent was [0.80,0.87] and for the prefactor was [280, 530] (g/mol). In ROMP of COD, in addition to elongation of linear chains, there is also competing intramolecular secondary metathesis that generates small cyclic oligomers (backbiting) resulting in approximately 15% loss of COD to form small cyclic species.[3]

Reactions stopped at short time[2] to look for molecular weights achievable at low conversion are summarized in Table B.1.
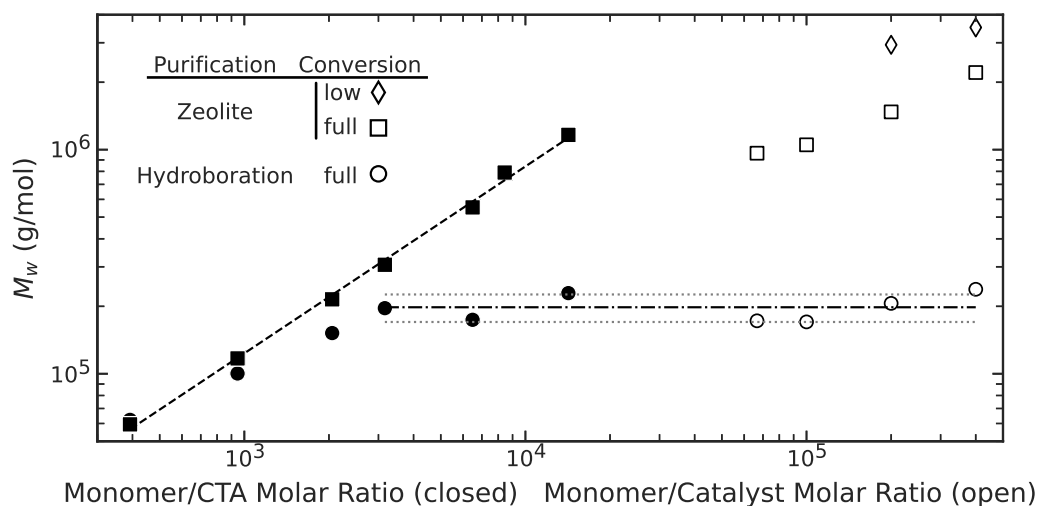
Figure B.2: Weight-average molecular weight (M_w) of polymers produced with (closed symbols) and without (open symbols) chain transfer agent (CTA) plotted as a function of monomer/catalyst molar ratio and a function of monomer/CTA molar ratio, respectively. Squares and circles indicate polymers produced from zeolite-purified and hydroboration-purified cyclooctadiene (COD), respectively, at full monomer conversion. Diamonds indicate polymers produced from zeolite-purified COD terminated at low conversion. Dashed line represents the power law regression of the molecular weights produced from zeolite-purified COD, $M_w[g/mol] = 390(COD/CTA)^{0.83}$, where COD/CTA is the monomer-to-CTA molar ratio. Dash-dotted line represents the average of the seven highest M_w obtained using hydroboration-purified COD (dotted lines above and below represent one standard deviation from this average, our best estimate of the uncertainty of the molecular weights represented in this figure).
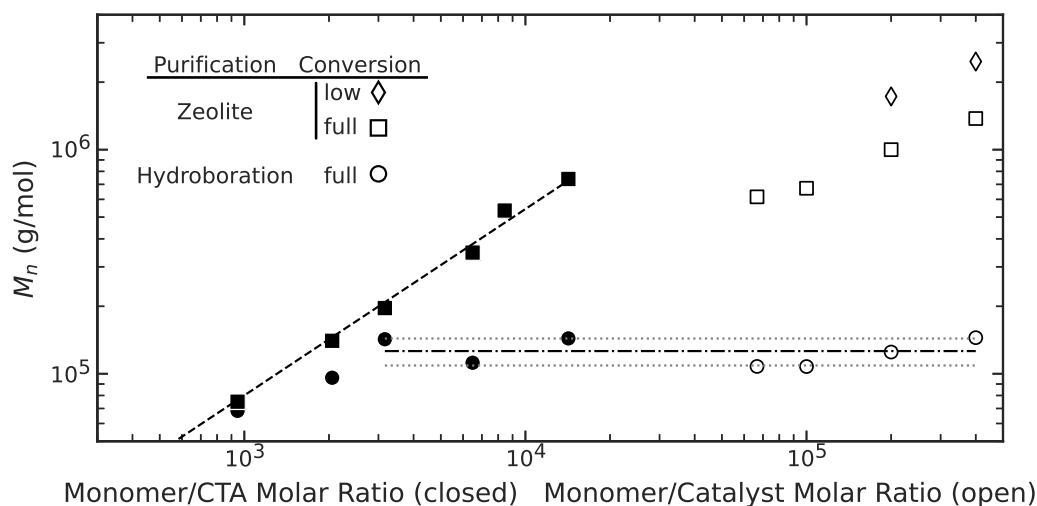
Figure B.3: Number-average molecular weight (M_n) of polymers produced with (closed symbols) and without (open symbols) chain transfer agent (CTA) plotted as a function of monomer/catalyst molar ratio and a function of monomer/CTA molar ratio, respectively. Squares and circles indicate polymers produced from zeolite-purified and hydroboration-purified cyclooctadiene (COD), respectively, at full monomer conversion. Diamonds indicate polymers produced from zeolite-purified COD terminated at low conversion. Dashed line represents the power law regression of the molecular weights produced from zeolite-purified COD, $M_n(g/mol) = 260(COD/CTA)^{0.83}$, where COD/CTA is the monomer-to-chain transfer agent molar ratio. Dash-dotted line represents the average of the seven highest M_n obtained using hydroboration-purified COD (dotted lines above and below represent one standard deviation from this average representing our best estimate of the uncertainty of the molecular weights represented in this figure).

References

[1] S. Ji, T. R. Hoye, and C. W. Macosko. "Controlled Synthesis of High Molecular Weight Telechelic Polybutadienes by Ring-Opening Metathesis Polymerization". In: *Macromolecules* 37.15 (July 2004), pp. 5485–5489. ISSN: 0024-9297, 1520-5835. DOI: 10.1021/ma0493067. URL: http://pubs.acs.org/doi/abs/10.1021/ma0493067 (visited on 03/23/2016).

[2] M.-H. Wei et al. "Megasupramolecules for Safer, Cleaner Fuel by End Association of Long Telechelic Polymers". In: *Science* 350.6256 (Oct. 2, 2015), pp. 72–75. ISSN: 0036-8075, 1095-9203. DOI: 10.1126/science.aab0642. URL: http://www.sciencemag.org/cgi/doi/10.1126/science.aab0642 (visited on 03/17/2016).

[3] H. Martinez et al. "Ring-Opening Metathesis Polymerization of 8-Membered Cyclic Olefins". In: *Polymer Chemistry* 5.11 (2014), p. 3507. ISSN: 1759-9954, 1759-9962. DOI: 10.1039/c3py01787g. URL: http://xlink.rsc.org/?DOI=c3py01787g (visited on 03/25/2019).

Appendix C

END-GROUP FIDELITY: SUPPLEMENTAL SAMPLE AND RHEOLOGY INFORMATION

C.1   Samples for Solution Rheology

High Concentration Samples

Table C.1 characterizes the polymers dissolved in decahydronapthalene with measured viscosities shown in Figures 5.2-5.6.

Low Concentration Samples

Table C.2 characterizes the polymers dissolved in decahydronapthalene with measured viscosities shown in Figures 5.7 and 5.8.

C.2   Viscosity of Similar Molecular Weight Polymers from Hydroboration-treated COD

In Figures 5.7 and 5.8, we compared the specific viscosities of the highest molecular weight samples produced from hydroboration- and zeolite-treated

Table C.1: Polymer Samples for High Concentration Solution Rheology

purification method	M	end-group	trans/cis ratio	M_n (Mg/mol)	M_w (Mg/mol)	Đ
ZSM-5	60k	DA	45/55	0.039	0.59	1.53
		NA	40/60	0.043	0.063	1.47
	200k	DA	33/66	0.14	0.21	1.53
		NA	42/58	0.13	0.20	1.52
hydroboration	60k	DA	46/54	0.043	0.062	1.43
		NA	43/57	0.042	0.059	1.41
	200k	DA	46/54	0.14	0.23	1.59
		NA	36/64	0.13	0.20	1.52

M: Molecular weight label,
DA: Diacid end group,
NA: Non-associative (cis-2-hexene).

Table C.2: Polymer Samples for Low Concentration Solution Rheology (COD/CTA of 14000)

purification method	end-group	trans/cis ratio	M_n (Mg/mol)	M_w (Mg/mol)	Đ
ZSM-5	DA	37/63	0.74	1.16	1.57
	NA	29/71	0.65	0.95	1.45
hydroboration	DA	46/54	0.14	0.23	1.59
	NA	36/64	0.13	0.20	1.52

DA: Diacid end group,
NA: Non-associative (cis-2-hexene).

Table C.3: DA PCOD from Hydroboration Purified COD

monomer/CTA ratio	trans/cis ratio	M_n (Mg/mol)	M_w (Mg/mol)	Đ
3200	63/37	0.14	0.2	1.38
6500	53/47	0.11	0.17	1.55
14000	46/54	0.14	0.23	1.59

COD. Here, in Figure C.1, we compared the specific viscosities of three self-associative polymers from hydroboration-purified COD at a concentration of 2.5 wt%, demonstrating that the sample shown in Figure 4 (monomer/CTA of 14,000) has the highest specific viscosity of these three samples, despite having a smaller number of CTA-controlled chain ends per polymer than the samples at lower monomer/CTA. The molecular weights corresponding to each monomer/CTA ratio are displayed in Table C.3.

C.3   Intrinsic Viscosity

Intrinsic viscosity data for polycyclooctadiene in decalin were fit to the Kuhn-Mark-Houwink-Sakurada (KMHS) equation (Figure C.2).
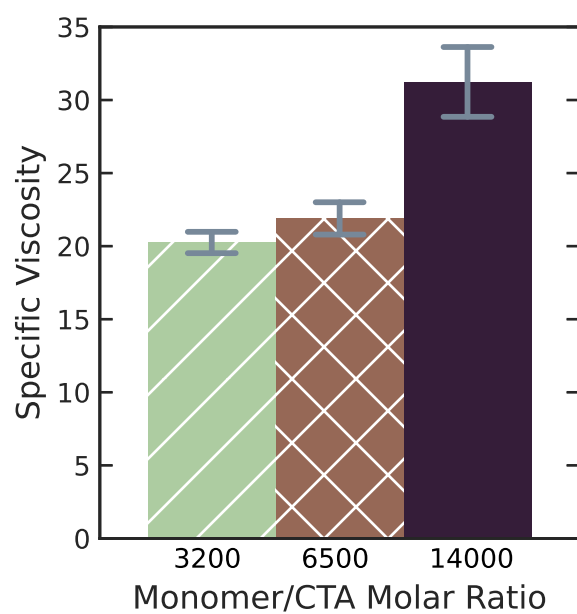
Figure C.1: Specific viscosities of solutions of three monomer/CTA molar ratios of self-associative (DA) polymers made from hydroboration-purified COD (hb) in decalin at a concentration of 2.5 wt %. Error bars represent 95% confidence interval.
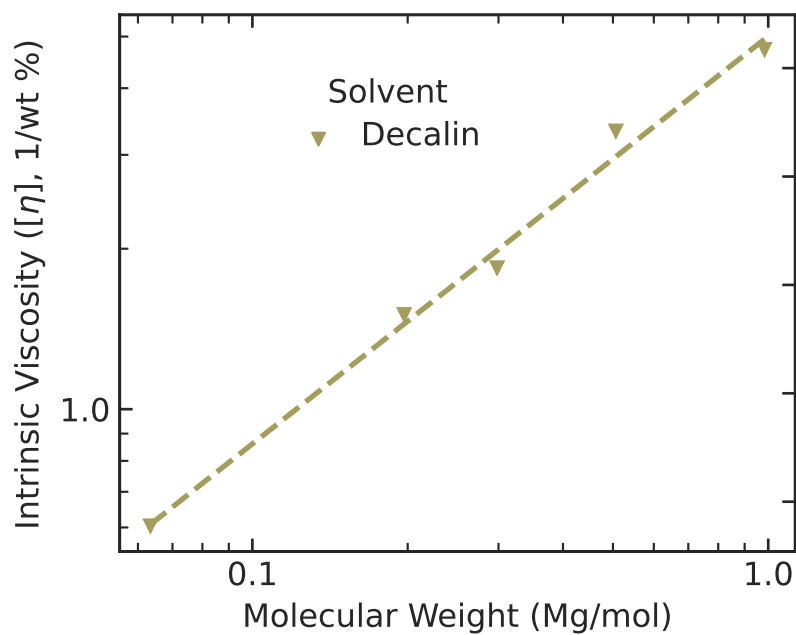
Figure C.2: Intrinsic viscosity ($[\eta]$, 1/wt %) as a function of weight-average molecular weight (M_w, g/mol) for polycyclooctadiene in decalin at 0°C (circles). Kuhn-Mark-Houwink-Sakurada equation fit to data (dashed line), $[\eta] = K M_w^a$ with $K = 1.4 * 10^{-4}$ and $a = 0.76 \pm 0.03$, with $[\eta]$ in (1/wt %) and M_w in g/mol. ($a \pm$ one standard deviation, K standard deviations were less than 10^{-8})